ON

LARGE TRANSVERSE MOMENTUM REACTIONS

Organiser: L M Lederman

INTRODUCTION

Large transverse momentum reactions were covered in three sessions. The first was devoted to a presentation of the results on hadron production at large transverse momentum submitted to the conference. In the second the related theoretical papers were reviewed in a single talk by Dr S D Ellis.

The final session dealt with the observation of lepton production. After papers from six experimental groups, Professor J D Bjorken made some remarks on the theoretical implications of the results. These remarks could not be included in these proceedings. Professor L M Lederman has written a brief summary of the session.

INCLUSIVE PION PRODUCTION AT HIGH p_T

G Jarlskog

CERN and Lund University

The first indication of surprisingly high cross-sections at large p_T came from the CERN-Columbia-Rockefeller (CCR) groups[1] at the CERN ISR, where the cross-section was found to be several orders of magnitude higher than the naive extrapolation of a linear exponential fit to the invariant differential cross section found for $p_T < 1$ GeV/c. Data also displayed a very strong s-dependence at large p_T. Later several other groups presented pion data at large p_T[2-5]. This data is consistent with a p_T^{-} and s-dependance given by

$$E \frac{d^3\sigma}{dp^3} = p_T^{-N} f(X_T), \qquad (1)$$

where $X_T = 2p_T/\sqrt{s}$, as suggested by hard scattering models. The CCR group found $n = 8.24$ and $f(X_T) = \exp(-13\, X_T)$ to fit their invariant cross-section for neutral pion production around 90° cm angle over the ranges $2.5 < p_T < 9$ GeV/c and $23.5 < \sqrt{s} < 52.8$ GeV.

The new results presented at this conference are listed in table 1.

TABLE 1

INCLUSIVE PION PRODUCTION

EXPERIMENT	PAPER	REACTION	$\sqrt{s}$ GEV	p_T GEV/C	θ_{cm}
COLUMBIA-NAL (FNAL)	1023	p+Be→γ+...	23.8	2.0-4.4	$65^\circ, 93^\circ$
NAL-NORTHERN ILL (FNAL)	745	p+C →γ+... p+p →γ+...	9.8-27.4	0.3-4.3	40°-110°
CHICAGO-PRINCETOWN (FNAL)	357	p+W →$\pi^{\pm}$+..	19.4-27.4	0.76-9.2	~90°
- " -	399	p+W →$\pi^{\pm}$+.. p+Ti→$\pi^{\pm}$+.. p+Be→$\pi^{\pm}$+..	23.8	0.76-6.1	~90°
BRITISH-SCANDINAVIAN (ISR)	834	p+p →$\pi^{\pm}$+..	23.4-63.0	0.15-4.8	40°-90°

Two papers are presented on the production of photons (interpreted as the decay products of neutral pions). The Columbia-FNAL group (paper 1023) have recorded photon spectra at $\sqrt{s}$ = 23.8 GeV using a one-arm magnetic spectrometer followed by lead glass converters and a hadron calorimeter. Beryllium foils of varying thicknesses were inserted into a secondary beam with 300 GeV protons incident, and the electron and positron spectra by γ-conversion were recorded. The cross sections on Be were renormalized to equivalent cross sections for nucleons by dividing by 9, the ratio of the atomic numbers of Be and H. The conclusions drawn from this paper are:

i) The π^o data at 90° agree with the modified CCR fit

$$E\frac{d^3\sigma}{dp^3} = \frac{15}{(p^2+1)^4} e^{-13X_T} \frac{mb}{(GeV)^2 sr} \quad (2)$$

ii) The shape of the inferred π^o spectra is the same as found for charged pions at the same energy[4]

iii) There is no angular dependence of the invariant cross section between θ_{cm} 65° and 93° (fig.1).

In the FNAL-Northern Illinois experiment (paper 745 and ref.5) the internal proton beam was utilized by using a gas hydrogen fit for calibration purposes and a rotating carbon fibre target for most of the data taking. The detector was a lead glass shower counter sensitive to one of the decay photons of the π^o.

The invariant differential cross section obtained over their angular range $40^o < \theta_{cm} < 110^o$ can be described by a product of two functions,

$$E\frac{d^3\sigma}{dp^3} = f(x_R)\, g(p_T),$$

where $x_R = 2p^*/\sqrt{s}$ is a radial scaling variable. This parametrization with $f(x_R) \sim (1 - x_R)^4$ and $g(p_T) \sim (p_T^2 + 0.86)^{-4.5}$ is adequate for $x_R > 0.2$ (fig.2) and $p_T > 0.5$ GeV/c.

New data on charged pion production at $\sqrt{s}$ = 27.4 GeV is presented by the Chicago-Princeton group (paper 357). The apparatus is described in ref.4. The main

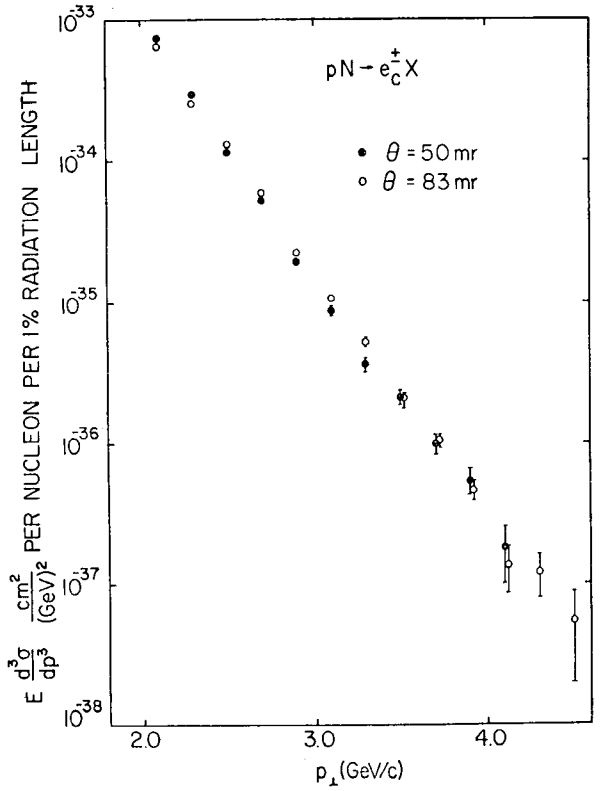

Fig. 1 Invariant cross section for conversion electrons (Columbia-FNAL).

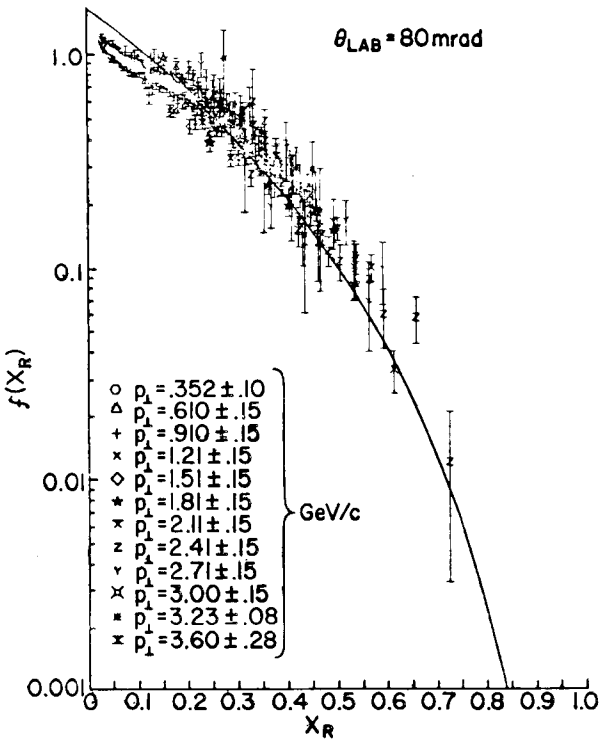

Fig. 2 The function $f(x_R)$ calculated for 12 fixed $p_\perp$ values for the 80 m rad data are compared with each other and with the functional form $(1-x_R)^4$.

experimental uncertainty was associated with the estimated 50% error in the number of incident protons. As in the previous measurements at $\sqrt{s}$ = 19.4 and 23.8 GeV, a tungsten (W) target was used. The new data cover the range $0.76 < p_T < 8.4$ GeV/c. In fig.3 the invariant differential cross sections of π^- are shown as a function of X_T. The data of the three different energies become parallel for $p_T > 0.4$ indicating a scaling behaviour in this variable. The data are well described by

$$E \frac{d^3\sigma}{dp^3} = s^{-n} e^{-a X_T}, \qquad (3)$$

where the total energy, $\sqrt{s}$, is used rather than p_T in order to get the same experimental form in X_T as used in ref.1. The best values above $X_T = 0.4$ are for π^+: $n = 5.7 \pm 0.2$, $a = 36.3 \pm 0.4$; and for π^-: $n = 5.4 \pm 0.2$, $a = 36.0 \pm 0.4$.

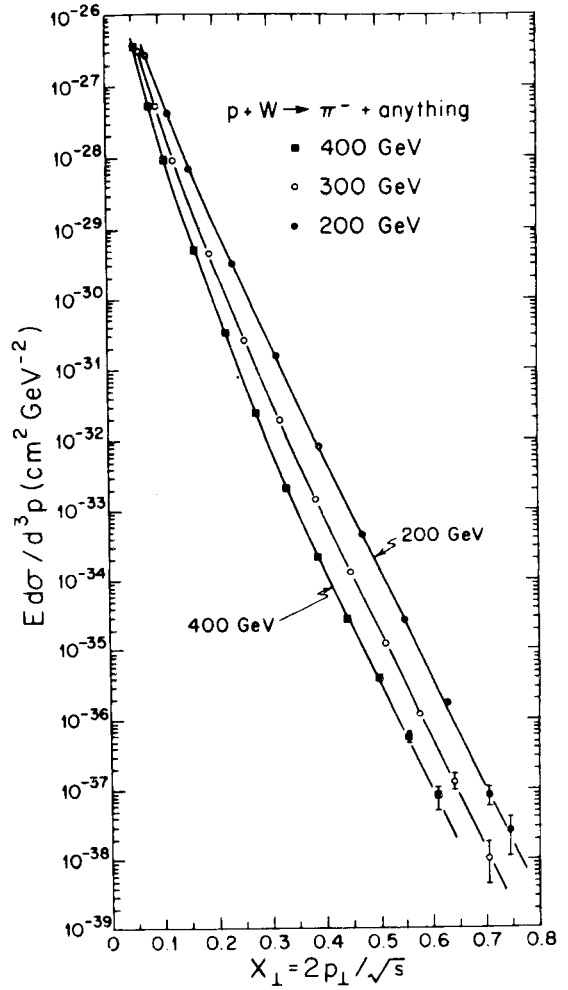

Fig. 3 π^- production cross section versus $x_\perp$.

In order to compare absolute cross sections on W with data on protons, a model dependent conversion of the cross-section has to be made. In order to investigate this the invariant production cross-section on titanium and beryllium were also measured at $\sqrt{s}$ = 23.8 GeV (paper 399). Assuming the cross section to be proportional to A^n, a momentum dependence of the power n was found, n increasing with p_T to reach a constant value of $\sim$ 1.1 for $p_T > 3$ GeV/c (fig.4).

For the reduction of the cross sections to the equivalent on nucleons, for simplicity, the ratio of the total absorption cross sections have been used, i.e. in the case of W the effective atomic number is assumed to be

$$A_{eff} = \sigma(W)/\sigma(p) = 1635/40 = 40.9$$

For Be an A_{eff} of 5.7 was used (this differs from the straight factor of 9 proposed in the Columbia-FNAL experiment).

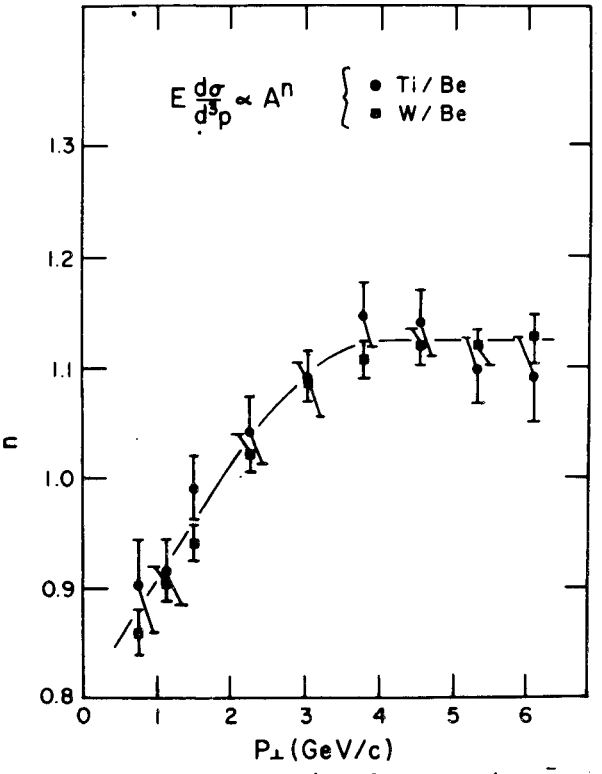

Fig. 4 The value of n derived from comparing π^- production from Ti and W to that from Be, assuming that the invariant cross section depends on the atomic number A via a power law.

The British-Scandinavian experiment (paper 834) at the ISR provide charged pion data at both low and higher momenta. The low momentum data (p_T < 1.2 GeV/c) was recorded using the spectrometer described in ref.3. For the high momentum part of the experiment (p_T > 1.2 GeV/c) two high pressure gas Cerenkov counters were added to the apparatus. At $\theta_{cm} = 89^\circ$ the pion data cover the range 0.15 < p_T < 4.8 GeV and $\sqrt{s}$ = 23.4 to 63.0 GeV. In addition, for $\theta_{cm} = 40^\circ$ and 60°, data are presented in the range 1.25 < p_T < 3 GeV/c and $\sqrt{s}$ = 44.6 amd 52.8 GeV. In the range of p_T below 1.2 GeV/c the invariant cross sections could be fitted by a quadratic exponential,

$$E\frac{d^3\sigma}{dp^3} = Ae^{Bp_T + Cp_T^2} \qquad (4)$$

When extended to include the high-momentum data, Eq.(2) does not give an acceptable fit for the pions. Instead, the data can be parametrized by a fit to the phenomelogical four-parameter formula.

$$E\frac{d^3\sigma}{dp^3} = D(p_T^2 + m^2)^n e^{ax_T}. \qquad (5)$$

Restricting the fit to the data above 1.2 GeV/c one finds m ∿ 1 GeV and n ≈ -4, in agreement with (2). Pions display an s-dependence which increases with p_T (fig.5).

The pion data have been fitted to the scaling formula (1) that was found to describe the behaviour of the CCR data on neutral pions[1] with N ≃ 8. Fig.6 indicates that the data on charged pions could approach the same scaling limit and only significantly deviate in regions of s and p_T not covered by Ref.1. The dashed line is a fit to the neutral pion data renormalised by a factor of 0.7.

Using the parametrization of the 89° data given by formula (5), the differential cross-section has been investigated over the p_T range from 0 GeV/c to 3 GeV/c to obtain $d\sigma/dy$ at $y_{cm} = 0$. The rise in the

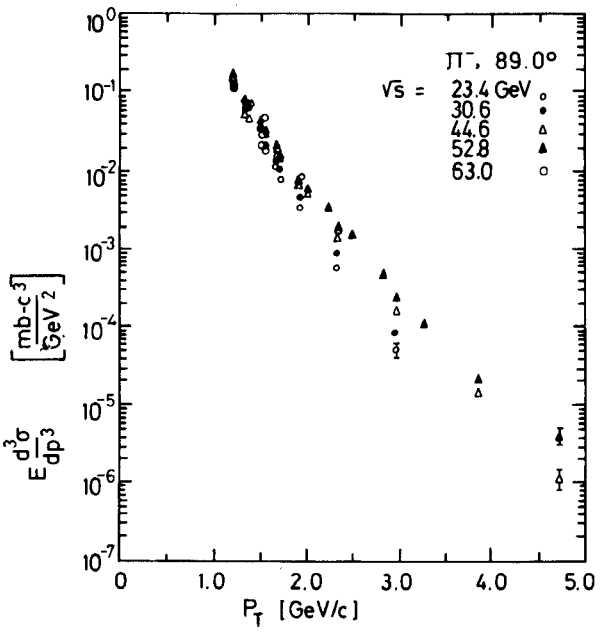

Fig. 5 The invariant differential cross section for the production of π^- at $\theta_{cm} = 89^\circ$ for five different energies of the ISR.

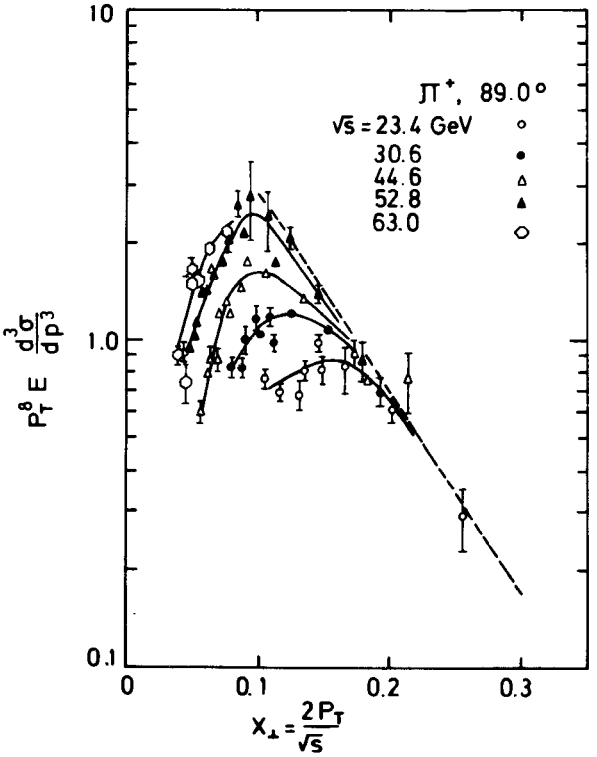

Fig. 6 π^+ data at $\theta_{cm} = 89^\circ$ for five different energies of the ISR, illustrating the possible approach to a scaling limit at high p_T satisfying the function

$$E\frac{d^3\sigma}{dp^3} = p_T^{-8} f(p_T/\sqrt{s}).$$

The straight line is a fit to π° data renormalized by a factor of 0.7.

pion cross section with energy is 24 ± 9% from $\sqrt{s}$ = 23.4 to 63.0 GeV. It should be stressed that the data below 1 GeV/c are partly preliminary (at $\sqrt{s}$ = 23.4, 44.6 and 63.0 GeV).

From the measurements at different angles, θ_{cm} = 40, 60 and 89°, the rapidity distribution at constant p_T is determined using fits to the momentum distribution to formula (4), applied to the high momentum data only. The rapidity distribution of cross-sections at $\sqrt{s}$ = 52.8 obtained over one unit in rapidity is given in Fig.7. Even at the highest value of p_T, π^+ and π^- show a remarkably flat distribution, as found previously at low p_T [6].

The π^+/π^- ratio above 1.2 GeV/c at 89° is essentially independent of p_T with about 15% excess of π^+.

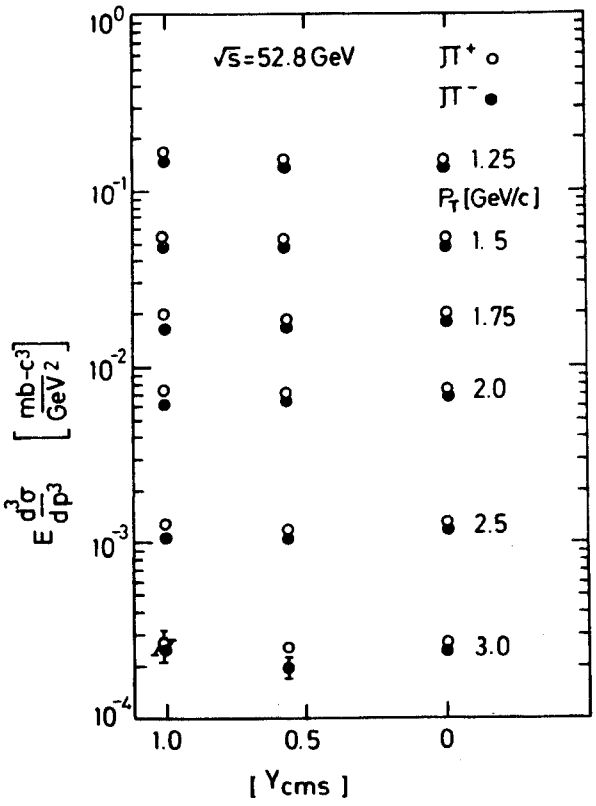

Fig. 7 The rapidity dependence of the invariant differential cross section for pions at $\sqrt{s}$ = 52.8 GeV and at fixed transverse momenta.

Conclusions

We have a good picture of the inclusive pion production at high energy over a large range in p_T although the precision in absolute normalization still needs to be improved. It should be stressed that at present it is very difficult to compare the data from nuclear targets with hydrogen data.

We can make the following observations:

1. The parametrization suggested by parton models

$$E\frac{d^3\sigma}{dp^3} = p_T^{-N} f(X_T),$$

with $f(X_T) = e^{-aX_T}$, gives a fair description of pion data at large p_T(or X_T), however with different values of the parameters N and a depending on the region in p_T and s over which the fits are done, typically giving N ∿ 8 at the ISR for $X_T \lesssim .5$ and N ∿ 11 at the larger values of X_T at FNAL. Fig.8 shows the variation of N as a function of X_T needed to bring the charged pion data of different energies of the FNAL together. No acceptable "universal" description of the overall pion data has been found.

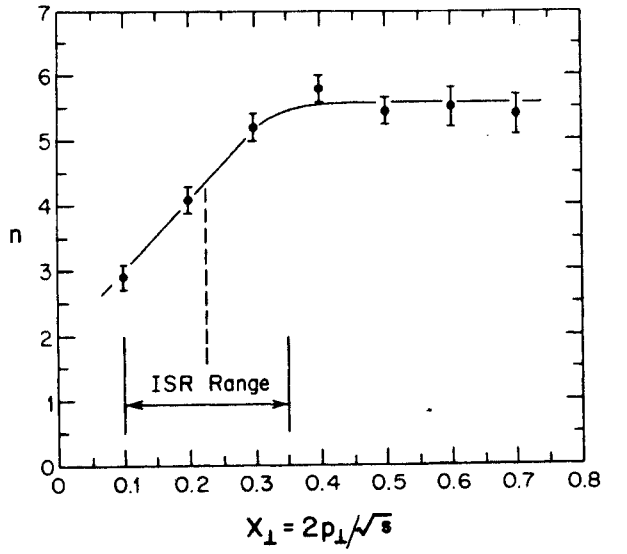

Fig. 8 Variation of exponent n, in the parametrization

$$E\frac{d^3\sigma}{dp^3} \propto p_T^{-n}$$

as a function of x_T, required to bring the charged pion data at different FNAL energies together.

2. As at low p_T, there is an extended central plateau in rapidity at large p_T.

3. The absolute yields of charged and neutral pions (as deduced from photon spectra) are very similar with a possible small surplus of π_o.
Since such a surplus would be of fundamental interest this question ought to be studied more.

4. The increase of $(d\sigma/dy)$ with s is 24 ± 9% over the ISR energies. Again a better accuracy in normalization at low p_T is called for in order to verify the magnitude of this important rise.

References

1. F W Busser et al., Phys. Letters, 46B, 471 (1973).
2. M Banner et al., Phys. Letters 44B, 537 (1973).
3. B Alper et al., Phys. Letters 44B, 521 (1973).
4. J W Cronin et al., Phys. Rev. Letters 31, 1426, (1973).
5. D C Careg et al., Phys. Rev. Letters 32, 24 (1974).
6. B Alper et al., Phys. Lett. 47B, 75 (1973).

THE PRODUCTION AT LARGE TRANSVERSE MOMENTUM OF PARTICLES HEAVIER THAN PIONS

Presented by H Frisch

Chicago University

New data on inclusive heavy particle production was submitted to the Conference by two groups:-

1) The British-Scandanavian (BS) Collaboration has submitted proton-proton data from the ISR covering the kinematic region $23 \leq \sqrt{s} \leq 63$ GeV, and $0.5 \leq p_\perp \leq 4.8$ GeV.
2) The Chicago-Princeton (CP) Collaboration has submitted data on proton-nucleus [1] collisions in the region $19.4 \leq \sqrt{s} \leq 27.4$, and $0.5 \leq p_\perp \leq 7.6$ GeV

The data are significant in that for the first time we have good data covering a large range in s at fairly large $p_\perp$.

In general the two experiments agree very well, although we shall see that there are some specific points of disagreement. The disagreement could be real in that the nuclear target produces both pp and pn collisions. However in some cases there are experimental details which may be responsible for at least some of the disagreement.

The gross features of the heavy particle data are listed below:

1) the invariant cross sections for inclusive $K^\pm$, P, and $\bar{p}$ production look much like those for π production.
2) Heavy particles are produced copiously at large $p_\perp$. For example, in much of the data I will show we see that the ratios K^+/π^+ and P/π^+ are greater than $\frac{1}{2}$.
3) Like the pion cross sections, the invariant cross sections for heavy particle production are s dependent large $p_\perp$, although not at small $p_\perp$. However the s dependences for K^-, p, and $\bar{p}$ differ from that of the pions, as we shall see in detail below.
4) The antiparticle-particle ratios for heavy particles are quite different from the π^+/π^- ratio in that it is quite sensitive to kinematic variables.

The gross similarity of the cross sections for the production of $\pi^\pm$, $K^\pm$, p and $\bar{p}$ is illustrated in Figure 1, which shows the invariant cross sections of the British Scandanavian group. One sees that all of the cross sections have the same general shape, with the exception that the $K^\pm$, p, $\bar{p}$ cross-

sections do not have the steeper slope at small $p_\perp$ as do the π's.

It is this steeper slope that makes the heavy particle fractions rise sharply with $p_\perp$. Figure 2 shows these particle fractions as measured by the B-S group at $\sqrt{s}$=52.8 GeV.

The Chicago-Princeton data at their three energies show the same effect, and also dramatically show the energy dependence of the various particle ratios. Their K^+/π^+ and K^-/π^- ratios, measured on a W target, are shown in Figure 3. One sees that the K^+/π^+ ratio rises with $p_\perp$, and levels off at a value near 0.6, independent of s. The K^-/π^- ratio, however, is energy dependent at large $p_\perp$, and is rising approximately linearly with $\sqrt{s}$.

The p/π^+ and $\bar{p}/\pi^-$ ratios are shown in Fig. 4. Both ratios are energy dependent, the P/π^+ falling as $\sqrt{s}$, the $\bar{p}/\pi^-$ rising to meet it also as $\sqrt{s}$.
(We note that as $\pi^+/\pi^- \sim 1.1\text{-}1.2$, if p and $\bar{p}$ were made in pairs p/π^+ and $\bar{p}/\pi^-$ would be almost equal).

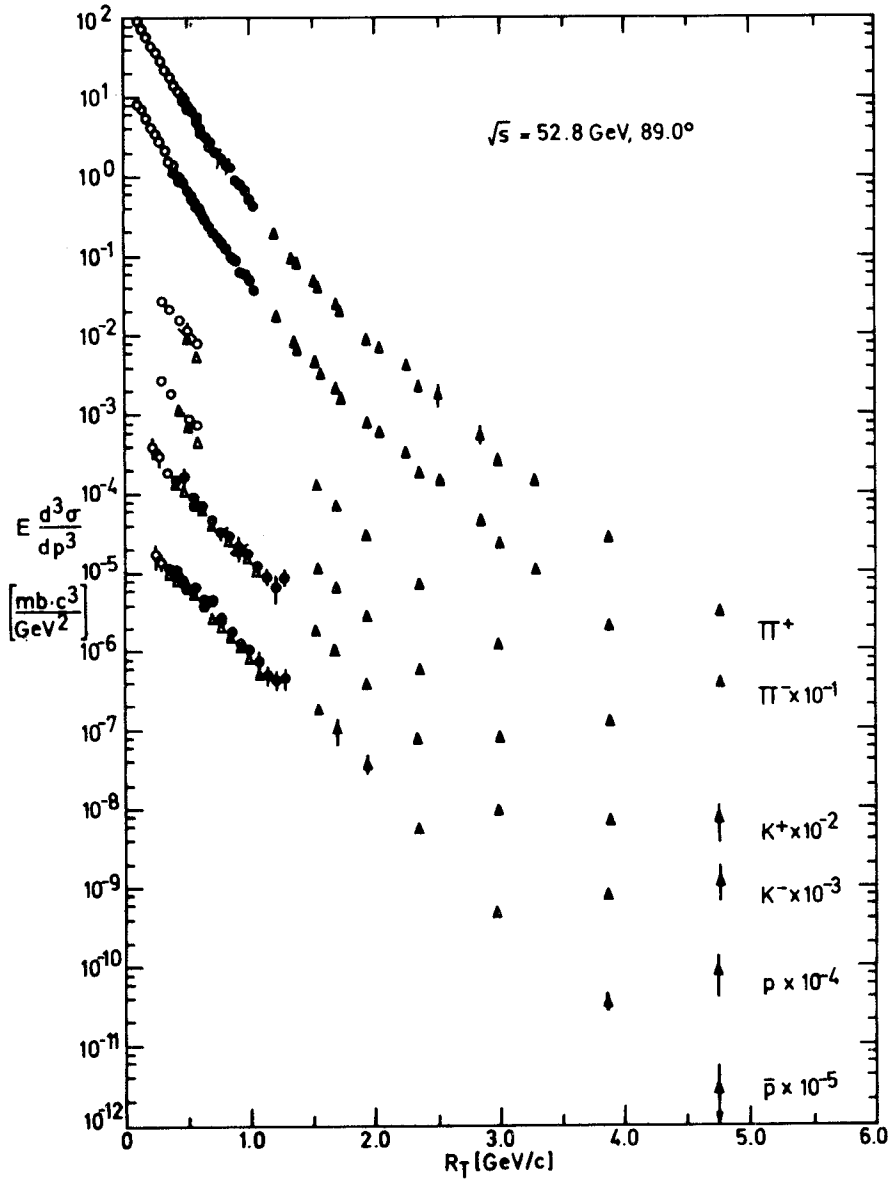

Fig. 1 The invariant differential cross section for the production of π, K, p and $\bar{p}$ at $\sqrt{s}$ = 52.8 GeV and $\theta_{cm} = 89^\circ$

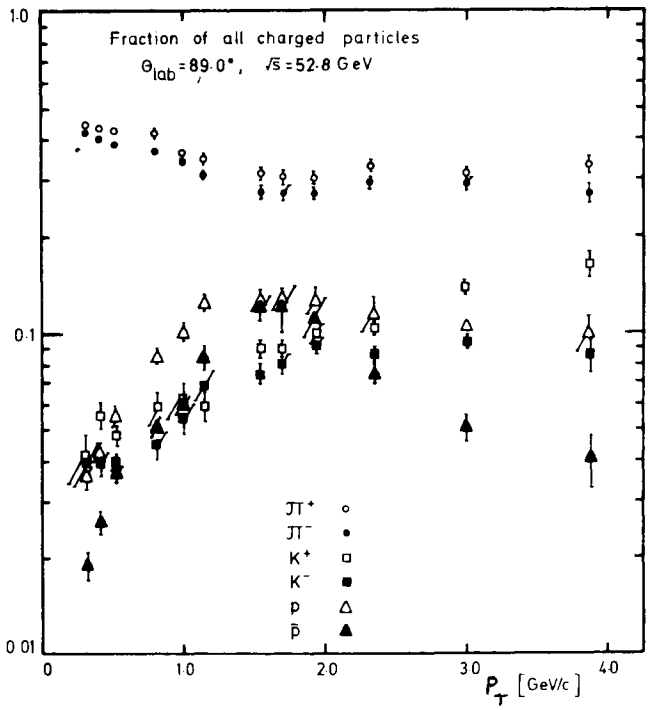

Fig. 2 The p_T dependence of the charged particle composition at $\sqrt{s}$ = 52.8 GeV for $|y_{cm}| = 0$

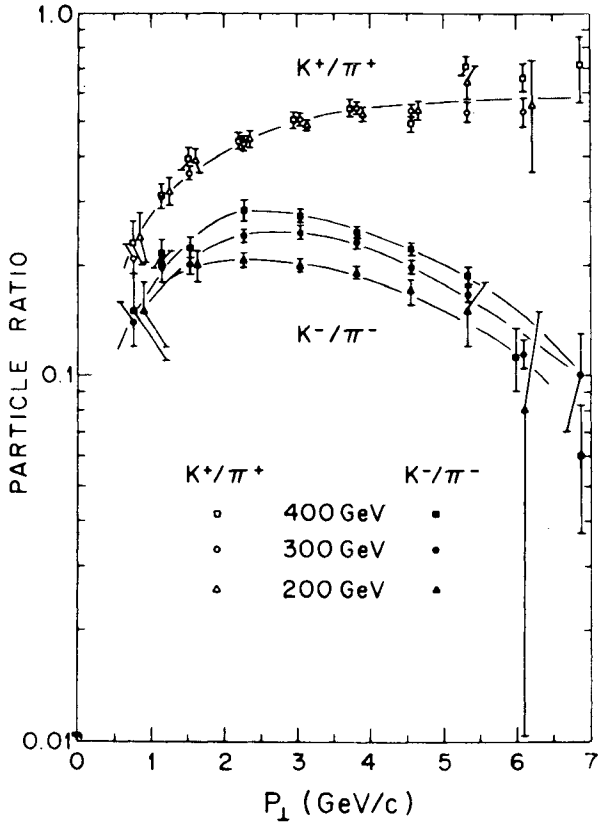

Fig. 3 K abundance relative to π versus $p_\perp$

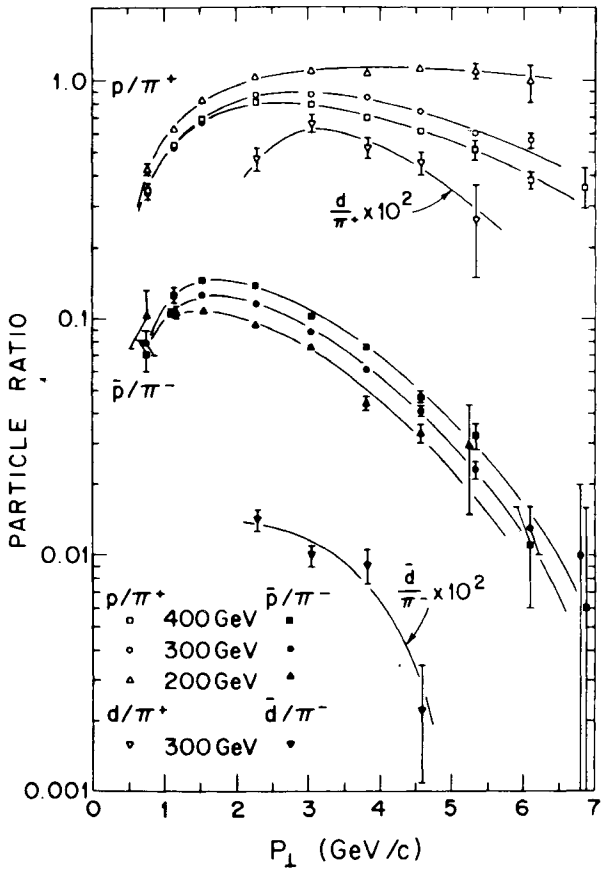

Fig. 4 p, $\bar{p}$, d and $\bar{d}$ abundances relative to π of the same charge versus $p_\perp$

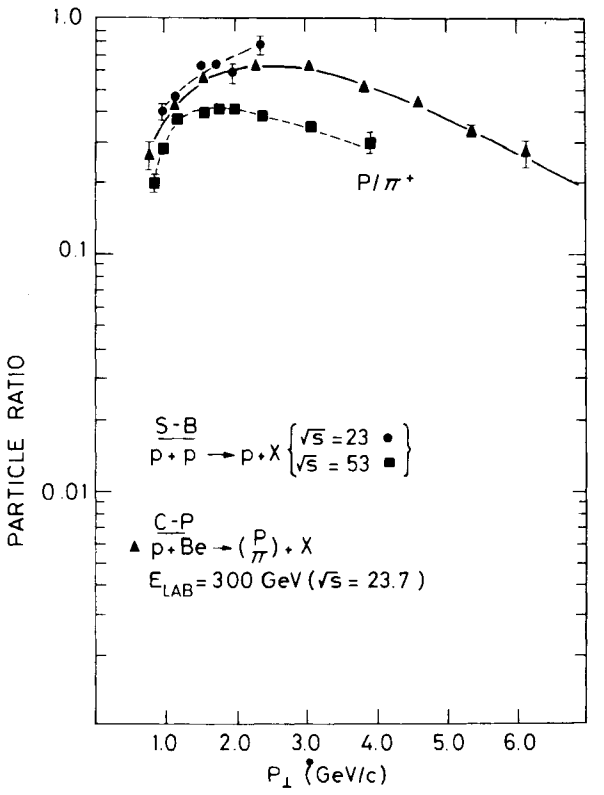

Fig. 5 p/π^+ relative abundance versus $p_\perp$. Comparison of B-S and C-P results.

A comparison of the B-S and C-P data on the p/π^+ ratio is shown in Figure 5. The two sets of data taken at $\sqrt{s}$ = 24 GeV are in reasonable agreement, and the measured decrease with energy in the B-S data is compatible with that of the CP data.

A similar comparison for the K^+/π^+ ratio is shown in Figure 6. (Here the p-W data is shown on the graph, while the dotted line approximately represents the p-Be data. Because the K^+/π^+ ratio shows an A dependence, the comparison should be made with the dotted line). Again the agreement is quite good, and the independence of the K^+/π^+ ratio seen in the C-P data holds true over a wide range of s.

The comparison of the $\bar{p}/\pi^-$ ratios for the two experiments is shown in Figure 7. Here the comparison of the data at $\sqrt{s}$=24 GeV is less happy than that for p/π^+ or K^+/π^+, the British Scandinavian points being significantly higher than those of Chicago-Princeton. However the energy dependence in the B-S data agrees well with that of the C-P collaboration, i.e. the $\bar{p}/\pi^-$ ratio arises with energy approximately as $\sqrt{s}$. Some part of this discrepancy may be due to a systematic uncertainty in the large absorbtion corrections for $\bar{p}$'s in the momentum range near 1.5 GeV in the B-S data.

The K^-/π^- ratios are in worse disagreement, as shown in Figure 8. Here not only do the data disagree at $\sqrt{s}$ = 24 GeV, but also the B-S data show no energy dependence, vs. the approximately $\sqrt{s}$ dependence of the C-P collaboration.

To summarize the data on the s-dependence of the particle ratios:

1) the K^+/π^+ ratio at large $p_\perp$ doesn't change with s as $\sqrt{s}$ goes from 19.4 GeV to 52.8 GeV.
2) the K^-/π^- ratio rises with $\sqrt{s}$ in the C-P data out changes little in the B-S data. There is also a disagreement at $\sqrt{s}$=24 between the two groups.
3) The p/π^+ ratio falls with $\sqrt{s}$, and both groups are in fair agreement.
4) the $\bar{p}/\pi^-$ ratio rises with $\sqrt{s}$ in both sets of data, but the two groups disagree in the ratios at $\sqrt{s}$=24 GeV.

The particle/anti-particle ratios are shown in Figure 9 as measured from a W target by the C-P collaboration. One sees that $p/\bar{p}$ and K^+/K^- rise as $p_\perp$ increases at fixed s, although at fixed $p_\perp$ the ratio falls as s increases. Figure 9 shows that the p and $\bar{p}$ production changes as one moves away from 90° keeping $p_\perp$ fixed, with the p increasing and the $\bar{p}$ decreasing. Such behaviour agrees with the above trend that as one goes toward the kinematic limit the particle/anti-particle ratio increases.

Footnotes 1) The C-P data was taken on W, Ti, and Be targets. We should note that in a paper submitted to the Conference the C-P group shows that the A dependence of the invariant cross-section follows a power law of the form $E\frac{d\sigma}{d^3p} \propto A^n$, with n increasing with $p_\perp$ to a value of 1.1 at large $p_\perp$.

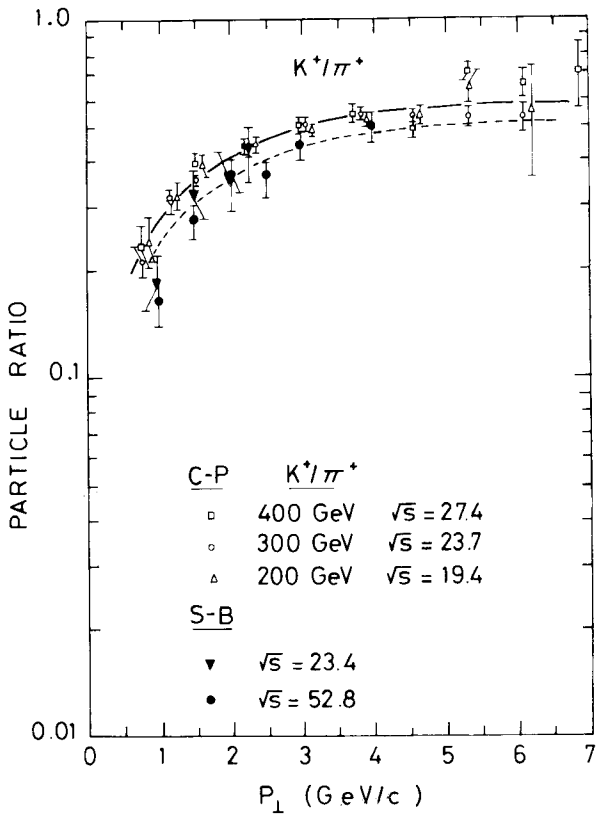

Fig. 6 K^+/π^+ relative abundance versus $p_\perp$. Comparison of B-S and C-P results.

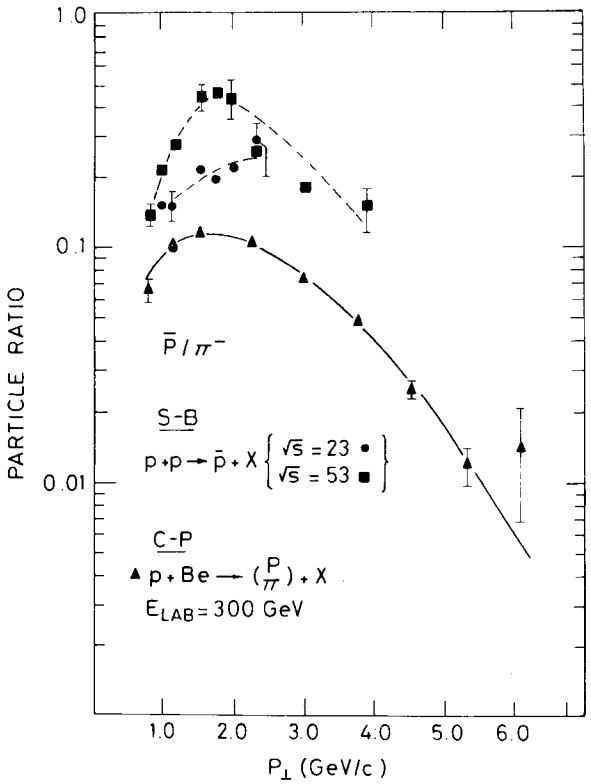

Fig. 7 $\bar{p}/\pi^-$ relative abundance versus $p_\perp$. Comparison of B-S and C-P resutls.

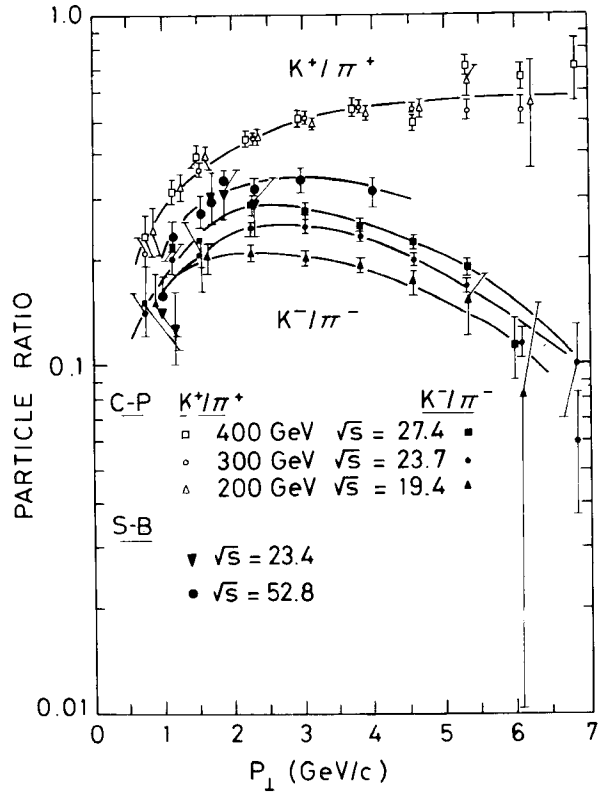

Fig. 8 Comparison of B-S and C-P results on K abundance relative to π.

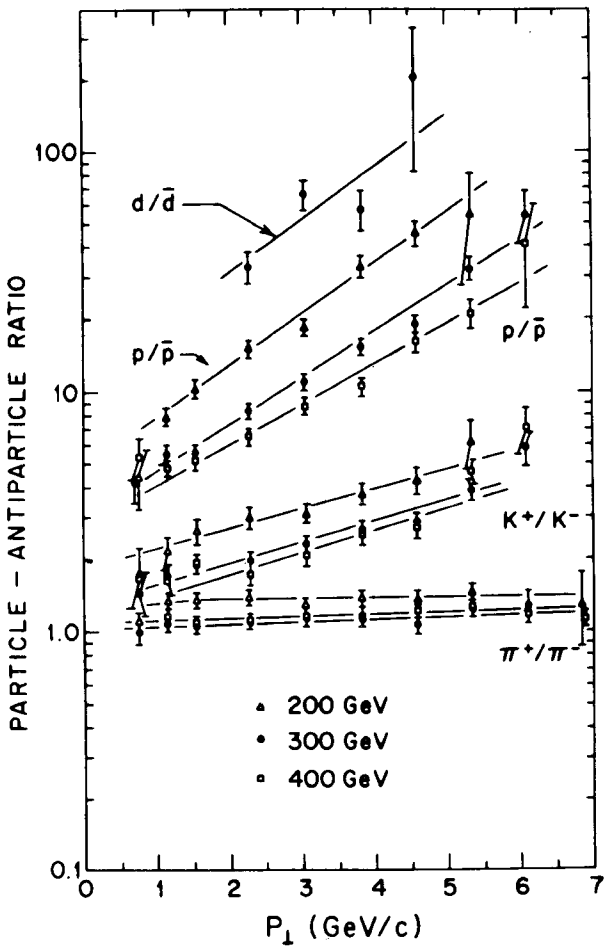

Fig. 9 Particle-antiparticle ratio versus $p_\perp$

CORRELATIONS IN HIGH TRANSVERSE MOMENTUM FINAL STATES

L Di Lella

CERN

1. INTRODUCTION

A study of particle correlations in high energy collisions leading to high transverse momentum secondaries can provide further insight into the dynamics of these processes. In particular, it is hoped to test the hypothesis [1] that hadron production at high values of the transverse momentum $p_\perp$ result from large angle scattering of elementary constituents within the proton (partons). In this case it is expected to observe "jets" of hadrons, with a total transverse momentum balancing that of the high $p_\perp$ secondary hadron which triggered the apparatus.

All the experimental results on this subject have so far been obtained at the CERN Intersecting Storage Rings (ISR). Most of them are limited by statistics to $p_\perp < 4$ GeV/c.

2. CHARGED PARTICLE MULTIPLICITIES AND ANGULAR DISTRIBUTIONS

The Pisa-Stony Brook (PSB) collaboration [2),3)] have used a system of counter hodoscopes covering a solid angle of almost 4π, triggered by a photon detector (a matrix of lead glass Cerenkov counters) located at 90° (see Fig. 1). Fig. 2 shows the average charged particle multiplicities at the five standard ISR c.m.s. energies ($\sqrt{s}$=23,31,45,53 and 62 GeV), as a function of the photon transverse momentum $p_\perp$, as measured in the hemisphere opposite to the photon direction. These data have been normalized to the value relative to the lowest $p_\perp$ bin ($p_\perp < 0.5$ GeV/c), in order to divide out most of the experimental errors and to stress the dependence on $p_\perp$. The raw normalizing multiplicities range from 5.1 at $\sqrt{s}$=23 GeV, to 8.2 at 62 GeV. It is seen that the normalized multiplicities increase roughly linearly with $p_\perp$ and display little s-dependence. However, in the hemisphere toward the photon, the data (see Fig. 3) show a strong s dependence: at the lower energies the normalized multiplicities decrease as $p_\perp$ increases, while they become flat or even increase slightly at the higher energies.

The angular distribution of charged particles associated with a high $p_\perp$ photon or π^o, has been measured by the PSB collaboration [2),3)] and by the Aachen-CERN-Heidelberg-Munich (MPI)(ACHM) Collaboration [4)]. The apparatus used in this latter experiment is shown in Fig. 4 : it consists mainly of two streamer chambers surrounding an ISR intersection region, and an array of lead glass Cerenkov counters to detect π^o's emitted at 90° in the lab system. Fig. 5 shows the difference of the η

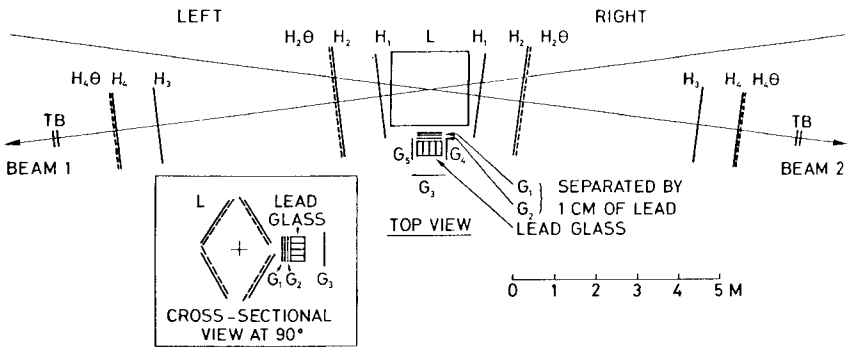

Fig. 1
Plan view of the Pisa-Stony Brook experimental set-up.

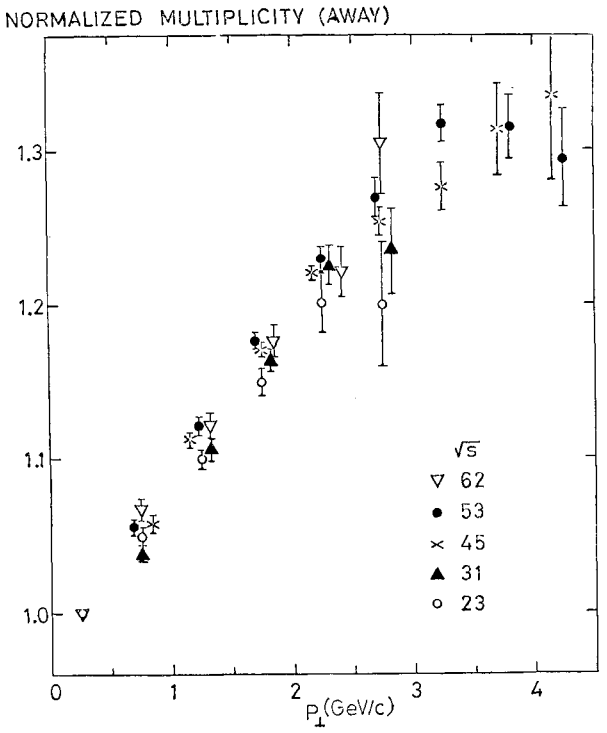

Fig.2 Normalised partial multiplicities as a function of the photon transverse momentum, in the hemisphere away from the detected photon.

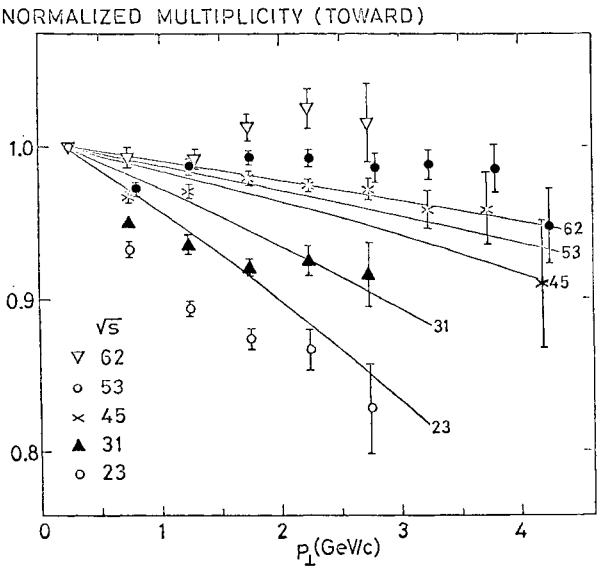

Fig.3 Normalized partial multiplicities as a function of the photon transverse momentum, in the hemisphere toward the detected photon.

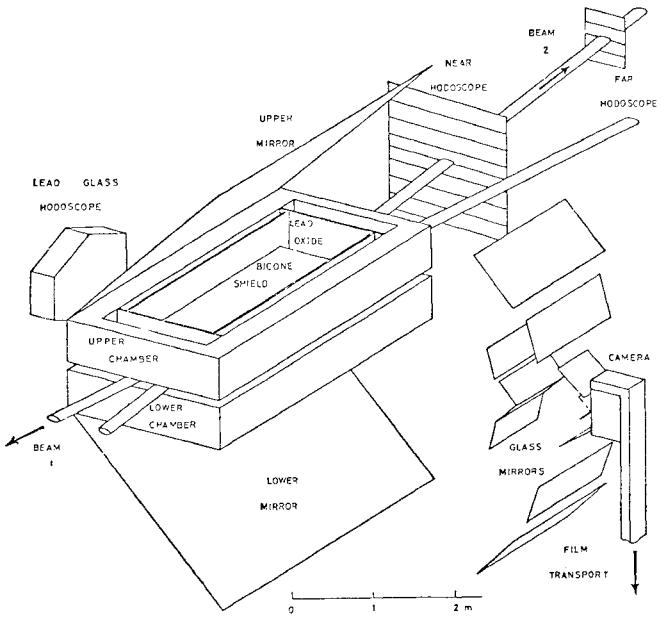

Fig.4 Experimental set-up used by the Aachen-CERN-Heidelberg-Munich (MPI) collaboration.

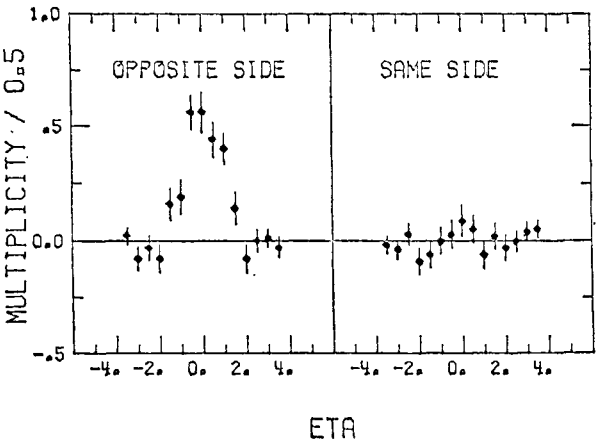

Fig.5 Difference of the η distributions at $p_\perp$ = 3 GeV/c and $p_\perp$ = 1 GeV/c, for the opposite and same hemispheres with respect to the π^o.

distributions (η=-ln tan $\theta/2$) for events with $p_\perp$ = 3 GeV/c and $p_\perp$ = 1 GeV/c, at a c.m.s. energy $\sqrt{s}$ = 53 GeV, for the opposite and same hemispheres with respect to the π^o. It is seen that the $p_\perp$ dependent enhancement in the opposite hemisphere, covers an angular region with a width $\Delta\eta$=±2. The difference of the ϕ distributions at $p_\perp$ = 3 GeV/c and $p_\perp$ = 1 GeV/c, for events with $|\eta| \lesssim 2$, is shown in Fig. 6 The enhancement is seen to occur in an azimuth interval $\Delta\phi$=±60°, centered around a direction opposite to the high $p_\perp$ π^o. Data from the CERN-Columbia-Rockefeller (CCR) collabroation[5], covering an angular range with $\Delta\phi$=±23°, $\Delta\eta$=±0.8 around 90° (see Fig. 7.), are shown in Fig. 8, for π^o's detected around 90° with $p_\perp$ values as high as 8 GeV/c, at $\sqrt{s}$=53 GeV.

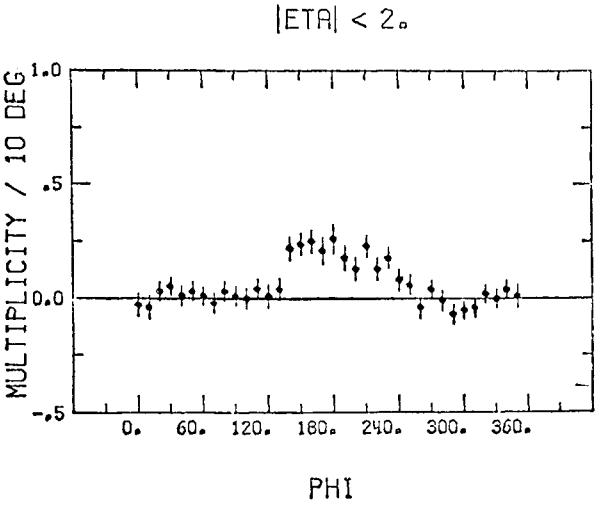

Fig.6 Difference of the ϕ distributions at $p_\perp$ = 3 GeV/c and $p_\perp$ = 1 GeV/c, for all charged particles with $|\eta| \lesssim 2$.

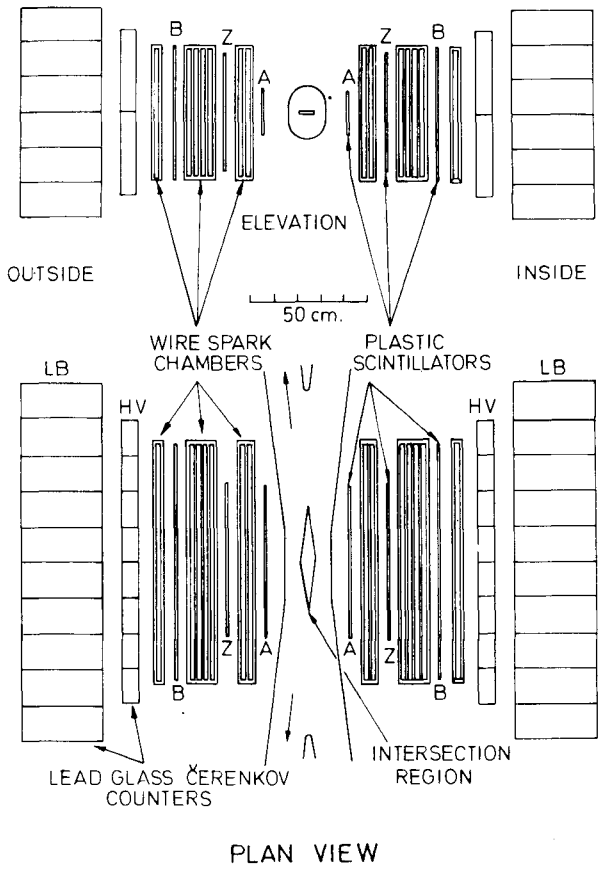

Fig.7 The CERN-Columbia-Rockefeller experimental set-up.

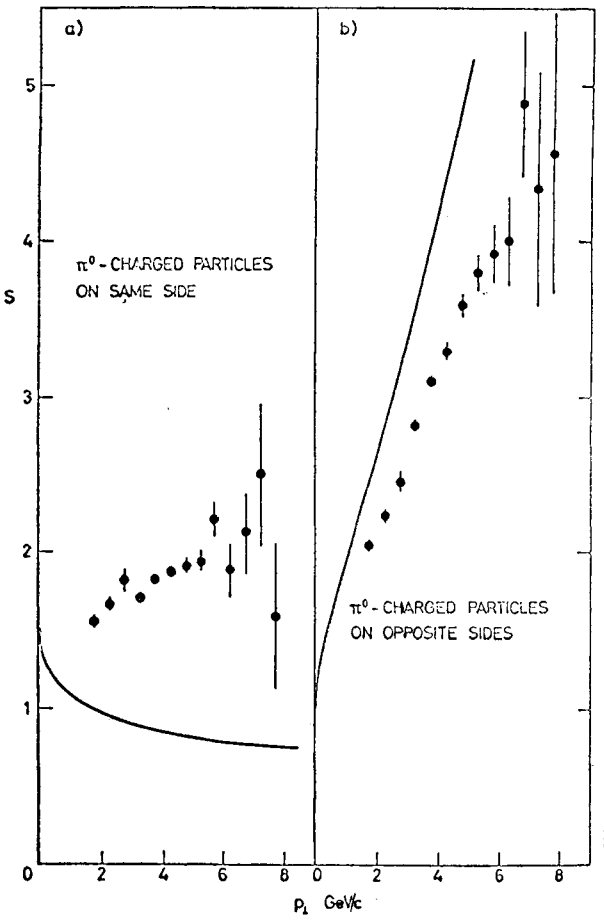

Fig.8 The ratio of the number of charged particles associated with a π^o meson of transverse momentum $p_\perp$ to the number of charged particles observed in a typical inelastic interaction.

These data are normalized to the average multiplicities, as measured for a typical inelastic interaction. The multiplicity in a direction opposite to the π^o is seen to increase roughly linearly with $p_\perp$ up to $p_\perp$ = 8 GeV/c, while on the same side as the π^o, it is approximately constant with $p_\perp$. In a direction opposite to the π^o, most of the enhancement can be explained by the Uncorrelated Jet Model [6] (see the full curves of Fig. 8), which uses only energy-momentum conservation and the limitation of transverse momentum. However, the data disagree with this model on the same side as the π^o.

In conclusion, one observes an enhancement of the charged particle multiplicity around a direction opposite to that of a high $p_\perp$ π^o emitted at 90°. This enhancement has the following features:

a) it covers an angular region with width $\Delta\eta=\pm 2$, $\Delta\phi=\pm 60^o$.

b) the multiplicity increases roughly linearly with $p_\perp$ up to at least $p_\perp \approx$ 8 GeV/c.

c) the rate of growth is 0.8 particles/GeV/c.

d) approximately 3.5 extra charged particles are produced when $p_\perp$ = 4 GeV/c.

Similar results have been obtained by the CERN-Daresbury-Rutherford-Liverpool collaboration [7], who detect high $p_\perp$ charged hadrons with a magnetic spectrometer at 60° and 90°, and study associated particle multiplicity by means of a barrel shaped counter matrix surrounding an ISR intersection region.

The PSB [8] and ACHM [4] collaboration have also measured the position of the multiplicity enhancement when the high $p_\perp$ π^o is detected at an angle different from 90°. In the PSB experiment [8], the lead glass detector is moved to 17.5° ($\eta_\gamma \simeq 1.9$). In the ACHM experiment [4], the π^o detector position is left unchanged, and data are taken with 11.8 GeV protons in one ring and 31.4 GeV protons in the other. These conditions give $\sqrt{s}$ = 38.2 GeV, $\eta_{\pi^o} = -0.5$.

In both cases the enhancement is seen to be centered at values of η which are not equal and opposite to those of the high $p_\perp$ photon or π^o. In the PSB experiment, the centre of the enhancement is at $\eta \approx -0.7$; in the ACHM experiment it is found between $\eta=0$ and $\eta=-\eta_{\pi^o}$. It is certainly difficult to explain these results in terms of kinematic effects only.

The ACHM collaboration [4] have also studied the angular correlation between two charged particles in the enhancement, in order to see if there is any evidence for jet structure. A normalised correlation function is defined as

$$R(\Delta\eta,\Delta\phi) = \frac{\sigma' \int \frac{d^4\sigma}{d\eta_1 d\eta_2 d\phi_1 d\phi_2}\, \delta(\phi_2-\phi_1-\Delta\phi)\delta(\eta_2-\eta_1-\Delta\eta)\, d\eta_1 d\eta_2 d\phi_1 d\phi_2}{\int \frac{d^2\sigma}{d\eta_1 d\phi_1}\frac{d^2\sigma}{d\eta_2 d\phi_2}\, \delta(\phi_2-\phi_1-\Delta\phi)\delta(\eta_2-\eta_1-\Delta\eta)\, d\eta_1 d\eta_2 d\phi_1 d\phi_2} - 1 \qquad (1)$$

where σ' is the partial cross section for the inelastic collisions being studied . The data are then compared with the predictions of two models: the first one, in which the extra particles produced in association with a high $p_\perp$ π^o are distributed at random within the angular band of the enhancement and the second, in which they are distributed in a way corresponding to a jet structure. As it can be seen from Fig. 9, the behaviour of R vs. $\Delta\eta$, as shown by the high $p_\perp$ data, does not agree with that obtained by a random distribution, and exhibits a clear short-range correlation in $\Delta\eta$. However, the same behaviour is found in the experimental data when lower transverse momentum π^o's are selected. This correlation in $\Delta\eta$ is also present in a direction normal to the plane containing the π^o and the beam momenta. It seems that the data can only be interpreted as giving evidence for a short-range

rapidity correlation, but the mechanism responsible for this phenomenon is unknown at present.

3. MOMENTUM CORRELATIONS

The CCR collaboration [5] have studied events at $\sqrt{s}$=53 GeV, where two high $p_\perp$ π^o's are produced on either the same side or on opposite sides of an ISR intersection region (see the apparatus shown in Fig. 7). Fig. 10 displays the correlation function

$$R(x_{1_\perp},x_{2_\perp}) = \frac{\sigma_{INEL}\ \frac{d^6\sigma}{dp_1^3 dp_2^3}}{\frac{d^3\sigma}{dp_1^3}\ \cdot\ \frac{d^3\sigma}{dp_2^3}} \qquad (2)$$

where $x_\perp = 2p_\perp/\sqrt{s}$, for the case of opposite side π^o's. The correlation is seen to increase with increasing $x_\perp$ of either π^o, and R is as high as $\sim 10^4$ for $x_{1_\perp} = x_{2_\perp} = 0.2$. This behaviour might be largely a consequence of momentum conservation, as shown by the solid curves of Fig. 10, which represent predictions based on UJM [6].

However, the correlation function R for same-side π^o's (see Fig. 11) is also positive and large (R$\sim$10 at $x_{1_\perp}=x_{2_\perp}=0.1$), an effect which cannot be explained

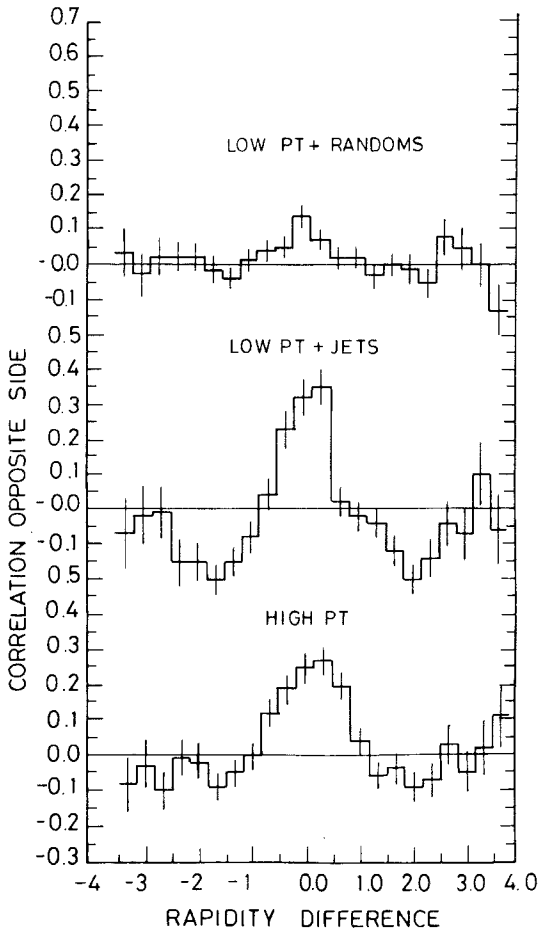

Fig.9 $\Delta\eta$ correlations of charged particles opposite to the π^o. Comparison of the data at $p_\perp$ = 3 GeV/c with the jet model and the random distribution model as described in the text.

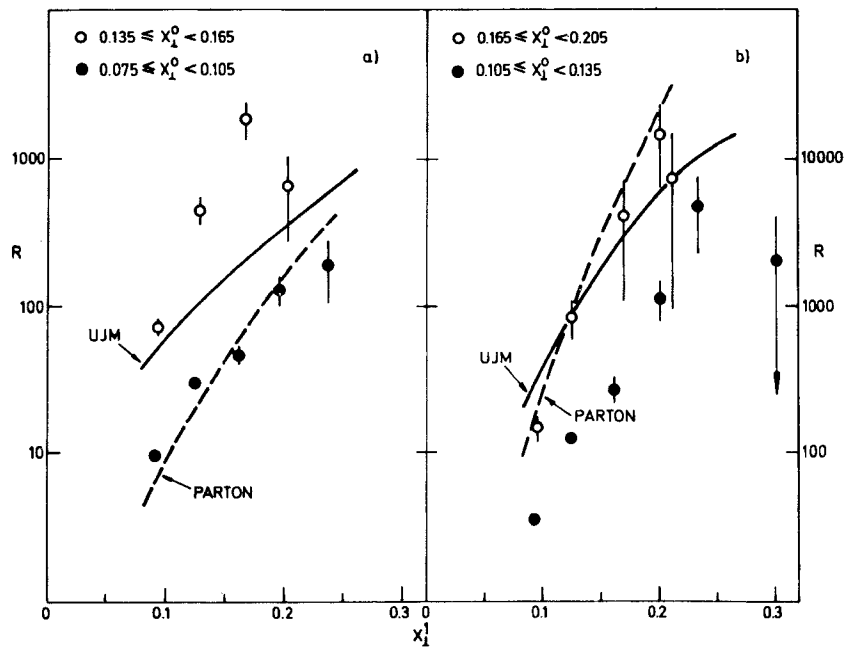

Fig.10 The correlation coefficient R for two π^o's with azimuthal separation $\sim 180^o$.

in terms of kinematics. An obvious possibility here is resonance decay, but the invariant mass distribution for the two π^o's (Fig. 12), does not show any evidence for resonances.

Preliminary data on momentum correlations between two high $p_\perp$ hadrons have been reported by the CERN-Columbia-Rockefeller-Saclay (CCRS) collaboration [9]. The experimental apparatus, shown in Fig. 13, consists of two magnetic spectrometers, each subtending an angular acceptance $\Delta\phi=\pm 7^o$ and $\Delta\theta=\pm 12^o$ around 90^o. A π^o detector, consisting of a matrix of lead glass Cerenkov counters, is located at the end of one of the two spectrometers. The results for charged hadrons with an azimuthal separation of approximately 180^o are shown in Fig. 14, where the correlation function R, as defined in (2), is displayed as a function of the two momenta p_1 and p_2. These results are consistent with those obtained by the CCR collaboration on opposite side π^o's and discussed above.

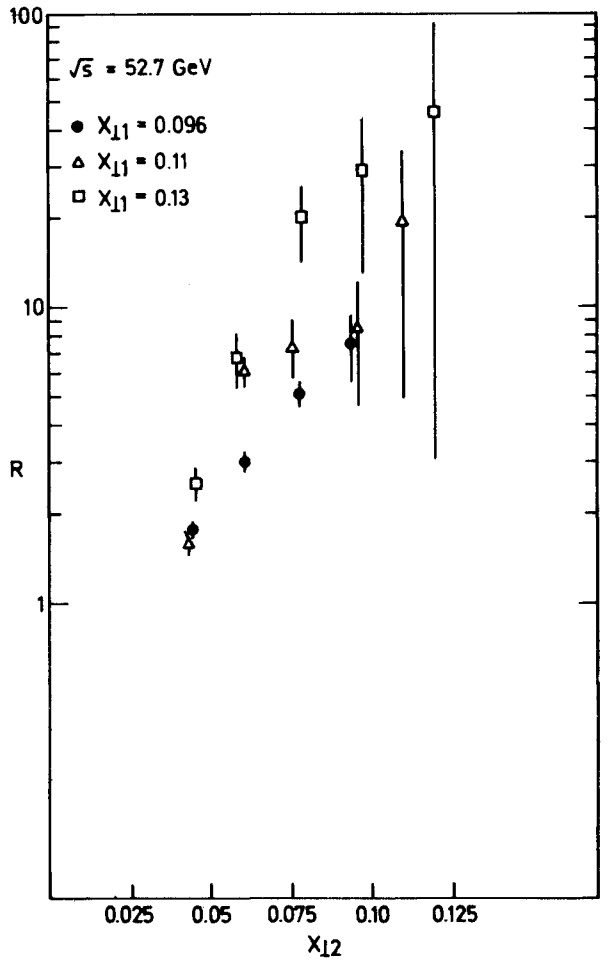

Fig.11 The correlation coefficient R for two π^o's with azimuthal separation $\sim 0^o$.

The momentum distribution of charged hadrons produced along a direction opposite to that of a π^o with $p_\perp > 3$ GeV/c, is shown in Fig. 15, normalized to the total number of events in which a π^o with $p_\perp > 3$ GeV/c is observed. The comparison with the inclusive momentum distribution for charged hadrons (also shown in Fig. 15) is another way to show the existence of a positive and large momentum correlation.

While this correlation might largely result from kinematic effects, the same side effects, shown in Fig. 16, need something more than this, since a positive and large momentum correlation is present here too.

4. CONCLUSION

Most of the effects observed in opposite direction with respect to that of a high $p_\perp$ hadron, can be largely explained in terms of kinematic effects. These effects have made any search for jets of hadrons opposite to a high $p_\perp$ hadron inconclusive - on the other hand, the positive momentum correlations observed between two high $p_\perp$ hadrons in the same azimuthal region, are certainly of dynamical origin and must be studied further.

It should also be very useful to measure the momenta of all the extra particles produced in a direction opposite to high $p_\perp$ hadron, as well as do special experiments in which not only single high $p_\perp$ hadrons are selected, but clusters of hadrons with a high value of the total transverse momentum.

REFERENCES

1) S M Berman, et al, Phys.Rev.D4,3388(1971).

2) Paper 988.

3) Paper 989.

4) Paper 1037.

5) Paper 728.

6) L Caneschi,VII Rencontres de Moriond(1973);
A Bassetto, et al, Nuclear Phys.B34,1(1971).

7) Paper 549.

8) Paper 990.

9) Paper 464.

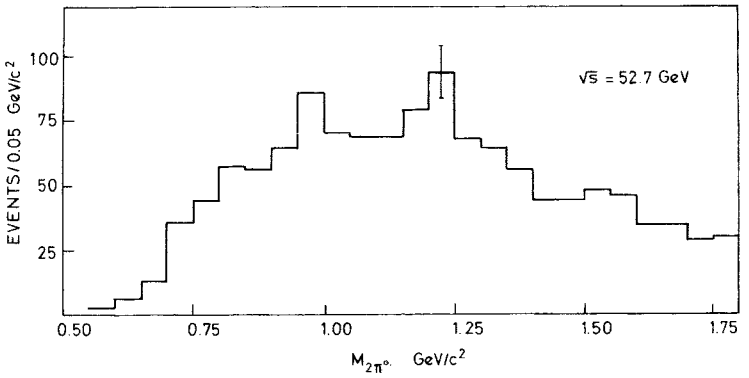

Fig.12 The distribution in invariant mass, $M_{2\pi^o}$ for two π^o's with azimuthal separation $\sim 0^o$.

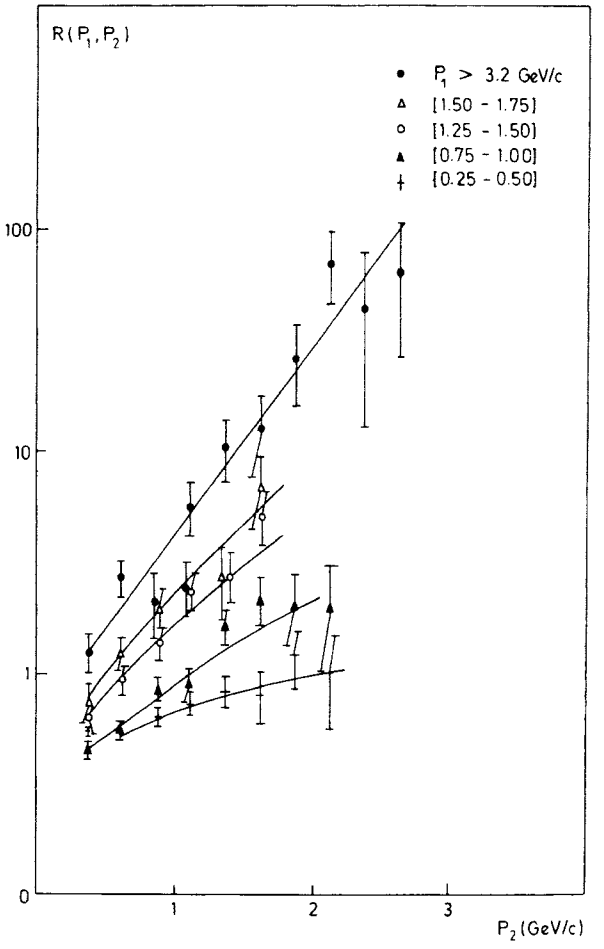

Fig.14 The correlation coefficient R for two charged hadrons with azimuthal separation $\sim 180^o$.

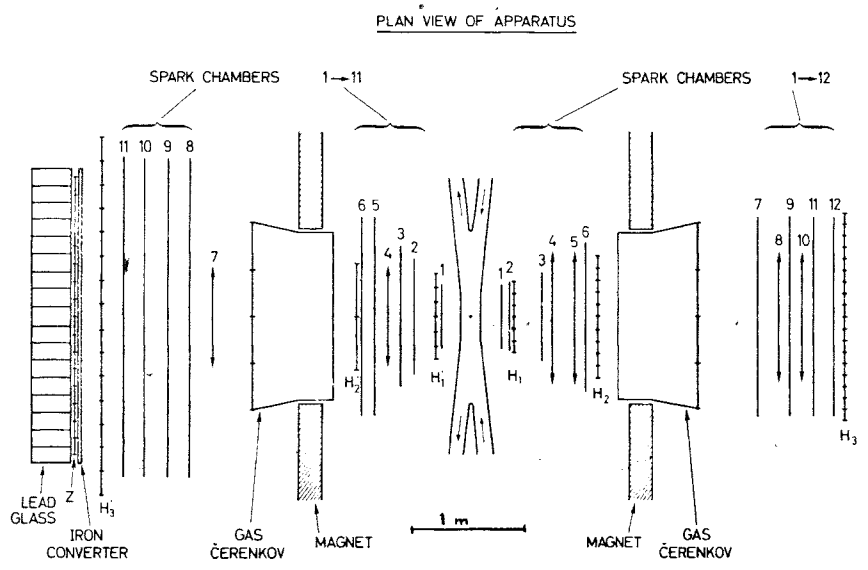

Fig.13
Experimental set-up used by the CERN-Columbia- Rockefeller-Saclay collaboration.

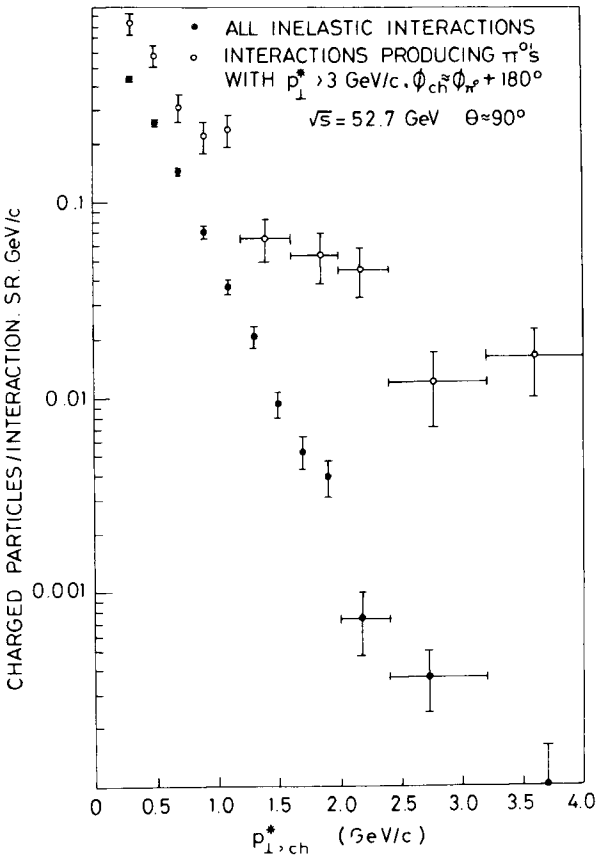

Fig.15 Momentum distributions of charged hadrons at 90°:
a) inclusive (full circles); b) produced together with a π^0 with $p_\perp$ > 3 GeV/c, with an azimuthal separation of $\sim 180^\circ$ (open circles).

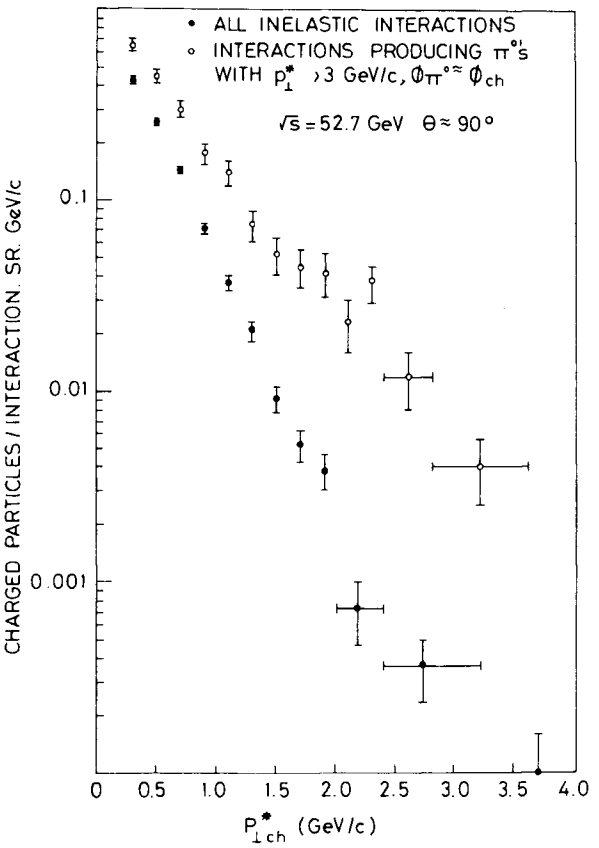

Fig.16 Momentum distributions of charged hadrons at 90°: a) inclusive (full circles); b) produced together with a π^0 with $p_\perp$ > 3 GeV/c, with an azimuthal separation of $\sim 0^\circ$ (open circles).

MULTIPLICITY RISE ASSOCIATED WITH TRANSVERSE MOMENTUM OF A PROTON IN pp AT 28.5 GeV/c

Presented by F Turkot

Brookhaven National Laboratory

A sharp rise has been observed [1] in the mean multiplicity, $\bar{n}_c$, associated with a fast forward proton in the reaction $p_1 + p_2 \to p_3 + MM$. It occurs for fixed missing mass, MM, when the four-momentum transfer, t, to p_3 exceeds 2 $(GeV/c)^2$, or $p_{3\perp} \sim 1$ GeV/c. The original data augmented by data at intermediate t values is given in Fig. 1; for MM < 2 GeV (not shown) no increase in $\bar{n}_c$ is observed. An abrupt increase of 0.6 in $\bar{n}_c$ (includes p_3) is seen in all MM bins in the $|t|$ interval 2.0-3.0 $(GeV/c)^2$, followed by a slower rise for $|t| > 3$ $(GeV/c)^2$.

In the parton interchange model of BBG [2] there are two diagrams giving rise to inclusive hadron production; one involves hadronic bremsstrahlung by the incident or final state proton and is important only at low t. Based on this idea Choudhury [3] has made a calculation that yields the qualitative features of Fig. 1. Fig. 2 illustrates the model; for

FIG. 2

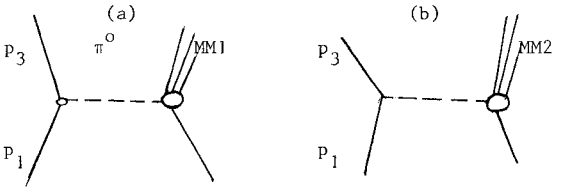

a fixed p_3 in CMS (hence the MM) the presence of the soft π^o in (a) gives MM1 < MM2 and a smaller $\bar{n}_c$. Fig. 2(a) falls more steeply with t than 2(b).

Several features of the distributions of the final state particles appear to support this type of mechanism:

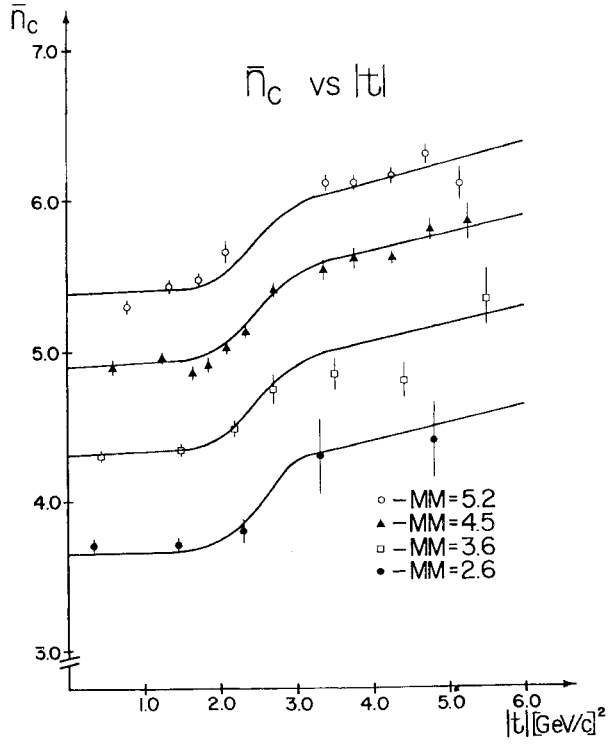

Fig.1 Variation of the average charged particle multiplicity, $\bar{n}_c$, with t_{13} for four intervals of MM.

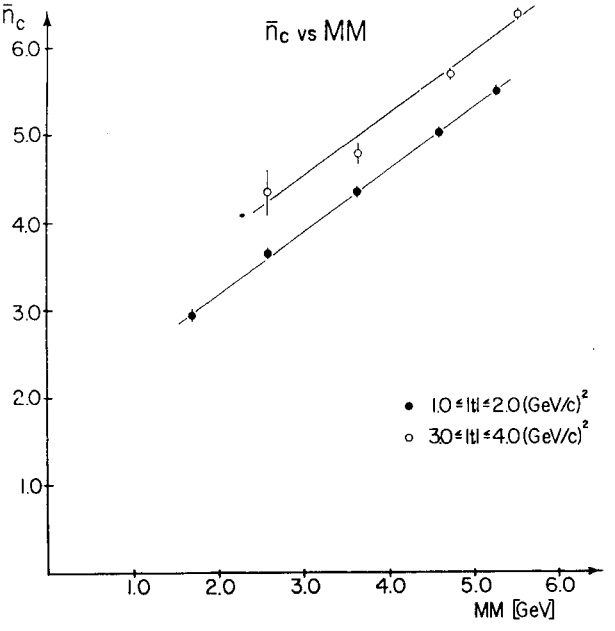

Fig.3 The dependence of $\bar{n}_c$ on MM for two intervals of t_{13}, one below the rise in $\bar{n}_c$, the other above.

1) We observe a certain behaviour of $\bar{n}_c$ and P_n (t,MM) vs MM for $|t| < 2$ (GeV/c)^2, P_n being the probability of n_c prongs. If we look at the same functions for $|t| > 3$ (GeV/c)^2 we see the same behaviour except that the MM scale has been shifted to larger MM by 0.8 GeV. This effect can be seen in Figs 3 and 4. The corresponding large t plot to Fig. 4 (not shown) agrees remarkably except for n_c=2, where it is lower.

2) In Fig 5 we show the scaled (KNO type plot) and $|t| < 2$ (GeV/c)^2 (data points) and $|t| > 3.0$ (solid line). One sees that $\langle(n/\bar{n} - 1)^2\rangle^{\frac{1}{2}}$ decreases by 10% at high t, an effect consistent with the proposed mechanism.

3) Table I shows where the increase in $\bar{n}_c$ occurs; it is all in the hemisphere opposite to P_3 as might be expected for Fig. 2 (b). It is also true that the angular distribution with respect to the MM direction at high t is quite symmetric. We conclude that the data are consistent with the picture of BBG and Choudbury, but not with a double-fragmentation model.

TABLE I

	SAME HEMISPHERE		OPPOSITE HEMISPHERE	
	POS.	NEG.	POS.	NEG.
$\bar{n}$	1.63	0.36	1.19	0.80
$\Delta\bar{n}$	0.03±.03	0.05±.02	0.33±.03	0.26±.03

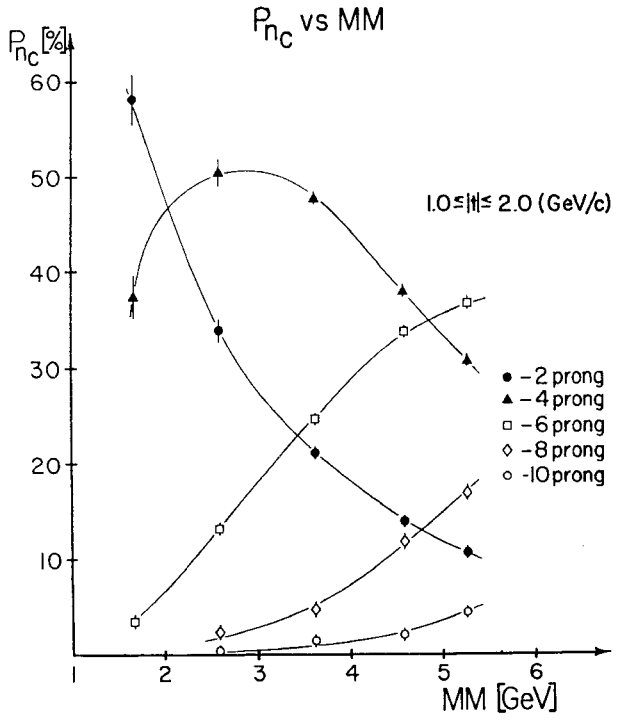

Fig.4 The probability for given number of prongs, P_{n_c}, vs MM for $|t_{13}| < 2.0$ (GeV/c)^2.

REFERENCES

1. A Ramanauskas et al., Phys.Rev.Letters,31, 1371(1973) and Anderson et al, Paper 375 submitted to this conference.

2. R Blankenbecker, S Brodsky and J F Gunion, Phys.Lett.,42B,461(1972).

3. S R Choudbury, A note on the Rise of Hadronic Multiplicity at Large Momentum Transfers, Purdue University Preprint (Paper 482 submitted to this conference).

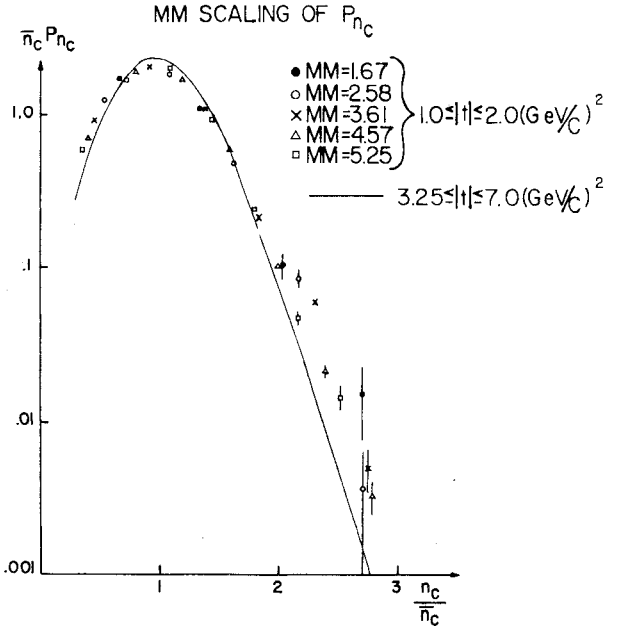

Fig.5 Scaled multiplicity distributions, $\bar{n}_c \cdot P_{n_c}$, for five MM intervals. The data points are for $|t_{13}| = 1.0 - 2.0$ (GeV/c)^2; the curve is the representation of the data for $|t_{13}| = 3.25\text{-}7.0$ (GeV/c)^2.

THEORETICAL MODELS FOR LARGE TRANSVERSE MOMENTUM PHENOMENA

S D Ellis*

CERN

I Introduction

During the last two years one of the most active areas of high energy physics research has been the study of events containing hadrons with large transverse momentum. The experimental situation is reviewed elsewhere in these proceedings. In the following report a review[1] is given of the various models which have been proposed as explanations of the observed behaviour of such large $p_\perp$ events. The intent is to provide a fairly inclusive summary of the most recent work. As a result, the discussion is seldom very detailed. The interested reader is referred to the original papers or to more specific reviews for a more complete exposition of any single model. Only definite models which have been utilized phenomenologically will be discussed.[2] It should be emphasized that there does not yet exist a real theory of large $p_\perp$ phenomena and current efforts have concentrated on the phenomenological study of these various models.[3]

The first two sections of this report will comprise a discussion of the two major classes of specific models, fireball models and hard scattering (parton) models, largely within the context of the single particle inclusive spectrum near $\theta_{c.m} \approx 90^o$. This will be followed by a brief discussion of the possible ways in which more detailed information on correlations and particle composition may be understood and used to discriminate between various models. In particular some discussion will be given concerning what can be expected when the large $p_\perp$ particle is observed away from 90^o. Then there will be a short summary of some of the other possible explanations for large $p_\perp$ events and more novel forms of analysis which have been suggested but which do not fit into the two classes mentioned above. Finally there will be a brief concluding discussion. Althought the major emphasis will be on inclusive processes, and in particular $pp \to \pi X$, there will also be some discussion of the most recent applications of various models to large $p_\perp$ exclusive processes.[3] This is a field of study with a rich history and the present coverage is far from complete, including only some of the most recent work. This situation is to some extent justified by the fact that the bulk of the large angle exclusive data is at quite low energies compared to the inclusive data.

2. Fireball Models

The majority of the models which have been advanced as relevant to large $p_\perp$ physics can be classified into two categories: fireball models and "hard scattering" or parton models. The former class is characterized by the transformation of some or all of the incident energy of longitudinal motion into one or more very massive hadronic states. By assuming that these states decay essentially isotropically, such events can lead to hadrons with large transverse momentum in the final state. The initial fireballs are themselves generally assumed to have only small $p_\perp$ so that the observed single particle spectrum is given only by the physics of the decay. For example, if the hadronic matter in a fireball of mass M reaches thermodynamic equilibrium and then decays in a statistical fashion, the normalized single particle cross section, at $\theta_{c.m} = 90^o$ and with $p_\perp \approx E \gg M$, will be given essentially by a

*on leave from FNAL

Boltzman factor.[4]

$$\frac{E}{\sigma}\frac{d^3\sigma(M)}{d^3p} \sim p_\perp^{\beta} \exp(-cp_\perp/M^{\alpha}) \qquad (1)$$

Here M^{α} is the effective temperature of the hadronic matter, β and α ($\alpha \leq 1$) are parameters related by $\beta = (1-3\alpha)\alpha$ and $\sigma(s,M)$ is the cross section to produce a fireball of mass M at energy s.

A specific example of Eq. 1 is the early nonrelativistic statistical model of Fermi[5] recently restudied by Meng-Ta-Chang.[6] In this case one has $M = \sqrt{s}$ and $\alpha = 1/4$, $\beta = 1$. For σ = constant Eq. 1 becomes

$$\frac{d^3\sigma}{d^3p} \sim \exp(-cp_\perp/s^{1/8}) \qquad (2)$$

which is compared to data in Fig. 1. Although the data may be consistent with a universal behaviour in $p_\perp/s^{1/8}$, the largest $p_\perp$ data would seem to argue against any simple exponential behaviour. Another, more sophisticated single fireball picture has been suggested by Heiko[7] who argues that the data indicate three distinct stages of evolution for the fireball. In particular there is to be an initial hot stage ($T \sim s^{1/4}$) which produces very large $p_\perp$ particles, a transition stage ($T \sim C + Ds^{1/4}$) producing intermediate $p_\perp$'s, and finally a cool stage ($T \sim T_o \sim M_\pi$) which yields the usual low $p_\perp$ spectrum.

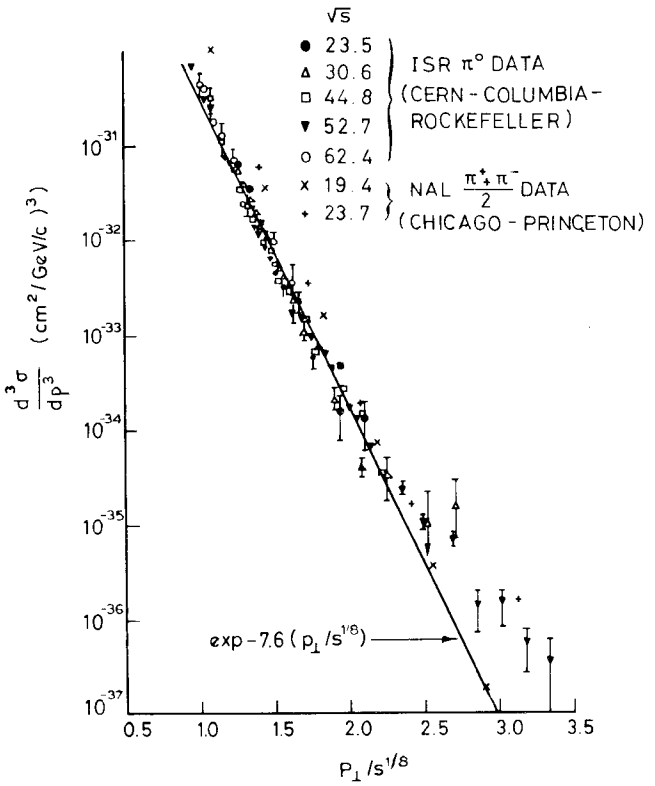

Fig. 1 Data for π production plotted in the form $d^3\sigma/dp^3$ versus $p_\perp/s^{1/8}$.

Another possibility is to utilize the freedom represented by the fireball production cross section $\sigma(s,M)$ in Eq. 1. In the case of a nontrivial distribution of fireball masses one must sum over the distribution to find (ignoring the longitudinal motion for simplicity).

$$E\frac{d^3\sigma}{d^3p} \sim \int_{2p_\perp}^{\sqrt{s}} dM\ \sigma(M,s)\ p_\perp^{\beta} \exp(-cp_\perp/m^{\alpha}) \qquad (3)$$

This formula illustrates that s dependence can arise both from that explicitly present in $\sigma(s,M)$ and from the fact that larger masses become accessible at higher s. Clearly a fairly complicated $p_\perp$ and s dependence can be achieved by a judicious choice of $\sigma(s,M)$. Such a procedure will be truly informative only if the required form of $\sigma(M,s)$ can be connected with other features of hadronic processes. Two possibilities for fireballs are to identify them with large mass diffractively produced states[8] or with the large mass tail of the mass distribution of the clusters[9] now being popularized as an explanation for short range correlations in the central region.[10]

At least two attempts to use a spectrum of fireball masses in order to explain the spectrum of particles at large $p_\perp$ have already been made. In the work of Sakai[11] a sequence of super resonances is postulated to start at $m_1 \sim 5$GeV with a spacing between resonances of $\Delta m \sim 5$-6 GeV. This author argues that evidence for such states already exists

in cosmic ray data. Assuming a six pion decay throughout and a resonance production spectrum falling as $1/m_R^2$, Sakai achieves a reasonable discription of the data at one s . A study of the predicted s dependence is certainly called for.

Another example of a mass spectrum is the recent work of Bouquet, et al.[12] Here each fireball decays as prescribed by the statistical bootstrap model. The actual number of fireballs produced in any event is allowed to vary. In the calculation particular care is taken to include recoil effects for the case of two fireball production. This is sufficient to produce large $p_\perp$ particles (via a random walk process) even though, on average, each emission involves only small momentum in the relevant fireball rest frame. By assuming a specific mass and momentum spectrum for the fireballs and accounting for overall energy-momentum conservation, a reasonable description of data at $\sqrt{s}$ = 44.8 and 52.7 is obtained. Clearly such models are of interest. However, since the fireball mass spectrum plays an essential role, it is extremely important that attempts be made to connect it to physics in other regions of phase space as discussed above. Said more generally, it is important to more directly motivate these models. Further it is necessary to study what fireball models predict about the other features of large $p_\perp$ events, for example, correlations and particle ratios.

3. Hard Scattering Models

The second basic class of large $p_\perp$ models is characterized by the presence of a "hard scattering" process. The basic assumption is the existence of interactions involving hadrons or hadronic constituents (partons) which are damped only weakly(i.e as some small power) in the momentum transfer and which can be treated as a local interaction. In this case large $p_\perp$ hadrons can be efficiently produced by a single "hard" interaction. The motivation for such models is the observed behaviour of lepton-induced inclusive reactions in the limit where both the energy loss and momentum transfer to the lepton are large. In particular, for the process ep → eX one finds experimentally that the inclusive electron cross section behaves as[13]

$$E\frac{d^3\sigma}{d^3p} \simeq \frac{\alpha^2}{s^2}\, g(t/s,\ M_x^2/s) \qquad (4a)$$

or in a more familiar form for hadronic processes

$$E\frac{d^3\sigma}{d^3p} \simeq p_\perp^{-4}\, f\,(P_\perp/\sqrt{s},\ \theta^*) \qquad (4b)$$

when s is large and t/s and M_x^2/s are fixed. Here α is the fine structure constant, s is the total energy, t is the momentum transfer to the electron, and $p_\perp$ and θ^* are the transverse momentum and angle of the electron in the e-p c.m system. Note that the behaviour indicated in Eq. 4 is just what would follow from dimensional analysis under the assumption that the hadronic part of the interaction contains no scale factors (i.e no explicit parameters with dimension). This suggests that hadrons are able to absorb large momentum transfers in a scale invariant fashion when probed by local interactions and when no restrictions are placed on the final state hadrons. It is generally also assumed in such models that hadronic form factors have a power dependence on the momentum transfer in exclusive processes involving local interactions. The end result of the above framework of assumptions is that inclusive particle production at large $p_\perp$ is expected to have the form

$$E\frac{d^3\sigma}{d^3p} \sim p_\perp^{-N}\, f\,(p_\perp/\sqrt{s},\ \theta^*) \qquad (5)$$

when s is large, $P_\perp/\sqrt{s}$ is fixed, and θ^* is not too near 0° or 180°.

This form of simple behaviour with a single power

times a function of only scaling variables(e.g $P_\perp/\sqrt{s}$ and θ^*) is characteristic of hard scattering or parton models and is to be contrasted with the generally more complicated behaviour expected in fireball models. In parton models one explicitly assumes that dimensional quantities (e.g. masses) become unimportant in the limit of large momenta and hence such models exhibit simple behaviour in dimensional variables (momenta) and complicated behaviour only in scale free variables (ratios of momenta). Fireball models, on the other hand , exhibit dimensional constants even in the large momenta limit and so can have complicated behaviour (e.g. exponential) in the momenta. The data from the ISR, e.g. those of the CERN-Columbia-Rockefeller Group[14] ($x_\perp = \frac{2P_\perp}{\sqrt{s}} \leq 0.4$), are consistent with Eq. 5 for N = 8. However, the data of the Chicago-Princeton[15] group at FNAL suggest N≈11 for $x_\perp \geq 0.4$. Thus the question of the existence at high energy of a single power law for the full $x_\perp$ range remains an open and extremely important question. In most of this report N is assumed to have the value 8. Emphasis will be placed on how the models are able to yield this value instead of the naive dimensional value N=4.

Hard scattering models are especially interesting in that the function f in Eq.(5) is generally related to the hadronic structure functions measured in lepton induced reactions (e.g. ν W_2), and there exists the exciting possibility of connecting lepton-hadron reactions to purely hadronic ones. The models discussed below share this feature of seeking to relate leptonic and hadronic processes. Differences arise from the details of the specific hard scattering process assumed. However, all the models treat the scattering as basically a two body interaction. Hence they all predict a coplanar topology for the large $p_\perp$ event exhibiting little correlation between large $p_\perp$ particles and those produced perpendicular to the plane containing the incident beam and the large $p_\perp$ particle. Also the models suggest "jet structure" wherein the large $p_\perp$ particles tend to appear within two well defined cones in momentum space on either side of the beam direction. Included in some of the models is the case when the jet contains only a single particle or resonance. It should be emphasized that clear "jet" structure can be manifest in the data only in the limit where the average momentum of a particle in the jet is much larger than the expected width of the jet. This condition does not seem to be fulfilled in present data.

The various specific parton models are illustrated in Fig. 2. Note the general kinematic similarity of the models. In all cases a constituent of one hadron (either a parton or a virtual pion) interacts with a constituent of the other hadron to yield the observed large $p_\perp$ pion and generally other hadrons with large $p_\perp$. Here a parton may or may not be a quark but is definitely structureless so that the experimental absence of structureless hadrons requires that partons do not appear as free particles in the final state. One may take the attitude either that partons are truely the elementary hadronic constituents and are just difficult to produce directly or that partons are only an intuitively appealing and economical language with which to represent the internal degrees of freedom of a hadron.

In Fig. 2a is illustrated the multiperipheral parton model of Amati, Caneschi and Testa[16] which is distinguished by its assumption of an underlying $\lambda\phi^3$ theory of scalar partons. Explicit scales enter the model via the dimensional coupling constants (λ has units of mass) and lead to N = 8 ($E\, d^3\sigma/dp^3 \propto \lambda^4$) with no constraints on the final

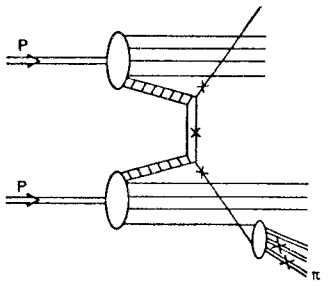

(a) MPModel[16)]

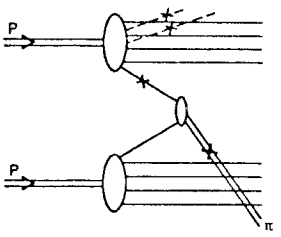

(b) Covariant parton model[17)]

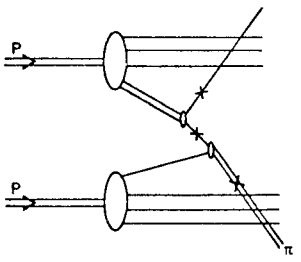

(c) Parton interchange model[18)]

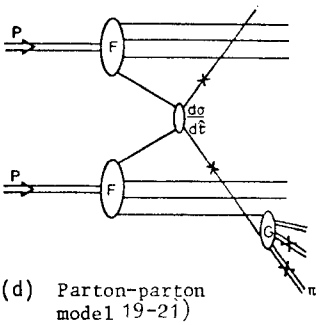

(d) Parton-parton model[19-21)]

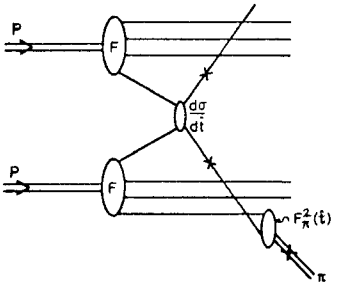

(e) Parton-parton model in the "quasi-exclusive" limit[22)]

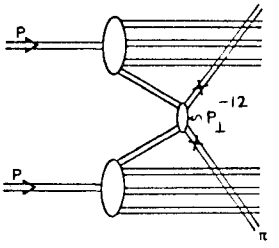

(f) ππ scattering[23)]

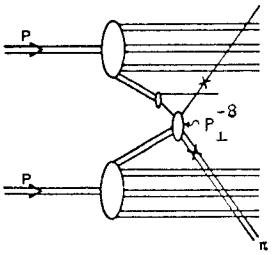

(g) π-parton scattering[23)]

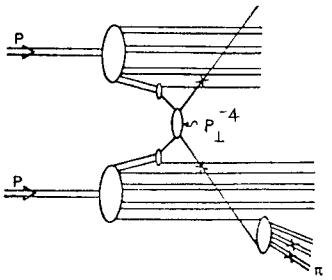

(h) Parton-parton scattering[23)]

Fig. 2 Pictorial representation of various parton hard scattering models for the process p + p → π + X, where the π has large $p_\perp$. The notation is double lines for hadrons, single lines for partons and crosses for particles with large $p_\perp$.

state structure except that the partons must evolve into the observed hadrons in a scale invariant fashion. The "co-variant" parton model of Landshoff and Polkinghorne[17] appears in Fig. 2b. Although the basic model as illustrated is quite general the specific example used for calculations by these authors corresponds to a single pion balancing the large $p_\perp$ of the parton emerging from the upper vertex in the figure. Thus the basic "hard" process is parton + antiparton → 2 mesons and again yields N = 8. The required extra dimensional factors (N=4 is the purely dimensional result) can be traced to the vertices where two partons "fuse" to form a pion and a scale, the size of the pion, naturally appears. These vertices are related to the pion form factor $F_\pi(t)$ and N = 8 arises if $F_\pi(t) \sim 1/t$ for large t. A related picture is the "constituent interchange model" of Brodsky, Blankenbecle and Gunion[18] (BBG) which, like the previous picture, explicitly avoids the notion of parton-parton scattering and instead utilizes the concept of a wave function which represents hadrons in terms of constituents. These constituents have a finite probability to carry large $p_\perp$ and be highly virtual and it is the interchange of such a highly virtual large $p_\perp$ parton which drives the basic "pion" + parton → pion + parton process as illustrated in Fig. 2c. Again the basic process yields only a single pion (or resonance) at large $p_\perp$ (not a full jet) and scales appear in the wave function (vertex) describing this particle. By relating this wave function to the pion form factor with the usual $1/t$ asymptotic behaviour one again finds N = 8. This concept of the production of a single pion (or meson resonance) carrying all of the large $p_\perp$ is illustrated in Fig. 3 and is hereafter labelled as a quasi-exclusive process. In contrast to the naive two-jet picture of the totally inclusive events, other large $p_\perp$ particles appear in the same direction as the trigger particle only when a well defined resonance is produced and subequently decays to yield the observed particle plus a few others.

The original parton-parton scattering picture, first studied by Berman, Bjorken and Kogut[19] (BBK) and later by others[20,21], is illustrated in Fig. 2d. As in the first model discussed, the scattered parton is required to evolve into the observed hadrons at the lower vertex (G). If this process introduces no scale and there is no scale in the basic parton-parton interaction, one finds N = 4 in contradiction with the data. In order to generalize this simple picture, it has been suggested, that one consider the "quasi-exclusive" limit of the parton-parton scattering model[22] as indicated in Fig. 2c. The scattered, large $p_\perp$, parton, presumably in cooperation with an antiparton, evolves into a single pion which carries all of the $p_\perp$. Again this "fusion" vertex is assumed to be related to the pion form factor (explicitly it is taken to behave as $F_\pi^2(t) \sim 1/t^2$ for $|t| \to \infty$). In parton language, the function G(y) ($y = P_\pi/p\text{-parton}$), which describes the process parton → π+X, is taken to have contributions from specific exclusive channels which appear near threshold (y → 1) as shown in Fig. 4 in analogy to the threshold behaviour of the usual structure functions (e.g. νW_2).

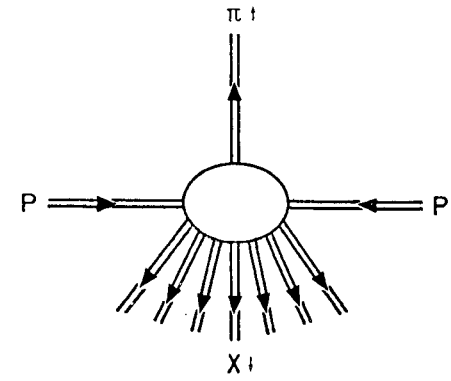

Fig. 3 Pictorial representation of a "quasi-exclusive" process as defined in the text.

These threshold contributions contain scale factors appropriate to the specific exclusive channels and decrease with momentum transfer in a fashion given by the appropriate form factor. Unlike the previous models, the present picture definitely predicts the dominance of a $p_\perp^{-4}$ behaviour at very large s or with different triggering technique. The N = 8 form is thought to dominate at the ISR because at these energies the suppression factor introduced by producing a 5 GeV/c pion directly from a 5 GeV/c parton, namely a factor $p_\perp^{-4}$, has less effect than the suppression introduced by requiring a much larger momentum parton which can yield a "full jet" containing the 5 GeV/c pion plus other hadrons. This explaination is borne out in explicit calculations[22] as long as the scale characterizing the exclusive channel effects is of order 4 GeV.

Similar conclusions are reached by Bardu, Barnett and Silverman [23] (BBS) in a model with three levels of "quasi-exclusiveness). These levels include virtual $\pi\pi \to \pi\pi$ (Fig. 2f with N = 12), virtual π + partons $\to \pi$ + parton (Fig. 2g with N = 8), and finally parton-parton scattering where the partons are from virtual pions (Fig. 2h, N = 4).

A recent entry to the list of large $p_\perp$ models which shares some features with both parton and fireball models, is the application of "massive quark model" to large $p_\perp$ inclusive processes by Preparata[24]. The distinguishing feature of this model is that the problem of free quarks is explicitly removed by putting the quark pole at infinite mass and simultaneously cutting off the quark propagator so that quarks can never be on-shell. The model has no explicit quark-quark interactions nor can the interchange of highly virtual quarks give a sizeable contribution. Only objects with hadronic quantum numbers can have large masses and, as illustrated in Fig. 5, the dominant terms of interest here involve quark-antiquark annihilation into massive fireballs. When the initial fireball decays into two smaller fireballs with large $p_\perp$ (Fig.5a), Preparata finds N = 4 and for the "quasi-exclusive" case with one massive fireball and a single hadron as decay products (Fig. 5b), he finds N = 8. Kinematic constraints at present energies suppress the first term and allow the model to explain the observed N = 8 behaviour at the ISR.

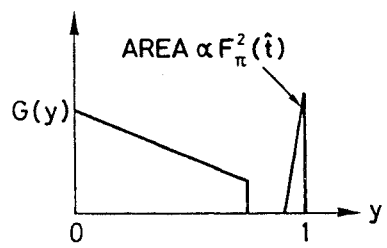

Fig. 4 Pictorial representation of the idealized structure function [22] discussed in the text.

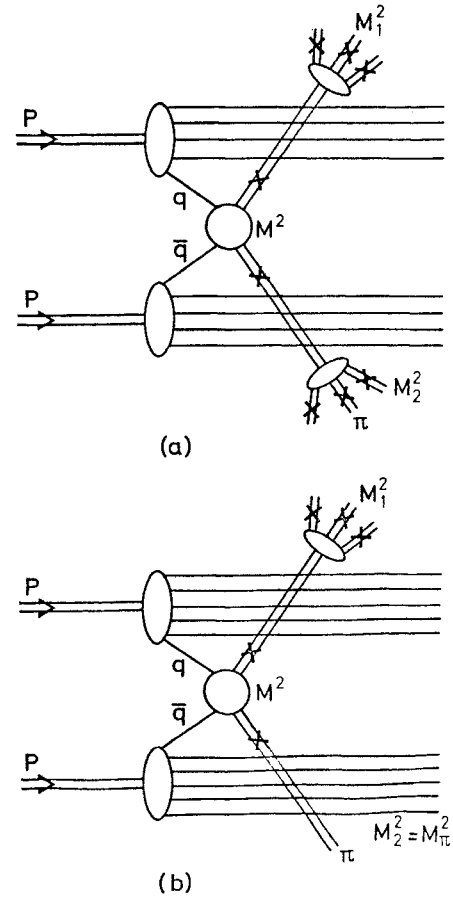

Fig. 5 Pictorial representation of the "massive quark model"[24] for pp $\to \pi$ + x. The notation is the same as Fig. 2. a) $p_\perp^{-4}$ contribution. b) $p_\perp^{-8}$ contribution.

In summary, parton models lead to $p_\perp^{-8}$ behaviour either because the basic parton-parton scattering has this behaviour, as in the first model discussed, or because in the present experiments the observed large $p_\perp$ is produced essentially by itself (quasi-exclusive process). This second feature is common to all of the other models with N = 8 and seems to be in reasonable qualitative agreement with the bulk of the data. The quality of the fit to the single particle data to be achieved in such "quasi-exclusive" models is illustrated in Fig. 6, taken from Ref. 22. The present data[25,26] on associated charged multiplicities indicate little variation with $p_\perp$ of the multiplicity in the same direction as the trigger particle but strong variation in the opposite direction as illustrated in Fig. 7. This would seem to be in good qualitative agreement with those "quasi-exclusive" models where the trigger particle is produced essentially by itself but its momentum is usually balanced by several particles (the remnants of parton decay ?). However, it should be noted that energy momentum conservation may already be sufficient to explain much of this effect[21]. There are also recent data with more complete momentum analysis[26] which indicate the existence of events where two large $p_\perp$ particles appear in the same hemisphere. In the "quasi-exclusive" context these events would arise from resonance production at large $p_\perp$ but as yet there is little evidence for resonance structure in the data. A more optimistic view for partonists is perhaps that these few events correspond to the true parton-parton → two-jet process with p^{-4} behaviour. These questions anxiously await further experimental and theoretical study.

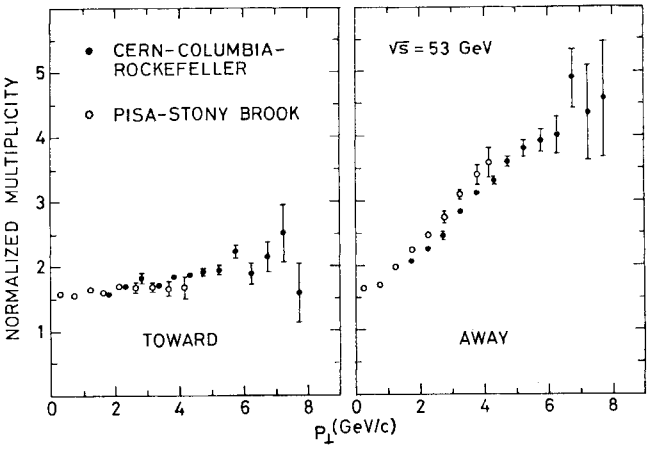

Fig. 7 Partial multiplicities around $\theta_{cm} \approx 90^o$ directly towards ($\phi \sim 0^o$) and away ($\phi \sim 180^o$) from the detected photons (π^o's) as a function of $p_\perp$. These data[25,26] are normalized to average inelastic multiplicities and not to multiplicities at low $p_\perp$.

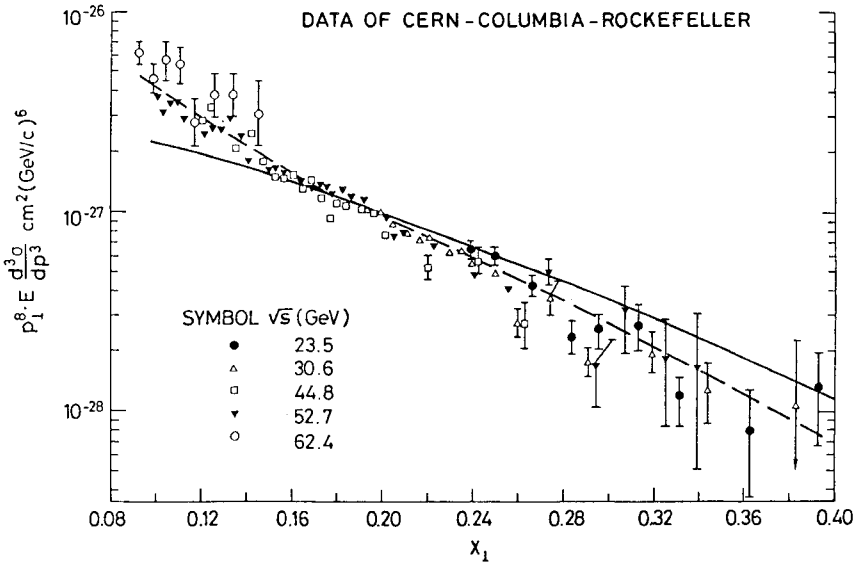

Fig. 6 Fit to the π^o data with the "quasi-exclusive" parton model[22]. The solid curve is for F(x) given by the experimental structure function νW_2 and the dashed curve is for $F(x) \sim (1 - x)^3$.

With respect to the Chicago-Princeton[15] data on nuclear targets at FNAL where N = 11 is suggested for $X_\perp >_o 4$, a description has been attempted within the context of the constituent interchange model.[27] Both a $(p_\perp{}^2 + m^2)^{-6}$ term with baryon production and the usual $(p_\perp{}^2 + m^2)^{-4}$ term are included and a reasonable description of the pion production data at both FNAL and the ISR is obtained. Another explanation has been given by Amati and Caneschi[28] utilizing the strong angular dependence in their multiperipheral parton model. Since these data are taken at fixed θ_{LAB}, θ_{cm} varies with s. However, θ_{cm} has already passed through 90^o at the highest energy (400 GeV/c) and the general consistency of the latest data with the lower energy data argues against such an explaination. Although it is perhaps premature to be comparing directly nuclear target and hydrogen target data, this sort of effort is certainly interesting, particularly if the observed particle ratios can also be understood.

Parton ideas have also proved useful in the study of exclusive processes in the limit of fixed angle as $s \to \infty$. With similar assumptions to those discussed above the usual parton model prediction is that in this limit the exclusive cross section should behave as

$$\frac{d\sigma}{dt} \sim s^{-n} f(\theta) \qquad (6)$$

Of course specific models make predictions for the value of the exponent n. An easy way to remember the results of many of the models is the so called "counting rule" suggested by Brodsky and Farrar[29] and Matveev, Musadyan and Tavkhelidze[30]. The rule states that n is given by the sum of the number of elementary constituents (quarks) present in the participating hadrons minus two. This yields, for example, $n_{NN} = 10$, $n_{N\pi} = 8$ and $n_{\pi\pi} = 6$. This rule was motivated by a study of certain limited sets of Feynman graphs and raised the hope that the asymptotic fixed angle behaviour of hadronic amplitudes might be determined by singularities arising from the short distance behaviour of some underlying field theory. Doubt has been cast in this conjecture, however, by the papers of Landshoff[31] and Ezawa[32] which point out the presence of other singularities in these amplitudes which are not related to the short distance behaviour of the fields and give behaviour violating the counting rule. Although the theoretical situation is therefore unclear, the basic form, Eq. 6, and the counting rule both seem to be satisfactory phenomenologically. Recent papers which discuss exclusive reactions and give specific forms also for $f(\theta)$ in Eq. 6 include those by Matveev, Musadyan and Tavkhelidze[33], Freund and Naudi,[34] Gunion,[35] and Preparata[36]. The constituent interchange model has also been used to study the transition from fixed angle behaviour to fixed t, Regge, behaviour.[37] Various other parton-motivated models have also been proposed[38,39] to describe both inclusive and exclusive data over the full kinematic region, including both large and small $p_\perp$. These last models tend to give different large $p_\perp$ results from those discussed earlier and high energy, fixed angle exclusive data should prove most informative.

Other aspects of various parton models have also been studied. For example Combridge[40] emphasises the interest of doing inclusive reactions with meson beams since the differences from the proton case, especially the anticipated asymmetry in θ, should yield important information. In another study, Scott[41] points out the important role of "leading particle" effects in the transition region between inclusive and exclusive processes at the edge of phase space.

A specific model field theory with fermion quarks

and scalar gluons has been studied by Efremov[42] using the assumption of short distance scale invariance and also utilizing certain rules for treating on-shell amplitudes which have been suggested from studies of Feynman diagrams. The results are of a specific nature and, hence, quite interesting. For example, it is predicted that $\pi\pi$, πN and NN will all exhibit the same s^{-10} behaviour for $s \to \infty$, θ fixed which is different from the results of the other models discussed above and seems also to be inconsistant with present data.

Overall, the application of simple parton concepts to large $p_\perp$ phenomena has been quite successful. However, the models have tended to become quite complex compared to the original naive picture and the development of more well defined theoretical guide lines, arising perhaps from the study of field theory, bag models, etc) is of extreme importance. Likewise the study of the complete event structure in such models will be very informative as is illustrated in the next section.

4. Particle Composition and Correlations

In the following brief discussion of particle composition and correlations the emphasis is on those features of the data which may serve to differentiate between the fireball and hard scattering pictures. Some characteristics of specific parton models are also described.

The question of particle composition has not yet been systematically studied in fireball models. However, on quite general grounds one may expect that for transverse momentum much larger there the particle masses, so that kinematic mass effects are no longer important,[43] fireball models will predict little variation with $p_\perp$ of the particle ratios. In particular one would expect particle/antiparticle ratios to be relatively $p_\perp$ independent at large $p_\perp$. This behaviour is to be contrasted to that in parton-quark models where the valance quarks play an increasingly dominant role as $x_\perp = 2p_\perp/\sqrt{s}$ increases and the particle ratios vary accordingly. In particular for proton-proton reactions one expects an increasing dominance of positive charge, nonnegative strangeness mesons for increasing $x_\perp$. The structure observed in both the British-Scandinavian[44] and the Chicago-Princeton[15] data seems to argue for the quark picture. However, the absence of scaling in the variable $x_\perp$, observed by the second group, is a serious problem. Further study is definitely needed. Finally, it is interesting to note that quark-parton models predict[21] that in events where a large $p_\perp$ π^+ is observed in one direction the most likely large $p_\perp$ particle in the other direction, for proton-proton reactions, is again a π^+. This is quite different from the $\pi^+ - \pi^-$ correlation observed at low $p_\perp$.

From the standpoint of correlations, the basic difference between fireball and hard scattering models arises from the expected event "shape". Fireballs which yield large $p_\perp$ particles are naively expected to give an isotropic secondary distribution in the fireball rest frame, except for the constraints of momentum conservation. Hard scattering models are expected to instead yield a definitely coplanar structure with only weak $p_\perp$ correlations for particles out of the plane defined by the beam and the large $p_\perp$ particle. Therefore one might expect that measurements of the average momentum and average multiplicity of other secondaries normal to the scattering plane in large $p_\perp$ events would be particularly informative. The observation of an appreciable increase in either quantity with increasing $p_\perp$ at fixed s or with s at fixed $p_\perp$ would suggest the presence of massive

fireballs, whereas no observed variation would indicate a scattering picture. Unfortunately it is also necessary to consider the following caveats. First, except in the case of single fireballs with $M = \sqrt{s}$, the process responsible for the large $p_\perp$ particle is not the only physics present. The hadronic matter not participating directly in the large $p_\perp$ process presumably also interacts to produce particles and is coupled to the primary process at least by energy momentum conservation. This will tend to produce more complicated correlations than in the naive expectations. Also in the limit of small fireball masses energy-momentum conservation will strongly influence the decay structure and distort the naive expectation. Clearly then, only a large increase in the multiplicity or average momentum normal to the large $p_\perp$ scattering plane will give an unambiguous answer, i.e. massive fireballs are present. Less dramatic effects require more careful studies in order to be correctly interpreted. The structure of the present multiplicity data from the Pisa-Stony Brook experiment[25] is shown in Fig. 8. The absence of strong variation near $\phi = 90^o$ in Fig. 86 would seem to argue against very massive fireballs. It will be interesting to see what else can be learned from such data by more detailed analyses. The measurement of the correlation between $p_\perp$ and the charged multiplicity toward and away from the large $p_\perp$ particle is shown in Fig. 7 and was discussed above as evidence for the quasi-exclusive" explaination of $p_\perp^{-8}$ behaviour in

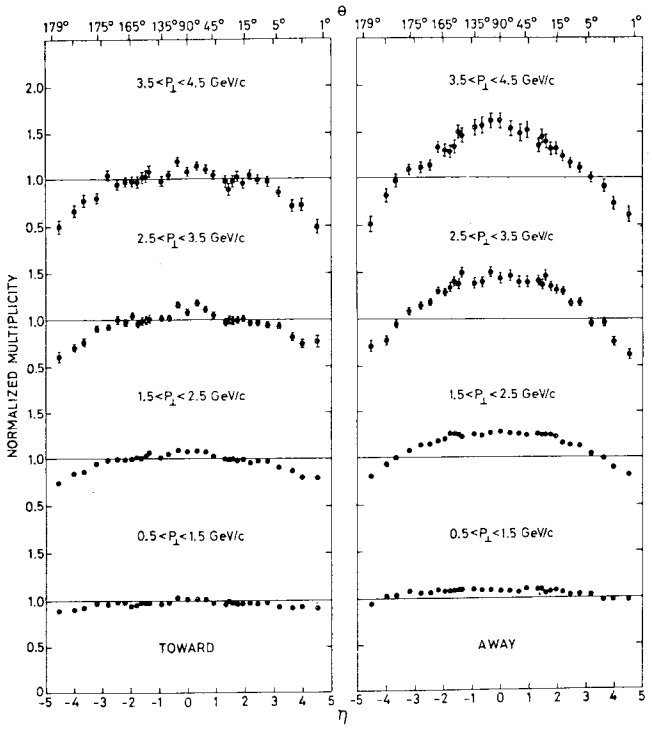

a) Multiplicities in the two 180^o azimuthal intervals towards and away from the detected photons as a function of $\eta = -\ln |\tan \theta/2|$.

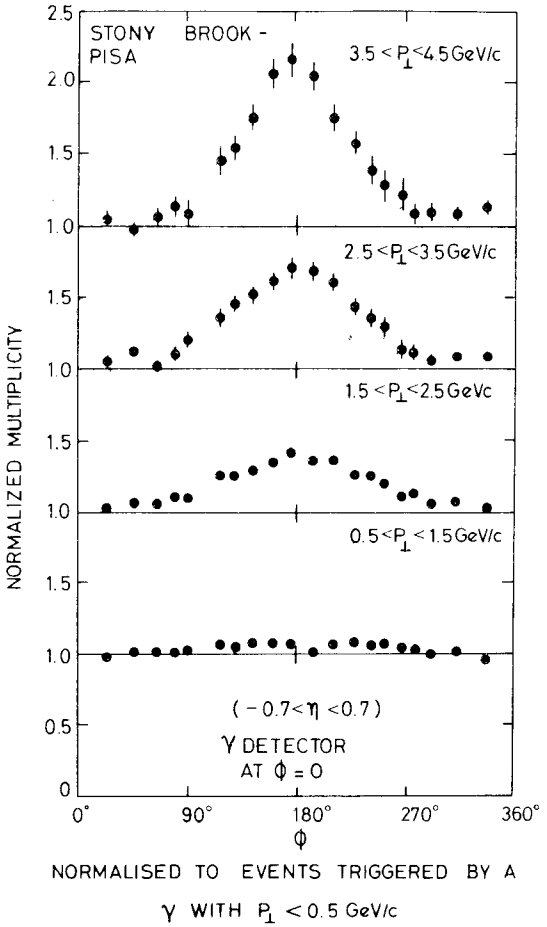

b) Multiplicities in the interval $-0.7 < \eta < 0.7$ as a function of the azimuthal angle measured from the photon detector.

Fig. 8 Data on partial charged multiplicities from the Pisa-Stony-Brook group at the ISR[25] for various $p_\perp$'s of the photon always normalized to the low $p_\perp$ bin.

parton models.

Another interesting question is how correlations vary as a function of the c.m. angle of the large $p_\perp$ particle. For example, in hard scattering models one naively expects a back-to-back configuration, whereas for relatively low mass fireballs one might expect $p_\perp$ to be balanced locally in rapidity (that is at the same $\theta_{c.m.}$ but 180^o away in ϕ). To actually utilize the data on these questions now becoming available[45,46] detailed calculations are, of course, required. As an example of what may be learned from such studies, Figs. 9-10 illustrate the results of calculations[47] in a few simple parton models (all with $p_\perp^{-8}$ behaviour). The models include a quasi-exclusive parton-parton scattering model[22] (QEPP), a simple BBG model[18] with $\frac{d\sigma}{d\hat{t}}\Big|_{\pi q} \propto (1/\hat{s}^4 + 1/\hat{s}^2\,\hat{u}^2)$[48] ($\hat{s}$, $\hat{t}$, and $\hat{u}$ refer to the variables in the quark scattering process), and a model of the BBS type[23] with $\frac{d\sigma}{d\hat{t}}\Big|_{\pi q} \propto 1/\hat{t}^4$. Hence the first and last models have essentially the same behaviour ($1/\hat{t}^4$) in the basic scattering process but differ in the constituents involved and their distributions (see Fig. 2 d and g). The QEPP model involves only parton distributions ($F_q \propto (1-x)^3$ was used) whereas the BBS model involves also a virtual pion distribution ($F_\pi \propto (1-x)^5$ was taken). The second and third models have the same constituent distributions but a different scattering structure. The models are all normalized at $\theta = 90^o$ and $x_\perp = 0.2$. The single particle distribution as a function of θ and $x_\perp$ is shown in Fig. 9 and indicates that the QEPP model so somewhat less θ dependent at fixed $x_\perp$. This difference arises from the more rapidly cut off constituent (virtual pion) distributions present in the other models.

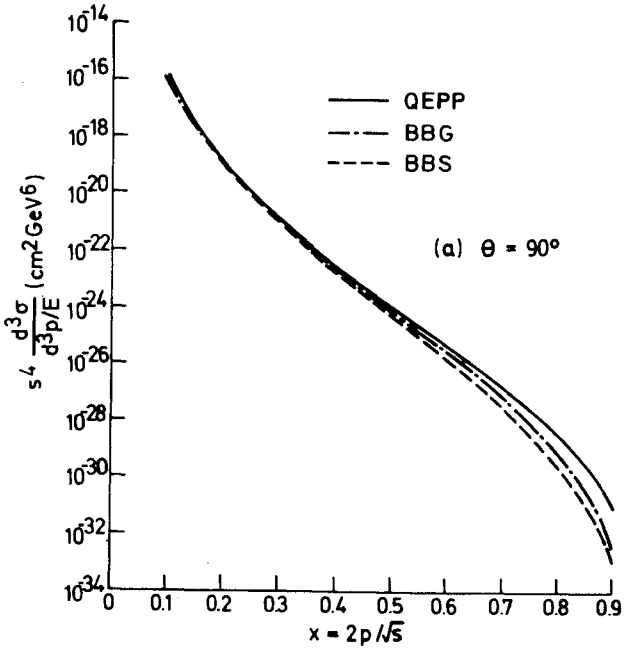

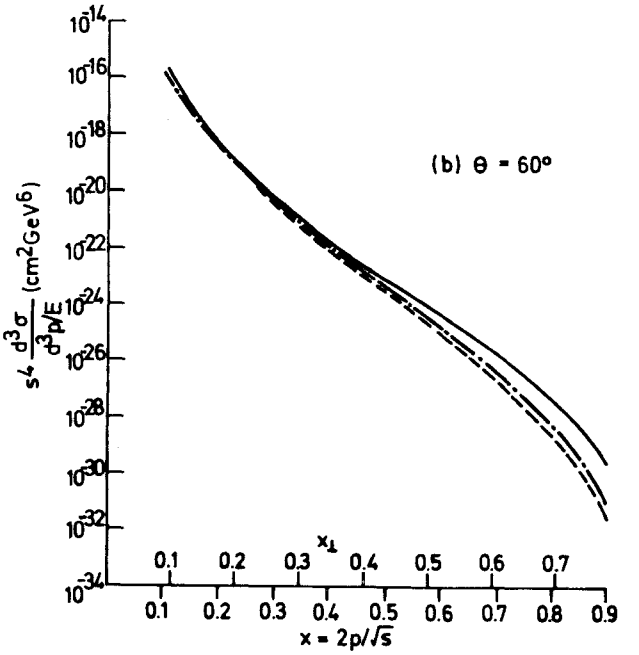

Calculations of the one pion - one parton (jet) cross-section are shown in Fig. 10. The cross-section

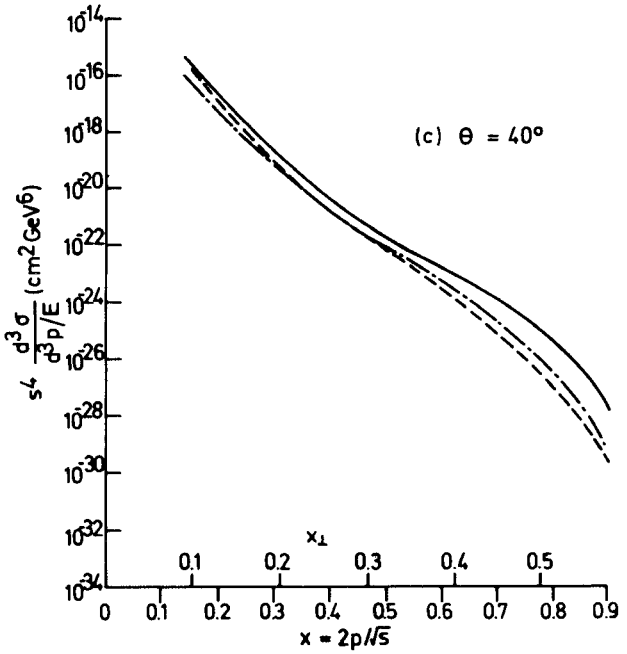

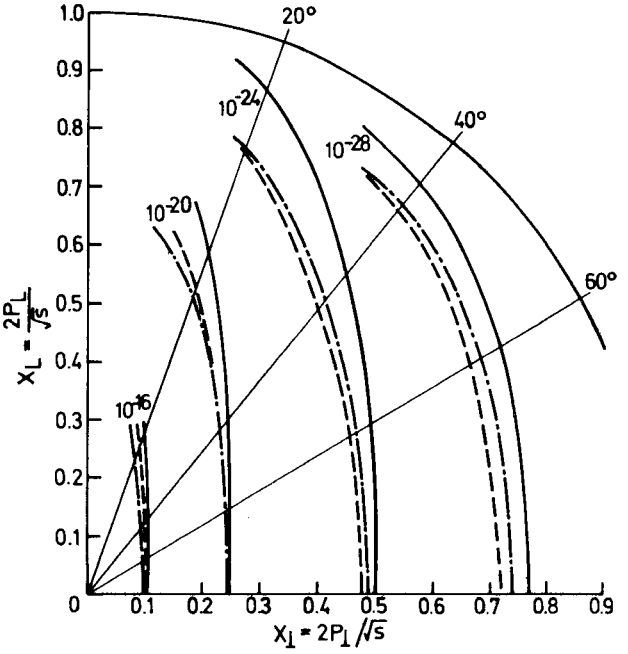

e) Topological plot of fixed values of the cross-sections in the $x_\perp$ - x_L plane.

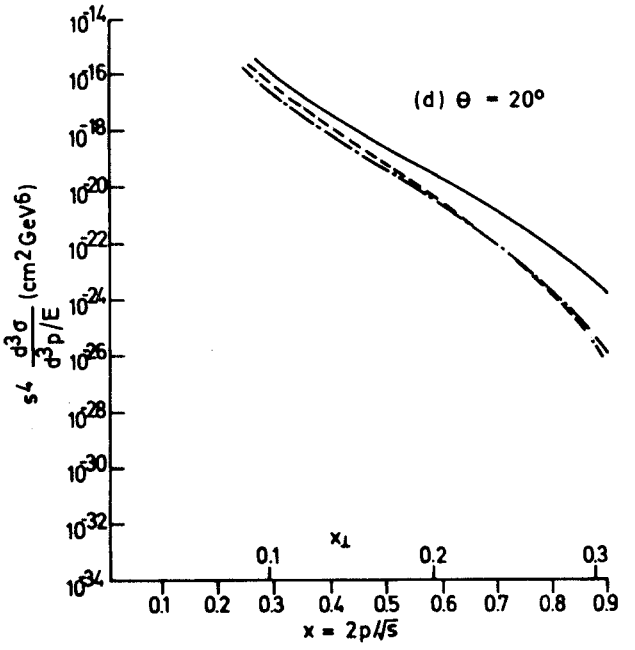

Fig. 9 Model calculations of the single-particle cross-section times s^4 versus $x_\perp$ at various values of θ. The three curves correspond to simple models of the "quasi-exclusive" parton-parton type[22] (solid curve), the BBG type[18] with $d\sigma/d\hat{t}|_{\pi q} \propto 1/\hat{s}^2\hat{u}^2 + 1/\hat{s}^4$ (dot-dash), and the BBS type[23] with $d\sigma/d\hat{t}|_{\pi q} \propto 1/\hat{t}^4$ (dashed). The calculations are all normalized to give the same value at x = 0.2, θ = 90°.

is plotted versus $\eta_{jet} = \ln(\tan\theta_{jet}/2)$, where θ_{jet} is measured from the same axis as θ_π but is 180° away in ϕ, for various values of θ_π with $x_{\perp\pi} = 0.2$. The intent is to study where in η the large $p_\perp$ of the pion is balanced, i.e. what is the η of the scattered parton. For questions of particle multiplicity alone one must smear the jet distribution by the average jet width ($\Delta\eta\sim1$) so that the two hump structure of the QEPP and BBS models is presumably washed out. Hence one expects a flat, broad multiplicity distribution in these models in contrast to the more peaked distribution of the BBG model studied here. Such a broad distribution is, in fact, in quite good agreement with the data of Fig. 8a. The real question is

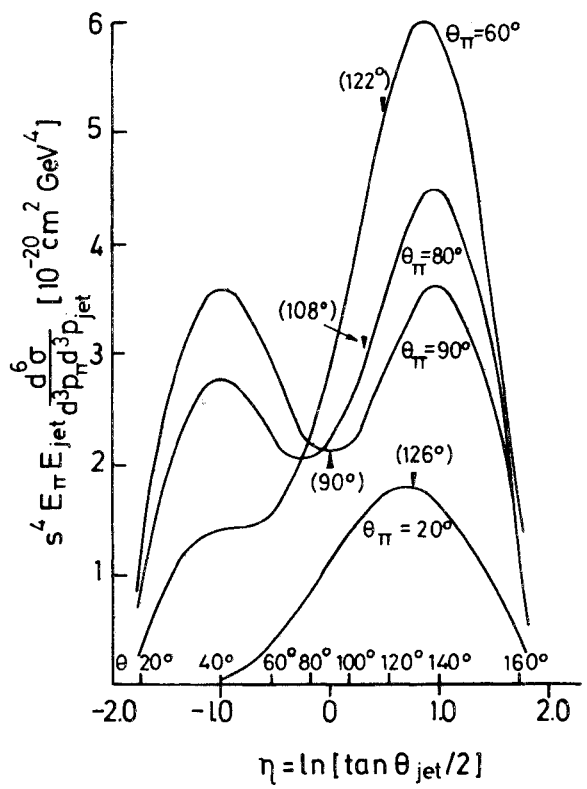

a) Simple quasi-exclusive parton-parton model[22].

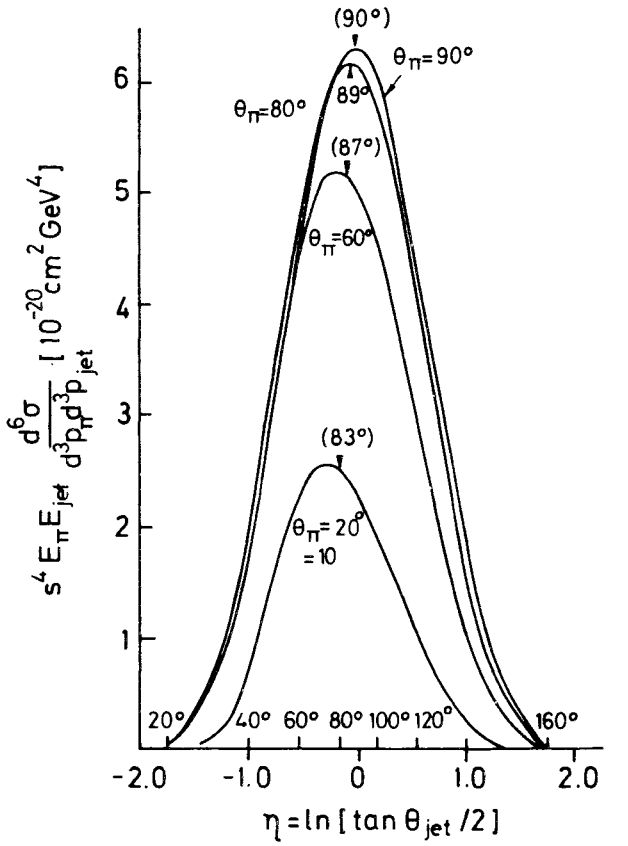

b) Simple BBG model[18] with $d\sigma/d\hat{t}|_{\pi q} \propto 1/\hat{s}^2\hat{u}^2 + 1/\hat{s}^4$.

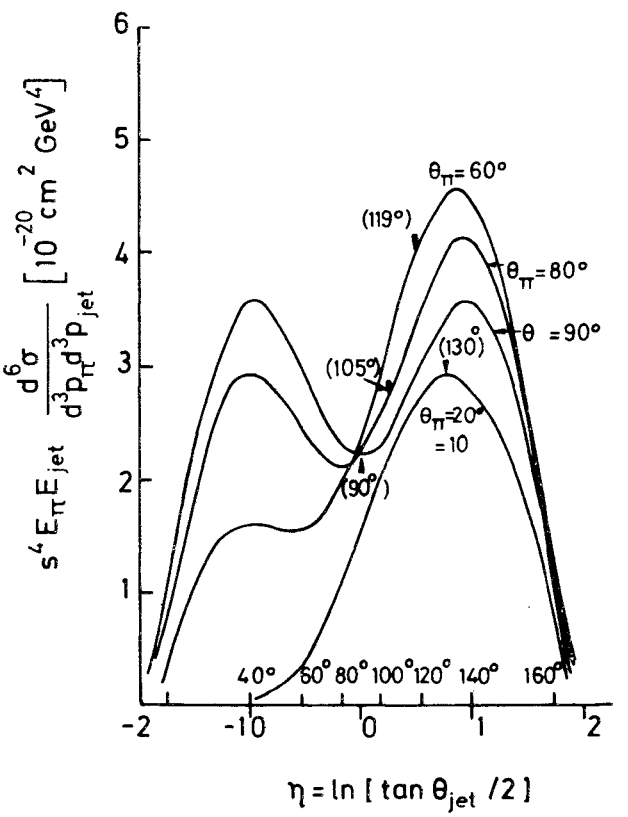

c) Simple BBS model[23] with $d\sigma/d\hat{t}|_{\pi q} \propto 1/\hat{t}^4$.

Fig. 10 Model calculations of the one particle-one jet double cross-section $s^4 E_\pi E_{jet}(d^6\sigma/d^3p_\pi d^3p_{jet})$ for various values of $\theta\pi$ as a function of $\eta = \ln\tan\theta_{jet}/2$ (θ_{jet} and θ_π measured from the same direction but 180° away in ϕ) with $x_\perp = 0.2$. The centre of gravity of each distribution is marked with a tick. The normalization is the same as in Fig. 9.

where the centre of gravity of the distributions (marked with a tick) move as θ_π is varied. In the first and third models the jet moves into the hemisphere opposite the π (approximate back-to-back behaviour) as naively expected. The relatively small magnitude of the effect is also not inconsistent with data[45,46]. Surprisingly the BBG correlation peak stays near 90^o with a slight tendancy to move to smaller θ (anti-back-to-back behaviour). The explanation for this is presumably the combination of the weak angular dependence of the assumed scattering process and the fact that the parton-pion c.m. system tends to be moving in the direction of the initial parton which carries higher momentum on average. If both particles appear near 90^o in their c.m. system then the motion of that system puts them in the same hemisphere of the overall c.m. system. A stronger angular dependence such as $\frac{1}{\hat{u}^4}$ [49] for the π-g process leads to results very similar to the other models. In any case such measurements are clearly useful for testing specific models.

5. Other Models

Besides the models discussed above, several other, generally novel, explanations of large $p_\perp$ phenomena have also been suggested. One formalism which seeks to explain the enhanced multiplicities observed in large $p_\perp$ events is the Bremsstrahlung of neutral vector mesons which is discussed by several authors.[50] The general picture is that for low momentum transfers some sort of multiperipheral mechanism is operative whereas at large $p_\perp$ Bremsstrahlung effects become important and lead to both power behaviour in $p_\perp$ and rising multiplicities. This picture also offers an explanation of the observed increase in multiplicity for increasing momentum transfer at fixed missing mass in the process $pp \to pX$.[51] A somewhat different Bremsstrahlung picture has also been studied by Choudhury[52] to explain this same data.

An extremely novel idea is the suggestion of Sen[53] that the observed properties of using σ_{TOT}, scaling in deep inelastic ep, and activity at large $p_\perp$ are all manifestations of a large transition in the hadronic matter. He suggests that this situation may then be studied in terms of an effective field theory wherein the use of perturbation theory is justified. Such a formalism might then allow, for example, the derivation of the counting rule discussed above. Another interesting idea is proposed by Teper[54] who attempts to set a lower bound on large $p_\perp$ inclusive amplitudes by using elastic unitarity to relate these amplitudes to the elastic amplitude at large t. The resulting analysis has strong model dependences but it is an interesting approach. This same author[55] has also suggested a model for large $p_\perp$ phenomena which kinematically looks almost identical to the BBS model[23] of Fig. 2f-h. However, in this case the central π-π dynamics is not to be taken from a parton model but rather from actual experiment which is here assumed to exhibit simple power behaviour. In this way Teper attempts to describe large $p_\perp$ events without introducing partons. In particular he finds a simple qualitative explanation of the observed particle ratios.

Finally D C Carey, et al[56] suggest that the empirical form

$$E^o \frac{d^3\sigma^i}{d^3p} \sim g(p_\perp)\, f^i(x_R) \qquad (7)$$

where $x_R = \frac{2|\vec{P}|}{\sqrt{s}}$, offers a good description of a large portion of the present large $p_\perp$ data over a wide range in s, $p_\perp$ and θ. The function $g(p_\perp)$ has the universal form $(p_\perp^2 + .86)^{-4.5}$ and $f^i(x_R)$ behaves as $(1-x_R)^{n_i}$ where n_i depends on the produced particle. Although this formula does not

fit well, the data of the CCR experiment[14], its simplicity and the apparent factorization are certainly interesting empirical features.

6. Summary

There is, as yet, no truly compelling single theoretical interpretation of large p_t phenomena. Models which itilize the notion of partons have been the most carefully studied and are generally consistent with the present data. However, other models, in particular fireball models, have also succeeded in explaining some of the features of the data. Clarification of the situation will require progress on at least two fronts. First, the specific models must be interrogated more fully in order to utilize the more detailed data now becoming available. For example, are the latest correlation measurements a problem for parton models? Are the particle ratios a serious threat to fireballs? At the same time, as the models mature and become more complex, it is imperative that one attempt to develop a foundation in more fundamental ideas in order to better motivate and simultaneously control the development of the models. There are also experimental questions of singular importance. For example, is a single power law behaviour adequate also at larger $p_\perp$'s at the energies of the ISR? Can the canonical two-jet $p_\perp^{-4}$ behaviour be found at larger energies or by means of more novel detection techniques? Clearly this field will remain interesting for some time to come.

Acknowledgements

The author gratefully acknowledges many helpful discussions with his colleagues at CERN. Special recognition goes to the session organiser, L Lederman, and the scientific secretaries, L Carroll and M B Green, for their assistance.

References

1. For other recent reviews of this topic see: S D Ellis, R Thun, IX[e] Rencontre de Moriond, 1974, CERN preprint TH 1874 (1974); S D Ellis, V[th] International Symposium on Many Particle Hadrodynamics, Eisenach-Leipzig, 1974, R Savit, preprint SLAC-PUB-1324 (1973); S V Brodsky, preprint SLAC-PUB-1329 (1973).

2. As an example of an alternate picture which has not been studied in detail in the present context but is in qualitative agreement with the data, see J Benecke, T T Chou, C N Yang, E Yen., Phys. Rev. 188, 2159 (1969).

3. For further discussions of this and related topics see also the reports of P V Landshoff and J F Gunion in these proceedings.

4. See for example: J Engels, K Schilling, H Satz, Nuovo Cim. 17A, 535 (1973).

5. E Fermi, Progr. Theor. Phys. 5, 570 (1950); Phys. Rev. 81, 683 (1951).

6. Meng Ta-Cheng, Freie Universitat,Berlin preprint FUB HEP 74/2 (1974).

7. L Heiko, Universite Catholique de Louvain preprint (1974), paper 158.

8. S Pokorski, L Van Hove, Nucl. Phys. B60, 379 (1973).

9. S Pokorski, L Van Hove, CERN preprint TH 1772 (1973) [to be published in Acta Phys. Polon B].

10. G Ranft, J Ranft, CERN preprint TH 1838 (1974); E L Berger, CERN preprint TH 1816 (1974).

11. S Sakai, Tokyo University preprint TUETP-73-6 (1973).

12. A Bouquet, University of Paris, Thesis; (1974); A Bouquet, V Letessia, A Tounsi, preprint PAR-LPTHE 74/1, IPNO 74-20 (1974).

13. For the present experimental situation see the report of F J Gilman in these proceedings.

14. F W Büsser, et al., Phys. Lett. 46B, 471 (1973).

15. J W Cronin, et al., Phys. Rev. Lett 31, 1426 (1973); see also EFI preprint, University of Chicago (1974), Production of Hadrons at Large Transverse Momentum at 200 , 300 and 400 GeV, paper 357.

16. D Amati, L Caneschi, M Testa., Phys. Lett. 43B, 186 (1973); and CERN preprint TH 1644 (1973).

17. P V Landshoff, J C Polkinghorne., Phys. Rev. D8, 4159 (1973); Phys. Lett. 45B, 361 (1973); and preprint DAMTP 73/31; Phys. Rev. D8, 927 (1973)

18. R Blankenbecler, S V Brodsky, J F Gunion., Phys. Rev. D6, 2652 (1972); Phys. Lett. 42B, 461 (1973); Phys. Lett. 39B, 649 (1972); Phys. Rev. D8, 287 (1973).

19. S M Berman, J D Bjorken, J Kogut, Phys. Rev. D4, 3388 (1971); J D Bjorken., Phys. Rev. D8,4098 (1973).

20. D Cline, F Halzen, H Waldrop., Nucl Phys. B55, 157 (1973).

21. S D Ellis, M B Kislinger., Phys. Rev. D9, 2027 (1974).

22. S D Ellis., Phys. Lett. 49B, 189 (1974).

23. M Bander, R M Barnett, D Silverman., Phys. Lett. 48B, 243 (1974).

24. G Preparata, CERN preprint TH 1859 (1974).

25. F Finocchiaro, et al., CERN preprint (1974), Measurement of Charged particle multiplicities associated with large transverse momentum photons in proton-proton collisions, paper 988; R Kephart, et al, CERN preprint (1974), s-dependence of charged particle multiplicities associated with large transverse momentum photons at the ISR, paper 989.

26. F W Büsser et al., CERN preprint (1974), Correlations between Large Transverse Momentum π^o mesons and Charge Particles or π^o mesons at the CERN ISR, paper 728.

27. R Blankenbecler, preprint SLAC-PUB-1438 (1974); talk presented at the IXth Balaton Symposium on Particle Physic, Hungary (1974).

28. D Amati, L Canuschi, CERN preprint TH 1854 (1974).

29. S Brodsky, G Farrar., Phys. Rev. Lett. 31, 1153 (1973).

30. V Matveev, R Muradyan, A Tavkhildze., Lett Nuovo Cim. 7, 719 (1973).

31. P V Landshoff, preprint DAMTP 73/36 (1973), (to be published in Phys. Rev.).

32. Z F Ezawa, preprint DAMTP 74/5 (1974), paper 120, (to be published in Nuovo Cim.).

33. V Matveev, R Muradyan, A Tavkhelidze, Joint Institute for Nuclear Research Report No. EZ-8048 (1974), paper 1101.

34. P G O Freund, S Nandi, University of Chicago preprint EFl 74/33 (1974), paper 833.

35. J F Gunion, University of Pittsburgh preprint PITT-126 (1974), paper 717.

36. G Preparata , CERN preprint TH-1836 (1974).

37. R Blankenbecler, S J Brodsky, J F Gunion, R Savit, SLAC-PUB-1294 (1973).

38. Y Igarashi, T Nishitani, Nagoya preprint (1974), paper 69; Y Igarashi, T Matsuoka, S Sawada, Nagoya preprint (1974), Paper 70; K. Awaya, S. Sawada, Nagoya preprint (1974), paper 71; Y Igarashi, T Matsuoka, S Sawada, Nagoya preprint (1974), paper 72.

39. K Kinoshita, Y Myozyo, Kyushu University preprint (1974), paper 113; K Kinoshita, H Noda, Kyushu University preprint KYUSHU-74-HE-7 (1974), paper 126; K Kinoshita, Y Kinoshita, Y Myozo, H Noda, Kyushu University preprint KYUSHU-74-HE-11 (1974), paper 125.

40. B L Combridge, University of Cambridge preprint (1974), paper 508.

41. D M Scott, preprint DAMTP 73/37 (1973), paper 250.

42. A V Efremov, Joint Institute for Nuclear Research preprint (1974), paper 674.

43. On quite general grounds one expects the relative proportion of heavy particles to increase with $p_\perp$ at small $p_\perp$ simply because kinematic mass effects are becoming less important.

44. B Alper, et al., CERN preprint (1974), High Transverse Momentum Charged Particle Production in Proton-Proton Collisions at the CERN-ISR,paper 834.

45. G Finocchiaro et al., CERN preprint (1974), Charged particle multiplicities associated with large transverse momentum photons at the ISR, paper 990.

46. B Betev, et al., CERN preprint (1974), Observation of proton-proton interactions with π^o of large transverse momentum at the ISR, paper 590.

47. S D Ellis, in the proceedings of the Vth International Symposium on Many Particle Hadrodynamics, Eisenach-Leipzig, 1974. See also the report of J F Gunion in these proceedings.

48. For a discussion of this form of $\frac{d\sigma}{dt}\Big|_{\pi q}$ see the last paper in Ref. 1. It is straighforward to get this result from the picture in Fig. 2c if the spin of the parton is ignored.

49. This form for $\frac{d\sigma}{dt}\Big|_{\pi q}$ is suggested by R Blankenbecler, IX^{e} Rencontre de Moriond, 1974. Still another form is discussed by J F Gunion elsewhere in these proceedings where calculations similar to those given here are presented.

50. H M Fried, Brown University preprint (1974), paper 35; A P Contogouris, J P Holden, E N Argyres, McGill University preprint (1974), paper 570.

51. A Ramanauskos, et al., Phys. Rev. Lett. 31, 1371 (1973).

52. S Rai Choudhury, preprint (1974), paper 482.

53. S Sen, Trinity College preprint (1974), paper 248.

54. M Teper, Westfield College preprint (1974), paper 298.

55. M Teper, Westfield College preprint (1974), paper 299.

56. D C Carey, et al., preprint NAL-PUB-74/49-THY/EXP (1974), paper 746.

THE OBSERVATION OF LEPTONS OF LARGE TRANSVERSE MOMENTUM

I. CERN-COLUMBIA-ROCKEFELLER-SACLAY COLLABORATION

Presented by S L Segler

Rockefeller University

A search for electrons of large transverse momentum emitted from proton-proton collisions has been performed at the CERN ISR at a centre of mass energy $\sqrt{s}$ = 52.7 GeV. Electrons are momentum analysed by a magnetic spectrometer and identified by a Cerenkov counter located inside the spectrometer (Fig. 1). A lead glass array [1,2] placed behind the spectrometer provides further electron identification and energy measurement. The apparatus is located at 90° with respect to the centre line of the incoming beam directions, the centre of mass motion being towards the detector (effective solid angle of .133 str).

An electronic trigger selected events which satisfied the following requirements: i) a coincidence between hodoscopes H_1', H_2', and H_3' indicating a charged particle transversing the magnetic field and incident on the lead glass; ii) a pulse from at least one of the eight cells of the gas Cerenkov counter, which had a threshold for charged pions of about 5.6 GeV/c and iii) an energy deposition in the lead glass array of at least 1.6 GeV.

Backgrounds that could have contributed to the events of interest consisted of: i) electrons from Dalitz decay of the π^o; ii) γ-ray conversion in the beam pipe, first spark chamber, or in the H_1', hodoscope; and iii) charged pions which somehow set the appropriate gas Cerenkov counter cell and interacted in the lead glass so as to deposit almost all of their energy.

Various cuts were applied off-line in order to reduce the backgrounds described above while at the same time maintaining good efficiency for events of interest. These requirements were: i) the energy distribution in the lead glass array was consistent with that expected for a real electron; ii) the charged particle had given a pulse height in H_1' corresponding to between 0.7 and 1.5 times minimum ionization and gave a spark in the first spark chamber in both x and y; iii) the momentum of the track and the energy deposited in the glass array must have agreed to within ± 30%. These

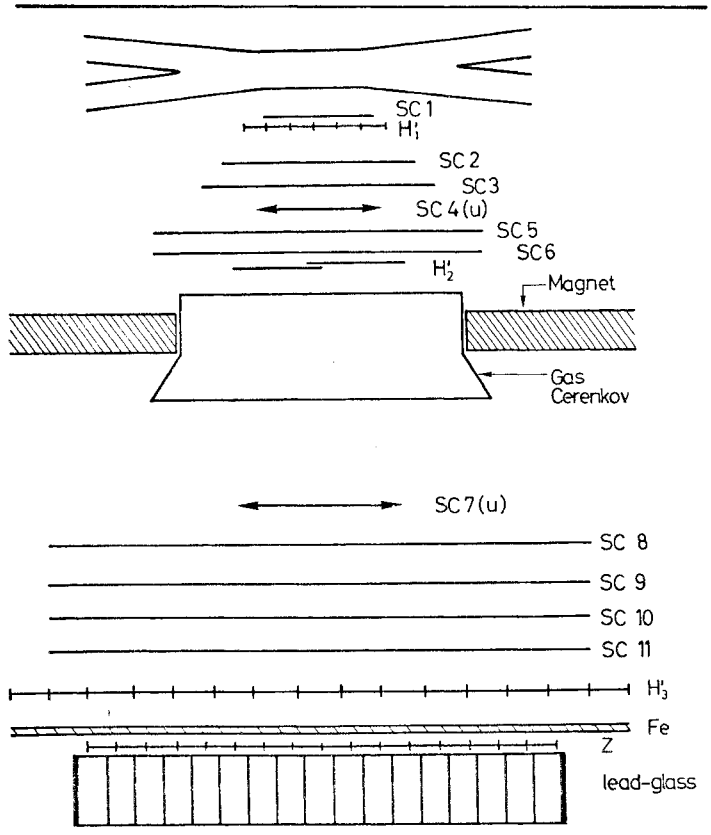

Fig. 1 Schematic diagram of the apparatus.

requirements resulted in an overall efficiency for single electrons of about 56%.

Dalitz decays and γ-ray conversions were suppressed by the requirement of single ionization in the H_1' counters. An experimental check was carried out to measure this background. Conversions were increased by inserting additional conversion material and extrapolating to zero thickness. The result is shown in Figure 2. The slope of the three points is seen to be very flat and, within errors, almost consistent with no change in the cross section at all. On the other hand, also plotted is the result obtained when two particles are required in the H_1' hodoscope. The steep slope obtained is what one would expect if all of the events were due to conversions. The contribution of this background was found to be 6.0 ± 4.0%. In addition, conversions in H_1' coupled with a random spark overlapping the track in the front chamber was empirically found to be .7±.2%.

A Monte Carlo computer programme was used to calculate the background contribution due to π^o-Dalitz decays. This programme was checked by comparing the prediction for conversions in the beam pipe with the event rates shown in Figure 2. The calculations agreed with the normalization error of the π^o spectrum used [2]. The background due to Dalitz decays was 5.6 ± 0.8%.

Charged pions were rejected by the combined requirement of a Cerenkov signal and equality of the magnetic and lead glass measurements. In addition, requiring that the particle shower in the iron before the Z hodoscope resulted in a reduction of $\pi^\pm$ relative to $e^\pm$ of a factor of 2.4. By comparing the cross section with and without this requirement, it was found that the cross section after correction was reduced only by 14 ± 2%. This corresponds to an upper limit on $\pi^\pm$ background of 20%.

The corrected electron spectrum corresponding to electrons of either charge divided by 2 is given in Figure 3. Within statistical errors, the numbers of positive and negative particles are equal. For comparison, the inclusive π^o spectrum for $\sqrt{s}$ = 52.7 GeV obtained from CCR [2] is also given. The electron spectrum is parallel within errors to the π^o spectrum and at a level of 1.3×10^{-4} relative to it. Due to different normalizations obtained by various groups at the CERN ISR for $\pi^\pm$ and π^o inclusive cross section measurements, this ratio could be in error by no more than a factor of 2.

A study was made of the vertical distribution of tracks at the interaction diamond for both charged

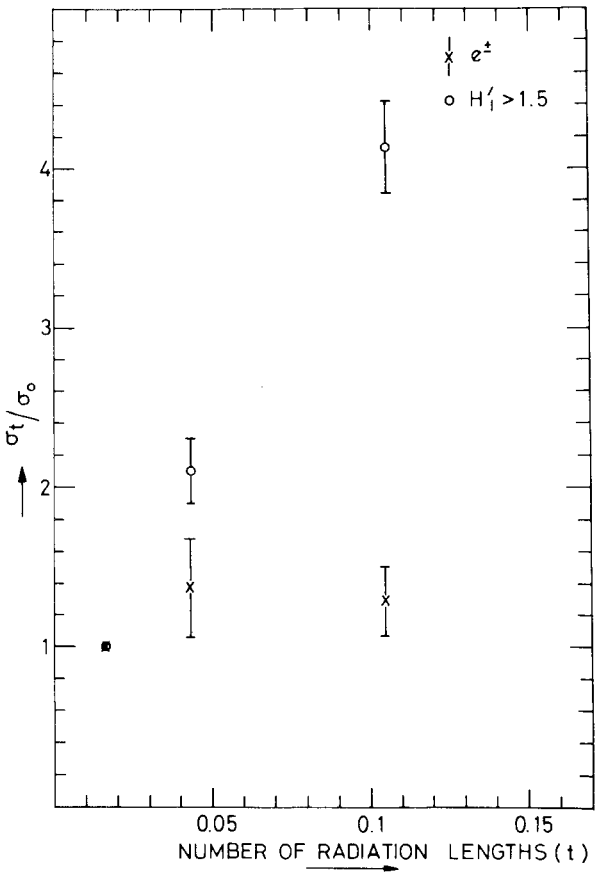

Fig. 2 The integrated cross section as a function of added converter thickness. This is given both for all cuts and for those events with two or more particles in H_1'.

pions and electrons. The fact that no broadening was observed for electrons indicates that any particle which may be decaying to give electrons must be short lived.

REFERENCES

1) J S Beale et al, Proc. Int. Conf. on Instrumentation for High Energy Physics, Frascati (ed. Laboratori Nazionale del CNEN, Frascati, 1973), p 415. To be published in Nuclear Instr. Methods.

2) F W Busser et al, Physics Letters 46B, 471 (1973).

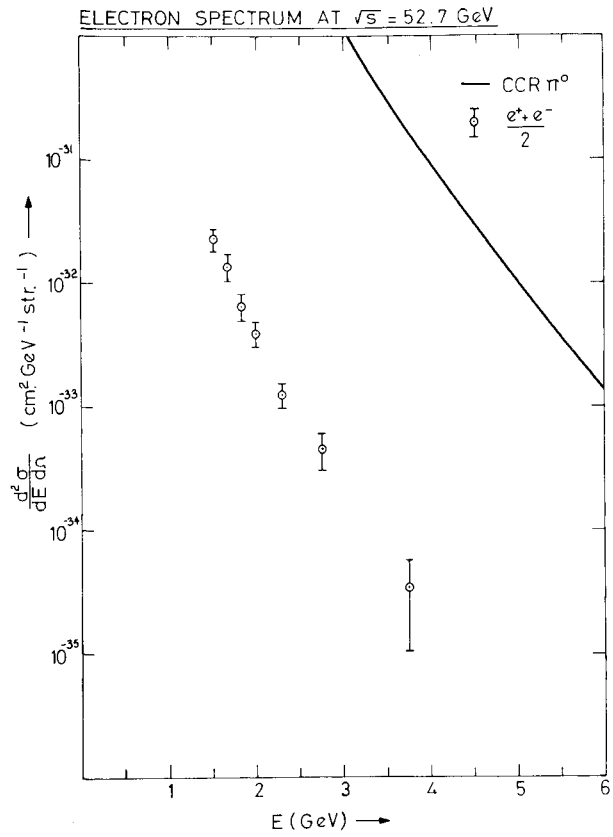

Fig. 3 The inclusive cross section, $d\sigma/dEd\Omega$, for electrons of either charge divided by two and plotted as a function of E. Also shown is the CCR π^0 spectrum.[2)]

II. COLUMBIA-FNAL COLLABORATION

Presented by T Yamanouchi

National Accelerator Laboratory

We describe here the observation of directly produced, high transverse momentum electrons and muons in proton-beryllium collisions at 300 GeV. Candidates for sources of such "direct" lepton production are: i) virtual massive photons, ii) vector mesons; $\rho,\phi,\omega,\ldots$. iii) intermediate bosons: $W^{\pm},Z^{o}$, ... iv) charmed particles, v) heavy leptons.

The virtue of electron detection is the high resolution possible; this is important in maintaining sensitivity to "bumps" which would be generated by a two-body decay $V \to e + X$ at a transverse momentum of $P = M_V/2$. Muon detection has the complementary advantage of having backgrounds (π,K decay) which are lower by a factor of $\sim$4.

The apparatus is shown in Fig. 1. The extracted proton beam strikes a thin Be target, 0.22 mm wide and $\sim$ 10 cm long. A 9 mr x 9 mr aperature is defined by a tungsten-lined steel collimator 8.2m long, tapered to minimize wall illumination. The production angle was measured horizontally, and data were taken at 50 mr and 83 mr, corresponding to 65^{o} and 93^{o} in the center of mass system.

Particles are detected only after magnetic deflection in the vertical plane. The "point" source target and angle in the vertical plane after the magnet

define the momentum; the horizontal plane trajectory was used to verify the target source.

The scintillation hodoscopes have a spatial resolution of 6 mm corresponding to a momentum resolution of 4% FWHM at 30 GeV/c. Two magnet settings cover the entire kinematical range ($P_\perp$ = 2 to 11 GeV/c) with good efficiency and large overlap.

Following the hodoscopes are two calorimeters, a total absorption lead glass electromagnetic shower detector and a steel-scintillator hadron detector.

The lead glass calorimeter consists of 45 identical blocks, arranged in three layers of 6, 6, and 15 radiation lengths along the beam direction.

A momentum analysis followed by shower detection in a lead glass spectrometer serves to provide hadron rejection of a factor of $\sim 10^5$. Efficiencies for electrons are determined by studying the effect of cuts on electron peaks produced by inserting foils in the intense γ-flux from the target.

In the electron experiment, we took data with foils of 2, 4, and 6% of a radiation length inserted in the secondary beam upstream of the magnets, to measure the spectra of electrons and positrons produced by γ conversions. A plot of the electron yield as a function of thickness is shown in Fig. 2. The uncorrected points are the raw data. Corrections were applied to take account of the energy loss due to bremsstrahlung by the electrons as they pass through the foils. (The slope of the resulting line gives the number of electrons from γ conversions per 1% radiation length).

The resulting electron yields were extrapolated to zero converter thickness to deduce the direct electron signal. Internal Dalitz conversion of the π^o parent spectrum can be subtracted in a trivial way since it is simulated by 0.8% of a radiation length. (The small effect of the finite mass of the Dalitz pair was calculated by a Monte Carlo program).

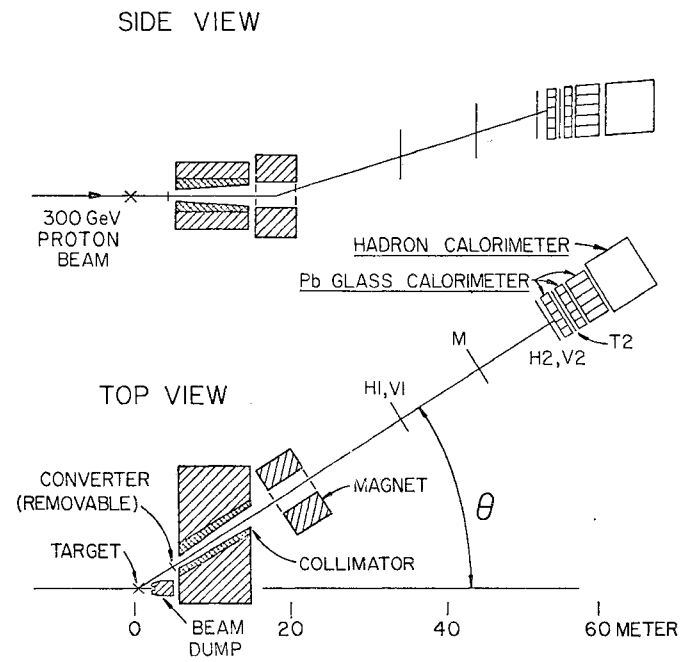

Fig.1 Experimental Apparatus for Electron Study.

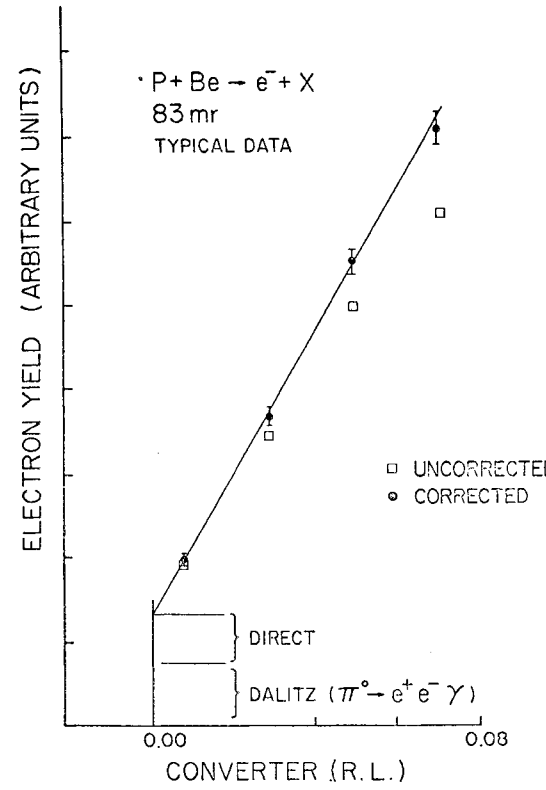

Fig.2 Yield of electrons vs foil thickness.

The direct electron signal at a consistent level of 10^{-4} of the π^o's persists in spire of a large series of critical tests.

The charge asymmetries of the directly produced electrons are given in Fig. 3. Positive and negative electrons have identical yields and are averaged to give the invariant cross section in Fig. 4. These data were taken on a Be target, and were normalized to a cross section per nucleon by dividing by 9, the ratio A(Be)/A(H). The overall cross-section normalizations are uncertain by 50%. Plotted errors are statistical only.

The data are seen to fall smoothly over 4 decades with no evidence of bumps. It should be noted that the acceptance is relatively flat out to $p_\perp \sim 11$ GeV/c, the kinematic limit. A list of background electron sources is given in Table I. They contribute negligibly to the signal.

To detect muons, a 0.9 m long hevimet filter was placed in the secondary beam line near the target

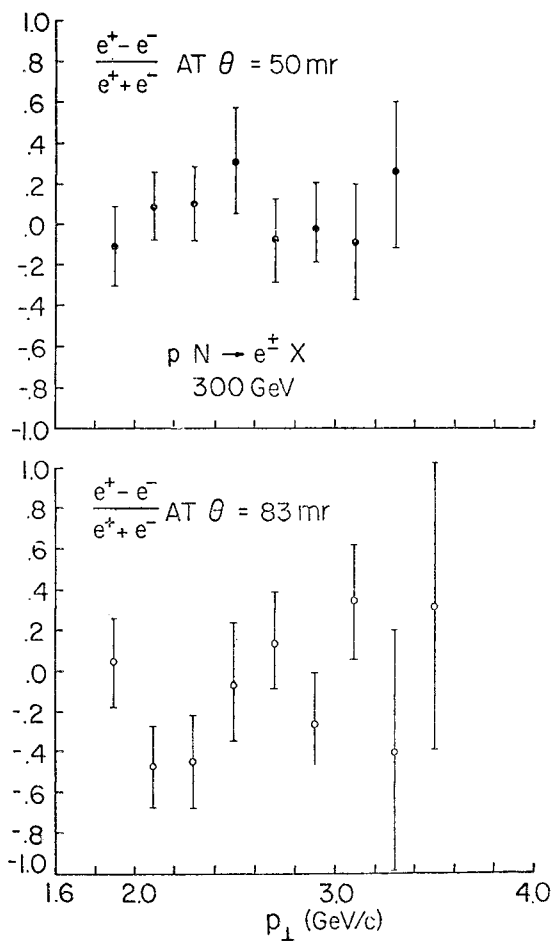

Fig.3 Comparison of positive and negative direct electrons.

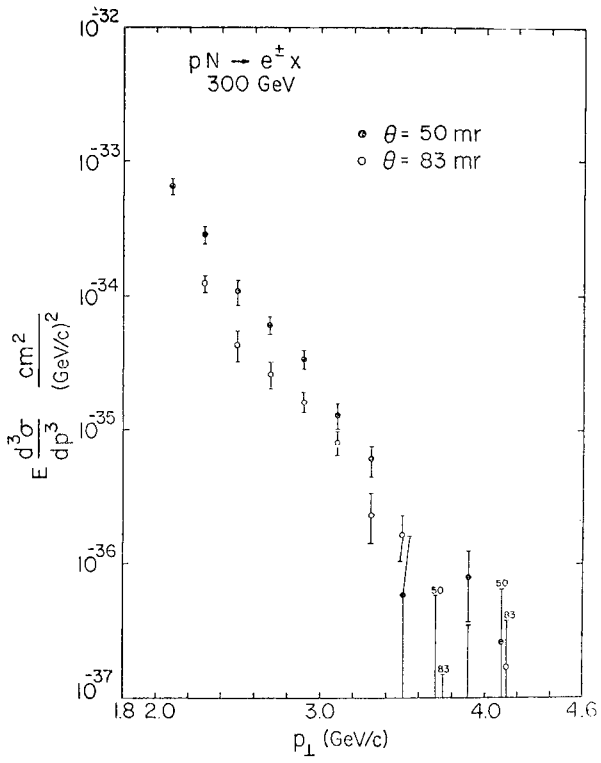

Fig.4 Invariant cross section for direct electrons.

TABLE I

Electron Sources, Normalized to π^o

$1.9 < P_\perp < 4$

$\pi^o \to \gamma e^+ e^-$	1×10^{-4}
$\eta^o \to \gamma e^+ e^-$	$1.5 \times 10^{-5} \times (N_\eta / N_{\pi^o})$
$\mu^- \to e\nu\bar{\nu}$	4×10^{-7}
$\pi^- \to e\nu$	4×10^{-8}
$K^- \to \pi^o e^- \bar{\nu}$	1×10^{-10}
$K_L^o \to \pi^+ e^- \nu$	2×10^{-10}
hyperons	$< 1 \times 10^{-10}$
signal	$\sim 1 \times 10^{-4}$ (90^o)

on a movable "sled" so as to decrease the decay-in-flight path of pions and kaons. The aperture of the detection system was fixed at ± 4 mr by additional x and y hodoscopes installed 9 m from the target. This arrangement insured that only a small change in the net "in-scattering" results from the motion of the filter. This effect, less than 30% for $P_\perp \geq 2.5$ GeV/c, is due to the changing lever arm of the multiple scattering and is evaluated by Monte Carlo. The only other effect of the filter motion is to vary the flight path and hence muons from π's and K's. Higher order effects result from secondary scatterings around the filter and from upstream sources. These effects are all rendered impotent by careful target reconstruction which was the main function of the added hodoscopes.

Typical results of a filter transit cycle are shown in Fig. 5. The point closest to "zero flight path" represents the distance of closest approach to the target (26 cm) plus a mean decay path in the hevimet (15 ± 5 cm) estimated by a Monte-Carlo cascade calculation.

The extrapolation to zero decay path shows a clear signal, equivalent to ∿ 50 cm of π, K decay path. Results of the cross section for muons (which we consider preliminary) are presented in Fig. 6. Again we observe no difference between positive and negative muons. Within the present systematic uncertainties these cross sections are consistent with those of the electrons (Fig. 4).

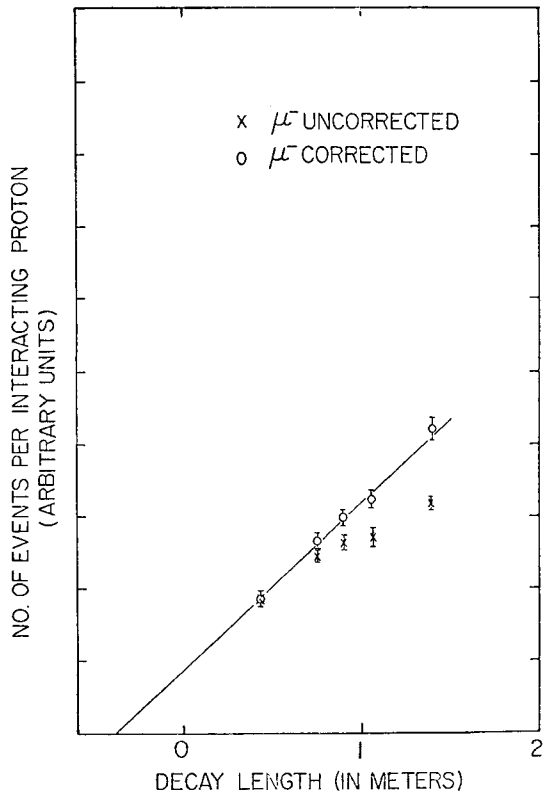

Fig.5 Yield vs. decay length. The slope gives the contributions of pions and kaons.

$(2.0 \leq P_\perp \leq 2.6$ GeV/c).

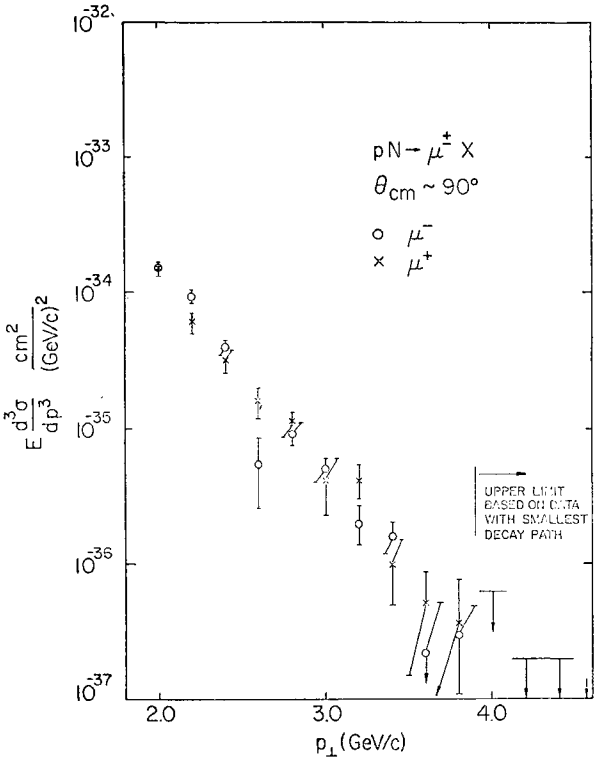

Fig.6 Invariant cross section for direct muons.

III. PRINCETON-CHICAGO COLLABORATION

Presented by P A Piroue

Princeton University

In an experiment, performed at the Fermi National Accelerator Laboratory we have observed muons produced directly in Cu and W targets by 300 GeV incident protons. We find a yield of muons which is approximately a constant fraction (0.8×10^{-4}) of the pion yield for both positive and negative charge and for transverse momenta ($P_\perp$) between 1.5 and 5.4 GeV/c.

We have used an apparatus described in a previous publication.[1] It consists of a single arm focusing spectrometer equipped with two Cerenkov counters and a calorimeter to identify hadrons, and a 15-ft.-long steel filter sampled each 2.5 ft. with dE/dx counters to identify muons. The spectrometer viewed secondaries produced in a heavy target at an angle of 77 mrad relative to the incident 300-GeV proton beam. This angle corresponds to $\sim 90^\circ$ in the nucleon-nucleon c.m. Direct muons from the target were separated from muons coming from π and K decays in flight with the aid of two absorbers which could be inserted into the spectrometer close to the target. The first absorber was a 23-in.-long W block with its upstream face 9.5 in. from the center of the target. The second absorber was a 42-in.-long Fe block with its upstream face 42 in. from the target. We used a 2-in.-long W target, primarily in runs with negative muons, and a 3-in.-long Cu target primarily in runs with positive muons.

Data were taken under three conditions: 1) no absorber, 2) W absorber inserted only, and 3) Fe absorber inserted only. Runs were made at 10 GeV/c intervals between 20 GeV/c and 70 GeV/c corresponding to transverse momenta ($P_\perp$) from 1.5 to 5.4 GeV/c.

For each absorber condition we measured the ratio of muons detected at the end of our apparatus to pions of the same charge detected by the apparatus when the absorber was absent.

For process (3) the ratio of muons to pions[2] was directly measured at each momentum and polarity in runs without the absorbers; the corresponding muon yield in the absorber runs is calculated from the observed penetrating pions. The remaining muon-yield, coming from processes (1) and (2), is then corrected by Monte-Carlo technique for the loss due to the absorber insertion (multiple scattering and change in $\Delta p_\perp$). Finally, the direct muon yield is obtained by linear extrapolation to zero decay path. The reduction of the raw data from a typical run at 40 GeV/c is presented in Table I. Figure I shows the extrapolation to zero decay path (dashed line); the solid line is the predicted slope. The points are plotted at a distance $(d+\lambda)$, where d is the distance between the target and the upstream end of the absorber, and λ is the measured interaction length in the absorber.

The predicted slope can be obtained from the rate of hadron decay between the target and the absorber. It was calculated by numerical integration as a function of momentum. The yield of decay muons between the target and absorber depends on both K and π decays. Kaons are twice as effective as pions in producing detected muons. Thus the slope is sensitive to the K/π ratio at the target. Figure 2 shows for both charges the predicted and observed slopes plotted against the inverse of the muon momentum.

The agreement between calculated and observed slopes is a significant verification of the corrections which are quite different in nature for the two absorbers.

Table II gives the ratio of direct muons to pions at target for all conditions. The most striking aspect of these results is the constancy of the ratio μ/π. The constancy for different target materials is particularly interesting. In a separate experiment, to be reported in a subsequent publication, we have found the yield of pions per interacting proton at 3 GeV/c $p_\perp$ to be 3.5 times larger from a W target than a Be target. This effect is believed to be due to secondary scattering in the nucleus. Since the direct muons follow the same pattern, a strongly interacting, short lifetime source is suggested for the muons. One such source can be the known vector mesons. If ρ^o, ρ^+, and ϕ^o were each produced with the same cross section as π, we would expect a ratio $(\mu/\pi) \times 10^{-4}$ of 0.49, 0.37 and 0.28 at $p_\perp$ of 1.5, 3.0, and 4.5 GeV/c, respectively. For all the observed direct muons to come from ρ^o and ϕ^o decays one would require ρ and ϕ productions to be each, at $p_\perp$ = 3.0 GeV/c ~3 times as large as the π cross section. This ratio rises [3] to ~6 at

	Tungsten	Iron
Observed muons	795±28	623±25
Observed pions	13580	4985
Ratio μ/π without absorber	$(2.03\pm0.10) \times 10^{-2}$	
Muons from hadron penetration of absorber (process (3))	276±13	101±5
Muons from processes (1) and (2)	519±31	522±26
Absorber loss factor	0.71±0.04	0.40±0.02
Corrected muons from processes (1) and (2)	731±60	1305±92
Pions at target	4.60×10^6	4.62×10^6
Muons/Pions at target	$(1.59\pm0.13) \times 10^{-4}$	$(2.83\pm.20) \times 10^{-4}$
Effective distance to target (meters)	0.35	1.25
Extrapolated μ/π at target	$(1.10\pm0.15) \times 10^{-4}$	

Table I Reduction of raw data to direct muon yield at the target. Processes (1),(2),and (3) are referred to in the text. Tungsten and Iron refer to the particular absorber used.

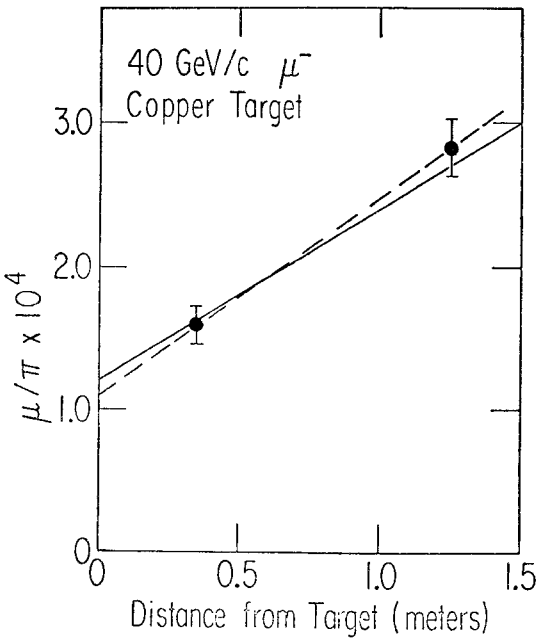

Fig.1 Plot of data reduced in Table 1. The dashed curve shows the linear extrapolation to the target. The solid line is the calculated slope.

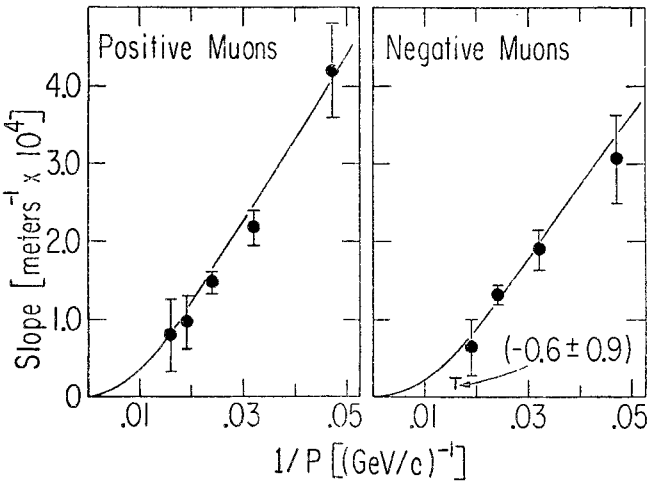

Fig.2 Plot of observed slope and calculated slope vs. reciprocal of the muon momentum. The points are the experimentally measured slopes; the solid line is the calculated slope.

$p_\perp$ = 4.5 GeV/c. This relatively large production ratio makes us wonder whether all the observed direct muons come from such a "mundane" source as the known vector mesons!

In Figure 3 we plot the invariant cross section per nucleon for inclusive muon production. Also plotted is the inclusive pion cross section x 10^{-4} and the inclusive muon cross section expected from a model based on parton-antiparton annihilation.[4] It is clear that the yield of muons is everywhere in excess of the parton model prediction.

REFERENCES

1. J W Cronin et al.,Phys,Rev.Letters 31,1426(1973).
2. For convenience we normalize to pions; the pions serve as a measure of all hadrons.
3. This point was drawn to our attention by L Lederman.
4. G R Farrar, California Institute of Technology preprint, CALT - 68 - 422, (1974); also private communication.

$P_\perp$ (GeV/c)	$\mu/\pi \times 10^4$ (Target) Positive	Negative
1.62	.66±.25 (Cu)	.86±.20 (W)
2.38	.72±.11 (Cu)	.67±.12 (W)
3.15	.88±.18 (Be)	- - -
3.15	.94±.16 (Cu)	.88±.12 (Cu)
3.15	.60±.15 (W)	.74±.16 (W)
3.91	.98±.23 (Cu)	.88±.26 (W)
4.67	.87±.30 (Cu)	1.02±.34 (W)
5.44	.94±.47 (Cu)	1.20±.46 (W)

Table II Ratio of directly produced muons to pions in the proton-nucleus collision. The observed pions emerging from the 0.4-interaction-length target are multiplied by a factor 1.25 to account for absorption in the target itself.

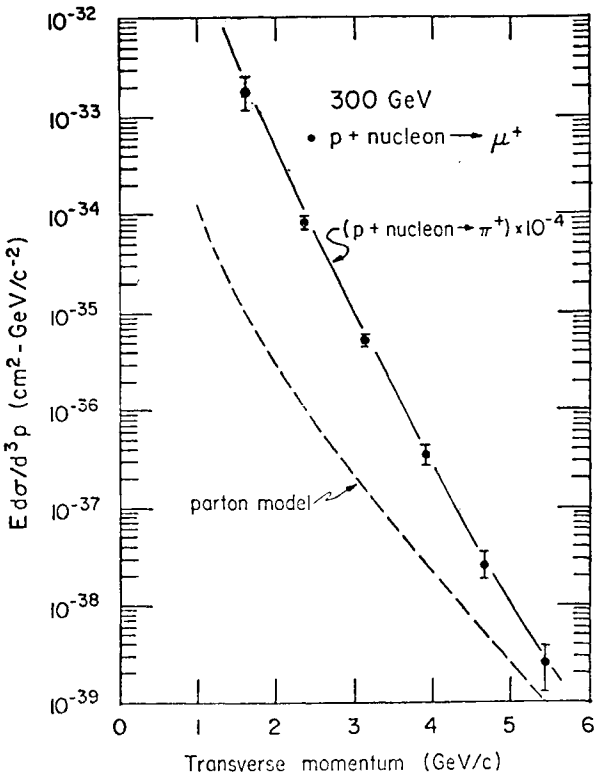

Fig.3 Plot of the invariant cross section for direct muon production vs. $P_\perp$. Also shown is the pion cross section x 10^{-4} and the cross section predicted by a parton model.

IV. WISCONSIN-HARVARD-PENN-CHICAGO COLLABORATION

Presented by R Imlay

University of Wisconsin

We have observed the prompt production of muons in nucleon nucleon collisions in an experiment at the internal target laboratory of Fermi National Accelerator Laboratory. The apparatus is shown in Fig. 1. A rotating carbon target intersected the circulating proton beam from 30 to 300 GeV. Penetrating particles produced near 85 mr in the laboratory passed through a series of absorbers and into a vertically bending magnetic spectrometer equiped with scintilation counters and multi-wire proportional chambers. Two gas Cerenkov counters and two lead glass counters were used for particle identification. An upper limit of 2% on hadron contamination was obtained using the lead glass counters.

Remotely controlled absorbers were used to vary the decay path available for pions and kaons from 40 cm to 110 cm. The rate of muons was measured as a function of this decay distance. An extrapolation to zero decay path yields the flux of prompt muons. Fig. 2 shows the yield of muons from pion and kaon decay compared with predictions based on pion and kaon production[2,3]. Fig. 3 shows the muon spectrum from pion and kaon decay compared with the predicted spectrum. Table I shows preliminary results for part of our data for the prompt muon to pion ratio obtained from the extrapolation plots. Relative corrections for multiple scattering of about 15% have been applied for the various absorber positions. We have checked that the corrections are insensitive to the estimated uncertainty in chamber and counter positions and pion and kaon production spectra.

We have used the two threshold gas Cerenkov counters to obtain limits on the invariant cross section for production of heavy penetrating particles. Table II shows the results as a function of mass m in GeV and lifetime τ in seconds.

REFERENCES

1. For related experiments see the following reports,
P J Wanderer et al.,Phys.Rev.Letters 23, 729 (1969).
J Christenson et al.,Phys.Rev.Letters 25, 1523 (1970).

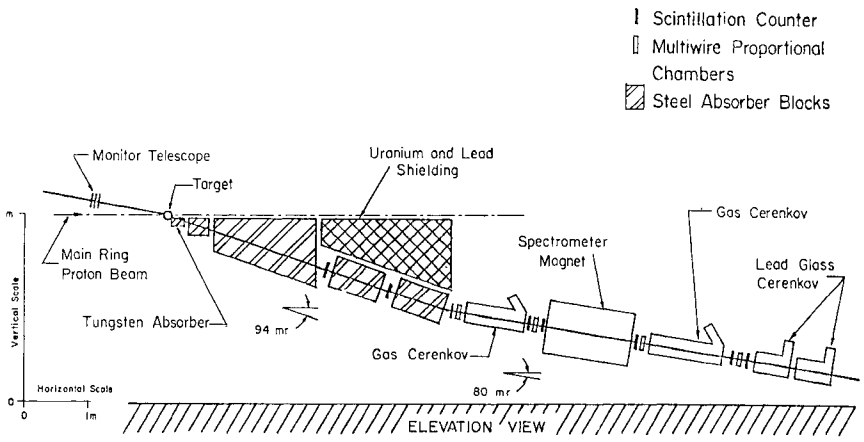

Fig. 1 Experimental arrangement.

Bondarenko et al.,Proceedings of XVI International Conference on High Energy Physics,Vol.2, p.329 (1972).

J Boymond et al.,Enrico Fermi Institute Preprint 74-24.

Fermi National Accelerator Laboratory experiment 70, unpublished.

2. D C Carey et al., Fermi Laboratory preprint NAL-74/48.

3. J W Cronin et al.,Phys.Rev.Letters 31, 1426 (1973).

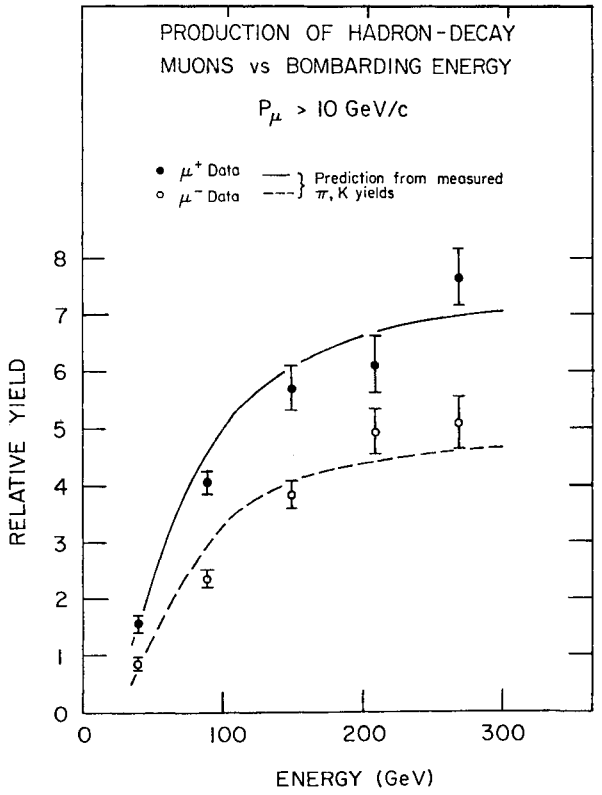

Fig. 2 Relative μ^+ and μ^- yields arising from π and K decay as a function of bombarding energy. The smooth curves are predictions based on the hadron production measurements of references 1 and 2.

TABLE II

p_T	Correction factor For short-lived particles	Cross section limit for $\tau = \infty$ cm^2/GeV^2	Mass
.85 to 1.25 GeV	exp [0 .3 x 10^{-8} M/τ]	2.6 x 10^{-34}	M>.8 GeV/c^2
1.25 to 1.7	exp [0.2 x 10^{-8} M/τ]	1.7 x 10^{-35}	M> 1.2 GeV/c^2
1.7 to 2.1	exp [0.15 x 10^{-8} M/τ]	7.3 x 10^{-36}	M> 1.6 GeV/c^2

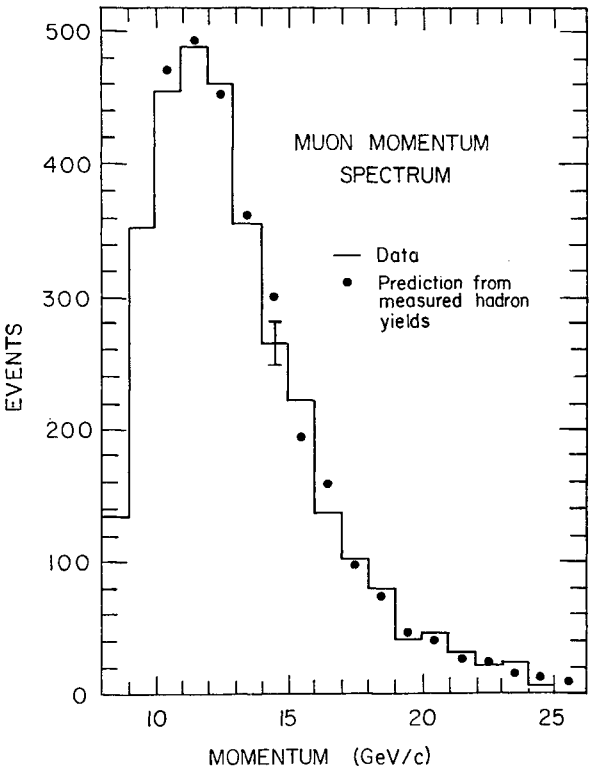

Fig. 3 Observed muon momentum distribution for one setting of the spectrometer's magnetic field. The low momentum cut-off arises from the spectrometer acceptance. The dots correspond to the distribution expected from the hadron production measurements of references 1 and 2, folded with hadron decay, multiple scattering, and detector acceptance.

TABLE I

Muon Charge	Proton Energy Range (GeV)	Muon Momentum Range (GeV/c)	Average Muon Transverse Momentum (GeV/c)	Prompt Yield (x 10^{-4}) N_μ/N_π
(+)	60-300	15-20	1.4	.66±.28
(-)	60-300	15-20	1.4	.77±.30
(+)	60-300	> 20	1.9	.82±.35
(-)	60-300	> 20	1.9	1.24±.39
(+) +(-)	60-180	15-20	1.4	.094±.34
(+) +(-)	60-180	> 20	1.9	1.41±.54
(+) +(-)	180-300	15-20	1.4	1.05±.35
(+) +(-)	180-300	> 20	1.9	.48±.31

V. BRITISH UNIVERSITIES COLLABORATION

Presented by R Cence

University of Hawaii

This experiment[1] was performed to search for muons with high transverse momenta as evidence for the existence of a massive object, (for example the Intermediate Vector boson) which has a muon decay. In the data reported here a minimum transverse momentum of 4 GeV/c was accepted, and hence the experiment was not sensitive to muons at lower transverse momenta reported to this meeting[2].

The data presented was taken in 450 HOURS at a mean luminosity of 1.47×10^{30} $cm^{-2}sec^{-1}$, and constitutes ~50% of the total data taken. The weighted average C.M. energy was $\sqrt{s}$ = 49.1 GeV. A total of 5.5×10^4 tracks were analysed, in which the muons had traversed > 13 Interaction lengths of material. Only tracks which had traversed at least 12 steel plates were included in the final data, to which geometrical cuts at the intersection region were applied to decrease the background from cosmic ray muons.

After subtracting the remaining backgorund muons from cosmic rays, and the meson decays, no signal was observed with a transverse momentum greater than 4 GeV/c. This result yields a value of

$$\frac{d\sigma}{d\Omega} \quad (pp \to \mu^{\pm}_{\circ}\ldots) \lesssim 5 \times \bar{10}^{36} \text{ cm}^2/\text{st} \quad (90\%\text{cl}).$$

This upper limit, and the model predictions using the modified Kuti-Wieskopf [3] parton distributions exclude W masses from 10 - 18 GeV/c^2, as shown in Fig. 1.

REFERENCES

1) P H Sharp, Proceedings 4th Int. Conf. on High Energy Collisions 2(1972) 215; G Manning, 16th Int. Conf. on High Energy Phys., 2(1972) 358.

2) Papers to this Conference: 218 Segler, CCRS ISR 571 Yamanouchi, Columbia/NAL, 398 Piroué, Princeton-NAL, 576 Imlay, Harvard-NAL-Wisconsin, 785 Nurushev, Serpukhov.

3) J Kuti and V Weiskopf, Phys. Rev. D4(1971) 3418; S Berman, J Bjorken and J Kogut, Phys. Rev. D4(1971) 3388; R McElhaney and S F Tuan, Phys. Rev. D8(1973) 2272; S Pakvasa, D Parashar and S F Tuan, Univ. of Hawaii Preprint, UH-511-177-74, May 1974.

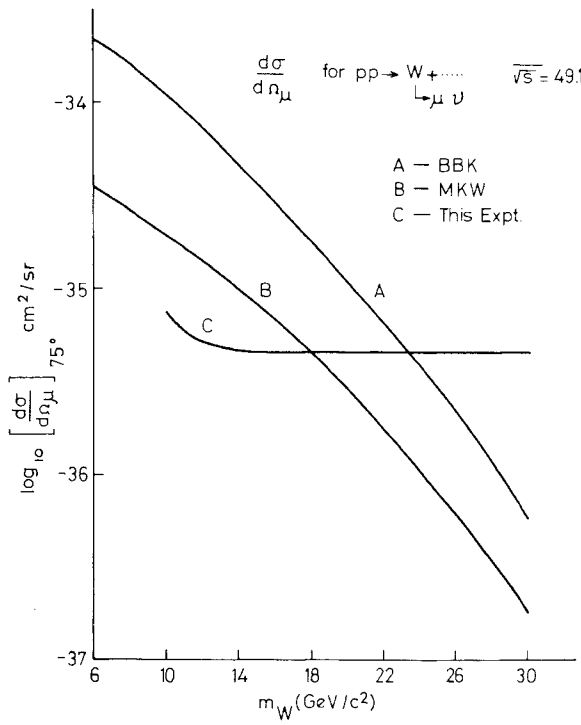

Fig. 1

VI. SERPUKHOV CONTRIBUTION

Presented by S Nurushev

The Institute for High Energy Physics

The energy spectrum and longitudinal polarization of muons with large transverse momentum (1.8 GeV/c $\leq P_\perp \leq$ 2.8 GeV/c) produced in the proton beam interaction with an internal copper target at the IHEP 70 GeV accelerator were measured. A beam of positive (or negative) muons was transported along a special muon channel made from magnetized iron placed at an angle of 9^o to an incident 70 GeV proton beam. It corresponded to particle production at about 90^o in the c.m. of two nucleons. Separation of muons produced directly in the target or connected with short-lived particle decays ("direct muon") was performed by changing the distance between the target and the copper absorber. Thus, in the experiment there was a possibility to measure the muon intensity from the hypothetical intermediate boson decay $W \to \mu e$, from muon pair production or from some similar process.

The apparatus and preliminary results were described elsewhere[1].

1. "Direct muon" intensity ($X^{\pm}$) was extracted by means of extrapolation of the experimental muon intensity dependence on the distance between the target and the absorber. In all the investigated transverse momentum intervals the value $X^{\pm}$ proved to differ from zero and was equal to 10^{-4} of pion intensity. This value was taken as the upper limit of "direct muon" production level rather than a precise number. Using some assumptions on the mechanism of production and decay of W-boson one can be used to estimate the theoretical and experimental values for σ_W B, where σ_W is the total cross section for intermediate boson production and B is the branching ratio of W-decay into muon and neutrino[2-4].

As is seen from Fig. 1 the experimental data contradict the fact of existence of intermediate boson in the mass interval from 6.5 to 8.5 GeV/c^2 based on the above assumptions.

The expected cross section for "heavy photon" B_o production (decaying into $\mu^+\mu^-$) was calculated from the relation

$$\sigma_{B_o} = \frac{3\pi}{2\alpha} M_{B_o} \left(\frac{d\sigma}{dq}\right)_{q = M_{B_o}}$$

and is plotted also on Fig. 1.

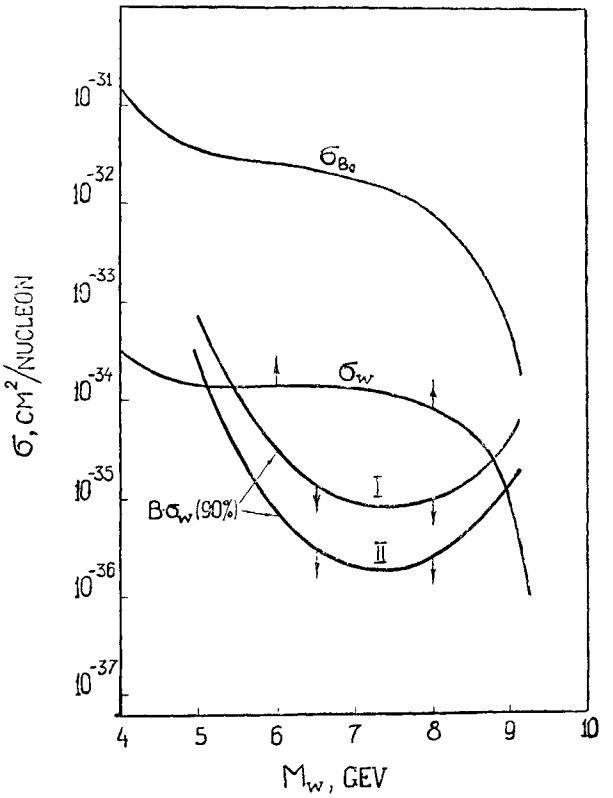

Fig. 1 Comparison of intermediate boson and heavy photon production cross sections (σ_W and σ_{B_o} respectively) with the experimental upper limit of cross sections. I - calculation with parton annihilation model; II - calculation with phase space model.

2. Muon pair production. Acceptance of the beam channel when displacing the absorber is the same for muons of both charges so if there are no "direct muons" the charge ratio of μ^+/μ^- must not depend on the absorber displacement. The results of charge ratio measurements for two absorber extreme positions (25cm and 85cm from internal target) as a function of muon energy indicate a presence of prompt muons. The invariant cross sections of "direct muon" production and π^+-meson production are compared on Fig. 2.

3. Measurement of the longitudinal muon polarization. Additional information about muon origin can be provided by measuring their polarization. Thus, muons produced on weak or semiweak lepton decays (or vector particles) have polarization $\eta = +1$ whereas muons from electromagnetic process have $\eta = 0$, and muons from weak scalar meson decays (π,K) have $\eta = -1$.

We have measured the polarization of muons with energy E = 14 GeV ($P_\perp$ = 1.8 GeV/c) by means of a system containing 12 carbon plates with dimensions 30 x 30 x 4 cm^3 alternated with scintillation counters ("sandwich"). The apparatus worked on-line with a computer. The electron angular distribution from μe-decay was measured for different distances between the target and the absorber, that is with changed relative weights for "direct muons". The asymmetry coefficient α is defined as a ratio of the difference between the number of decays into the front and rear hemispheres to their sum. The measured values of α yield the following results for "direct muon" intensities:

$X_o^+ = (1.5 \pm 4.0)/10^{12}$ proton (for $\eta = 0$)

$X_1^+ = (0.7 \pm 1.8)/10^{12}$ proton (for $\eta = +1$)

REFERENCES

1) G B Bondasenco et al., Proc. of the XVI Intern. Conf. on High Energy Physics 2(1973) 329.

2) L M Lederman and B G Pope, Phys. Rev. Lett. 27(1971) 765.

3) T H Christen et al., Phys. Rev. D8(1973) 2016

4) S D Drell and T M Yan, Phys. Rev. Lett. 25(1970) 1523, Yu A Golulkov et al. Yadernaya Fisica 18(1973) 393.

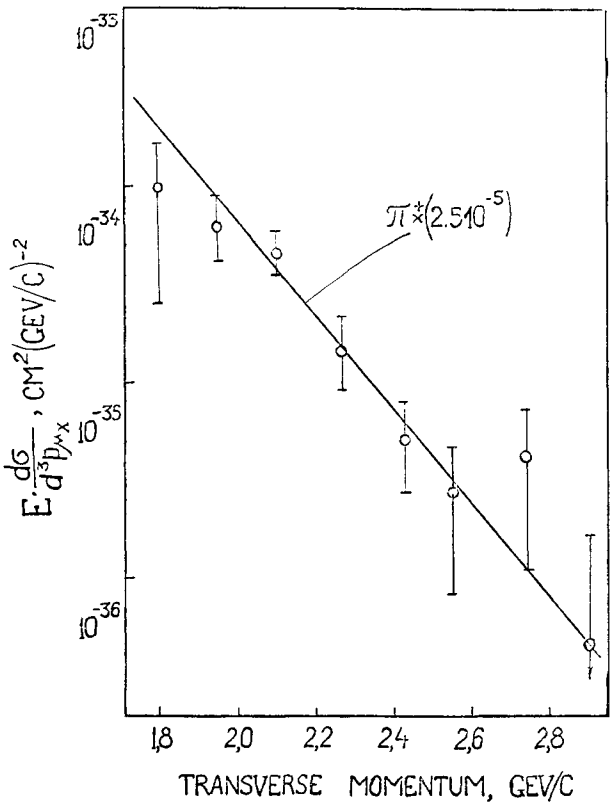

Fig. 2 "Direct muon" production cross section as a function of transverse momentum.

CHAIRMAN'S SUMMARY

L M Lederman

Columbia University

1. $\left(\frac{e}{\pi}\right)^+ \cong \left(\frac{e}{\pi}\right)^- \cong \left(\frac{\mu}{\pi}\right)^+ \cong \left(\frac{\mu}{\pi}\right)^- \cong 10^{-4}$
2. This is independent of P_T from 1.5 to 5 GeV/c.
3. This is independent of nucleon target size.
4. This is independent of CM viewing angle.
5. This is independent of s from $\sqrt{s}$ = 7 to $\sqrt{s}$ = 53 (See Fig. 1).

All of these statements may be true to within a factor of 2 or so.

(A BNL point is taken from a comment by R Adair). The implications are that leptons and pions have a common origin. Statement 5 implies the source mass must be less than 3-4 GeV (no threshold effects) for

$$p + p \to X + \text{anything}$$
$$\qquad\quad \hookrightarrow \text{leptons}$$

or less than 1.5-2 GeV for pion production e.g. Charmed particles. Statement (1) in its lack of charge asymmetry is discouraging for charmed meson sources analogous to K-mesons. The agreement of the ISR with NAL rules out low masses (M_X > few hundred MeV) because narrow angle leptons are vetoed in the ISR measurements.

The ISR muons and NAL electrons set limits on the production of single leptons e.g. from $W^{\pm}$ up to the kinematic limit. However, it is out of fashion to convert these limits to mass limits because the necessary models are currently discredited.

The lack of $P_\perp$ "bumps" means there are no significant heavy objects (M from 3 → 10 GeV) decaying into two leptons.

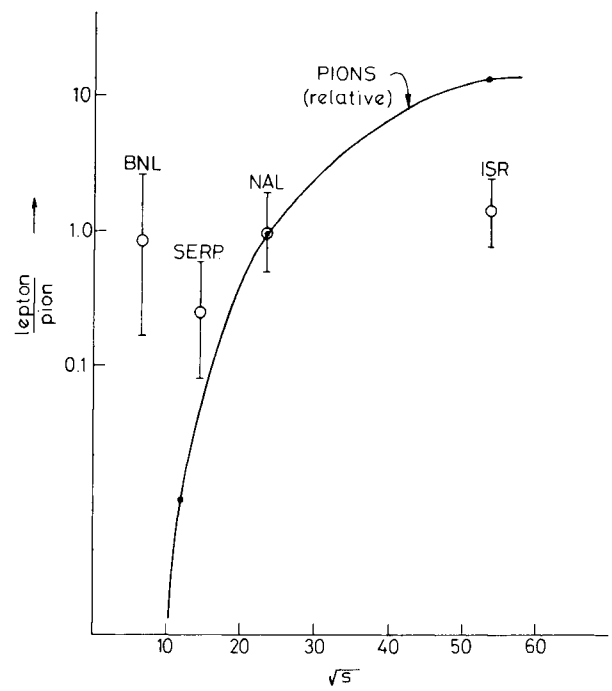

Fig. 1 lepton/pion ratio vs $\sqrt{s}$ compared to pion production ($P_\perp \sim 3$ GeV). Errors are estimated freely.